Development of a scalable bioprocess for the expansion and differentiation of human pluripotent stem cells into progeny for diabetes cell therapies

A thesis submitted by

Elena Jacobson

in partial fulfillment of the requirements for the degree of

Doctor of Philosophy in Chemical Engineering

Tufts University

August 2020

Adviser: Emmanuel Tzanakakis

Abstract

Recent advances in the differentiation of human pluripotent stem cells (hPSCs), including embryonic (hESCs) and induced pluripotent cells (hiPSCs), to clinically relevant cell types pave the way for hPSC use as cell therapies. However, the clinical potential of hPSCs hinges on development of bioprocesses for the robust, scalable, and economical generation of therapeutically useful cell types. Stirred suspension bioreactors (SSBs), which are the workhorse of the biotechnology industry, fulfill these requirements. Unlike static cultures, SSBs allow monitoring and control of cultivation parameters including feeding, pH, agitation, and dissolved oxygen (DO). Densities of 10^6-10^7 cells/mL or greater are typical in SSBs, suggesting more efficient utilization of media and factors relative to planar cultures. Such densities also underline the manageable working volumes necessary for producing 10^8-10^9 cells/patient for cell therapy regimens currently under development or in practice. One problem that arises in SSBs is high levels of lactate, which have been shown to slow hPSC growth rate. In spite of this, the metabolic changes that the lactate incurs on hPSCs has yet to be evaluated.

As an example of cell type which hPSC can be differentiated into, definitive endoderm (DE) cells are the progenitors of diverse cell types in organs such as the pancreas, liver, and lungs. These organs are targeted by major diseases like diabetes, cirrhosis, chronic obstructive pulmonary disease (COPD), and cancer. Therefore, DE and the pancreatic lineage are a useful differentiation pathway for hPSCs. Nonetheless, *in vitro* hPSC differentiation to pancreatic β-cells needs to be further matured *in vivo* in order to exhibit glucose stimulated insulin secretion (GSIS). The most mature β-like cells that have been developed utilize planar differentiation and an cell line that allows the sorting of insulin-expressing cells and reaggregation for future maturation. Nevertheless, for use as a cell therapy, a scalable differentiation system is necessary. In addition,

many of the differentiation protocols that currently exist use animal-derived components, which incurs lot-to-lot variability and risk of cross-contamination, and thus are not ideal for clinical applications. This suggests the need for xenofree expansion and differentiation in a scalable system.

In this work, we develop an aggregate planar DE differentiation protocol free of animal-originating components (xenofree) for a hESC (H9) and hiPSC (IMR90) line and achieve up to 87% $FOXA2^+/SOX17^+$ cells. We optimize the xenofree aggregate culture expansion of these cell lines in an SSB with pH and DO control, while maintaining pluripotency (>85% $OCT4^+$) and viability (>85%). Then we apply the xenofree DE differentiation protocol to the hPSC aggregates and attain 89% $FOXA2^+/SOX17^+$ cells or ~8 DE cells per seeded hPSC in the SSB. Lactate exposure, of the range seen in our SSB expansion, of hPSCs for 6 days showed that concentration over 2.5 g/L (~22 mM) had an effect on the growth rate, while pluripotency marker expression did not change. Finally, a hESC (MEL1 $INS^{GFP/W}$) line was differentiated to the pancreatic cell lineage, first in a spinner flask, achieving ~33% INS^+ cell, then in the SSB, yielding up to ~20% INS^+ and 40% $NKX6\text{-}1^+$ cells.

Overall, this work provides bioprocess improvements for the expansion of hPSCs and manufacturing of DE cell progeny and pancreatic islet cells.

Acknowledgement

I would like to thank my advisor, Professor Emmanuel (Manolis) Tzanakakis, for his guidance and support during my PhD. I would also like to thank my committee members: Professor Kyongbum Lee, Professor Qiaobing Xu and Professor Laertis Ikonomou for their invaluable advice while pursuing my PhD and work on my dissertation. As well as our collaborators at the University of California, San Francisco, Professor Matthias Hebrok and Gopika Nair and the other lab members who helped train me: Charity Juang, Mei Lan Li, and Michael Saxton. Additionally, I would like to thank my current and previous colleagues: Roofya Rahmati, Preeti Ashok, Fan Zhang, Zijing Chen, and Demetrios Stoukides. For those that taught me all the lab techniques and helped troubleshooted results and experiments with me and for everyone's support and friendship. Finally, I would like to thank my parents and friends for their never-failing support of all my endeavors.

Contents

1 Background 1
1.1 Pancreatic Development 2
1.2 hPSC differentiation toward pancreatic β-cells 8
1.3 Xenofree differentiation to Definitive Endoderm 12
1.4 Scalability of hPSC culture 13
1.5 Expansion of pluripotent stem cells 14
1.5.1 Stem cell culture media and coatings 14
1.5.2 Feeding strategies 15
1.5.3 Stem cell expansion systems 16
1.6 hPSC metabolism 19
1.7 Effects of lactate 20
1.8 Motivation for the present study 22
2 Materials and Methods 24
2.1 Human pluripotent stem cell culture 24
2.2 Definitive endoderm differentiation in multi-well plates 24
2.3 Bioreactor cultivation 27
2.4 Cell Seeding for lactate experiments 28
2.5 INS GFP cell line cultivation 29
2.6 Aggregate size distribution 30
2.7 Flow cytometry 30
2.8 Immunostaining 31
2.9 Quantitative Polymerase Chain Reaction (qPCR) 31
2.10 Lactate measurement 32
2.11 Statistical Analysis 32
3 Planar Suspension Differentiation of hPSCs to Definitive Endoderm 33
3.1 Introduction 33
3.2 Results 34
3.2.1 Differentiation of hPSCs to DE cells in multi-well plates 34
3.2.2 Xenofree differentiation in multi-well plates 38
3.3 Discussion 41
4 Expansion of hPSC aggregates in an automated bioreactor 45

4.1 Introduction 45
4.2 Results 46
4.2.1 Expansion of hPSCs in the bioreactor 46
4.2.2 Effect of exogenous lactate on monolayer and suspension aggregate culture 50
4.3 Discussion 51
5 Scalable differentiation of hPSCs toward insulin expressing cells 56
5.1 Introduction 56
5.2 Results 57
5.2.1 Scalable Differentiation of hPSCs Toward Insulin expressing Cells 57
5.2.2 Scalable Xenofree Differentiation of hPSCs To Definitive Endoderm 63
5.3 Discussion 66
6 Conclusions and Future Work 68
6.1 Impact of Work 68
6.2 Future Work 70
6.2.1 Expansion of hPSC in an automated SSB 70
6.2.2 Lactate metabolism and effects on hPSCs 71
6.2.3 MEL1 Differentiation toward insulin expressing cells 73
7 References 84

List of Tables

Table 1. Secretagogues for β-cell insulin secretion machinery. 6
Table 2. AW protocol for DE differentiation of H9 and IMR90 hPSCs. 26
Table 3. xfAW protocol for DE differentiation of H9 and IMR90 hPSCs. 27
Table 4. hPSC differentiation to β-like cells 76
Table 5. Differentiation components and their functional roles 78
Table 6. Protocols for Definitive Endoderm differentiation of hPSCs 79
Table 7. Xenofree and feeder-free human pluripotency medium 80
Table 8. hPSC bioreactor expansion studies 81
Table 9. Experimental protocols for testing different concentrations of canonical Wnt activation with CHIR and activin A application length for DE differentiation of H9 hESC aggregates. 82
Table 10. Experimental protocols for testing different concentrations of xfKSR and xfB27 for DE differentiation of IMR90 aggregates. 82
Table 11. Yield of DE cells/well reported here and by Diekmann et al. (Diekmann et al., 2019). 83
Table 12. Yield of DE cells/mL reported here with the xfAW protocol and by Sahabian et al. (Sahabian et al., 2019). 83

Table of Figures

Figure 1-1. Schematic of diabetes pathologies: A) Normal, B) Type 1 Diabetes (T1D), C) Type 2 Diabetes (T2D). Created in Biorender. 2

Figure 1-2. Schematic of pancreas development with stage specific markers and the signaling pathways that were activated (↑) or inhibited (⊤). 4

Figure 1-3. Schematic of the preproinsulin to insulin processing. Created in Biorender. 5

Figure 1-4. Schematic of β-cell insulin release (Lang & Light, 2010). 7

Figure 1-5. Examples of large-scale adherent, two-dimensional (2D) culture systems: A) Roller bottle (created in Biorender), B) Pall Corporation Xpansion® Multiplate Bioreactor System, C) Nunc™ Cell Factory™ Systems, D) Corning® CellSTACK® Chambers, E) HYPERstack, F) CellCube. 17

Figure 1-6. Examples of bioreactor system: A) DASbox ® Mini, B) Mobius® 3L, C) BioLevitator™. 18

Figure 1-7. Example of control of agitation (stirrer), temperature (temp), pH (ph), and dissolved oxygen (do) by our bioreactor my-control. Decrease to zero stirring rate is during medium changes. 18

Figure 1-8. Diagram demonstrating glycolysis and lactate production which leads to medium acidification (decrease (↓) pH). Created in Biorender. 20

Figure 2-1. Schematic of the experimental strategies for DE differentiation of hPSCs in multi-well plates and an automated bioreactor. I: multi-well differentiation; II: multi-well with expansion and differentiation. III: bioreactor with expansion and differentiation. Some pictures created in Biorender..... 26

Figure 3-1. A) Micrographs of aggregates differentiated with GDF8/CHIR/BSA (left, (Zhu et al., 2016)) or with AW protocol (right) at the final day of DE differentiation. Arrows indicate lysed cells. Scale Bars: 200 μm. B) Representative flow cytometry density plots of $SOX17^+/FOXA2^+$ cells at the final day of DE differentiation for IMR90 hiPSCs (top) and H9 hESCs (bottom) treated with GDF8 for DE differentiation after priming step. 35

Figure 3-2. Representative flow cytometry density plots of $SOX17^+/FOXA2^+$ cells from H9 planar aggregates subjected to the initial trial DE protocols A) 3, .3 μM CHIR (day 1-2), flow from day 3 and 4, B) 50 ng/mL WNT3A (day 1), flow of day 4 C) 25 ng/mL WNT3A and 1.5 μM CHIR (day 1), 2.5 ng/mL WNT3A and .15 μM CHIR (day 2) , flow of day 4 D) 3 μM CHIR (2 days), .3 μM CHIR (day 1-3) flow of day 3. 36

Figure 3-3. Flow cytometry analysis of SOX17+/FOXA2+ cells from IMR90 and H9 planar aggregates with AW protocol at the final day of DE differentiation. Results are shown as mean±SD along with representative density plots. 37

Figure 3-4. Representative images of IMR90 and H9 aggregates on days 0 (D0) and final day of AW DE differentiation (Day 3 (D3) or Day 4 (D4)). Scale Bars: 500 μm (top row), 200 μm (bottom row). 38

Figure 3-5. Representative flow cytometry density plot of $SOX17^+/FOXA2^+$ cells from IMR90 planar aggregates with trial xenofree protocols at the final day of DE differentiation. A) 1% xfB27 and 30% xfKSR. B) 1% xfB27 and 20% xfKSR. C) 2% xfB27 and 20% xfKSR. D) 1% xfB27 and 30% xfKSR. xfB27: xenofree B27 supplement, xfKSR: Xenofree KnockOut Serum Replacement. 39

Figure 3-6. Flow cytometry analysis of IMR90 and H9 cells following xfAW and AW differentiation in 6-well plate planar cultures. A) DE markers. B) Pluripotency markers of H9 cells. C) Pluripotency markers of IMR90 cells. *p≤ 0.05, **p ≤ 0.01, *** p ≤ 0.001, ****p ≤ 0.0001. Results are shown as mean±SD. 40

Figure 3-7. Representative immunocytochemistry of IMR90 aggregate after xfAW differentiation DAPI (blue), SOX17 (green), FOXA2 (red), OCT4 (no staining), and MERGE. Scale Bars: 100 μm. 40

Figure 3-8. A) Representative images of IMR90 and H9 hPSC aggregates at day 0 (D0) and 3 (D3) or 4 (D4) of the xfAW protocol. Scale Bars: 500 μm (top row), 200 μm (bottom row). B) and C) Representative cell aggregate sizes over the course of xfAW differentiation. B) IMR90 cells. C) H9 cells. Results are shown as mean±SD. 41

Figure 4-1. A) and B) Live cell concentration (cells/mL) and viability (%) for expansion in the bioreactor with essential 8 (E8) medium, H9 and IMR90. C) and D) Aggregate size analysis of IMR90 and H9 cells propagated in bioreactor cultures with essential 8 (E8) medium, H9 and IMR90. Results are shown as mean±SD. 47

Figure 4-2. Representative images of IMR90 and H9 hPSC aggregates 6 to 192 h in the bioreactor with essential 8 (E8) medium. Scale Bars: 100 μm. 47

Figure 4-3. A) Lactate and glucose concentrations for H9 and IMR90 aggregates over the course of bioreactor culture with essential 8 (E8) medium. Arrows indicate medium changes. B) Flow cytometry analysis of H9 cells for pluripotency marker expression during bioreactor expansion with essential 8 (E8) medium. *p ≤ 0.05, *** p ≤ 0.001, ****p ≤ 0.0001. Results are shown as mean±SD. 48

Figure 4-4. Immunocytochemistry of pluripotent markers (NANOG and OCT4) and nucleus staining (DAPI) of cells seeded as single cells in a monolayer and grown for 3 days after bioreactor culture with essential 8 (E8) medium. Scale Bars: 100 μm. 48

Figure 4-5. IMR90 and H9 bioreactor expansion in StemMACS A) Live cell concentration (cells/mL) and viability (%). B) Aggregate size analysis. C) Flow cytometry analysis for pluripotency marker expression. *p≤ 0.05, **p ≤ 0.01, *** p ≤ 0.001, ****p ≤ 0.0001. Results are shown as mean±SD. 49

Figure 4-6. Comparison between three H9 bioreactor expansion runs in StemMACs medium (A) Live cell concentration (cells/mL) and viability (%). (B) Aggregate size analysis. C) Flow cytometry analysis for pluripotency marker expression. *** p ≤ 0.001, ****p ≤ 0.0001. All results are shown as mean±SD. 50

Figure 4-7. Flow cytometry analysis for pluripotency marker expression ($NANOG^+/OCT4^+$ co-expressing cells) of IMR90 cells cultured as monolayer or aggregates in E8 Flex or StemMACs medium after six days with different concentration of sodium lactate (0, 2.5, 5 g/L). *p≤ 0.05, **p ≤ 0.01. Results are shown as mean±SD. 51

Figure 4-8. Aggregate size analysis of IMR90 at day 2 and 6 of culture with 0, 2.5, and 5 g/L sodium lactate in StemMACS medium. Results are shown as mean±SD. 51

Figure 5-1. Spinner flask culture: A) Flow cytometry analysis of $SOX17^+/FOXA2^+$ cells at DE. Results are shown as mean±SD. B) Representative density plot. C) Representative images of aggregate at DE. Scale Bars: 200 and 500 µm. 58

Figure 5-2. Relative expression of pluripotency and DE markers compared to control without differentiation factors. 58

Figure 5-3. SSB culture A) Flow cytometry analysis of $SOX17^+/FOXA2^+$ cells at DE. Results are shown as mean±SD. B) Representative density plot. C) Representative images of aggregate at DE. Scale Bars: 200 and 500 µm. 59

Figure 5-4. Comparison between well, SSB, and spinner flask culture. A) Flow cytometry analysis of $SOX17^+/FOXA2^+$ cells at DE. B) Aggregate size analysis. C) Relative expression of pluripotent and DE markers compared to control without differentiation factors. Results are shown as mean±SD. *p≤ 0.05, **p ≤ 0.01, ****p ≤ 0.0001. 59

Figure 5-5. Representative images of aggregates on day 5 of culture with cysts/cavities. Scale Bars: 200 µm (left) and 100 µm (right). 60

Figure 5-6. Spinner flask culture. A) Aggregate size analysis. Results are shown as mean±SD. B) Representative images of aggregates over the length of culture. Scale Bars: 200 µm. 61

Figure 5-7. Spinner flask culture, 25 days (D25) A) Flow cytometry analysis of pancreatic markers. B) Flow cytometry analysis of pancreatic markers at one and two (2X) million cells/mL density. C) Relative expression of pancreatic compared to control without differentiation factors for well culture day 12 (D12) and spinner flask culture day 15 (D15). Results are shown as mean±SD..... 61

Figure 5-8. SSB culture. A) Aggregate size analysis. Results are shown as mean±SD. B) Representative images of GFP expression by aggregates toward the end of culture. Scale Bars: 500 µm, Inset bar: 200 µm. 62

Figure 5-9. SSB culture. A) Flow cytometry analysis of pancreatic markers day 19-38. B) Relative expression of pancreatic markers day 19-24 for well and day 27-38 for SSB compared to expression at well (planar) cultures day 16 (D16). Results are shown as mean±SD..... 63

Figure 5-10. IMR90 and H9 DE differentiation in SSB A) Live cell concentration (cells/mL) and viability (%). B) Flow cytometry analysis for DE markers ($SOX17^+/FOXA2^+$) and pluripotency marker ($NANOG^+/OCT4^+$) expression. **p ≤ 0.01. Results are shown as mean±SD. C) Representative images of aggregates at the last day of culture (Day 10). Scale Bars: 200 µm and 500 µm. 64

Figure 5-11. A) Flow cytometry analysis of hPSCs in the bioreactor compared to the well after expansion and xfAW differentiation. *p≤ 0.05 and **p ≤ 0.01. B) Flow cytometry analysis of cells

expanded in the bioreactor and differentiated in 6-well plates (well after bioreactor expansion: WABE) compared to expansion and differentiation in the bioreactor. **$p \leq 0.01$. (C) Aggregate size analysis for bioreactor and WABE H9 cell aggregates at 240 h. (D) Pluripotency marker expression after expansion (and before priming/differentiation) as determined by flow cytometry for the well and bioreactor. *** $p \leq 0.001$. All results are shown as mean±SD..... 65

Figure 5-12. Flow cytometry analysis of H9 cells at the final day of DE differentiation treated with the same basal media but no activin A and CHIR. Results are shown as mean±SD..... 65

1 Background

Approximately 9% of the worldwide population suffers from diabetes. Diabetes is characterized by hyperglycemia due to autoimmune destruction of insulin-producing β-cells (type 1 diabetes; T1D) or insulin resistance exacerbated by exhaustion and depletion of β-cells (type 2 diabetes; T2D) (Figure 1-1) (Jacobson & Tzanakakis, 2017). All patients with T1D and some with T2D (~30%) require exogenous insulin administration, but this typically results in suboptimal glucose control. Whole pancreas or pancreatic islet transplantation has the potential to restore normoglycemia, but this is limited by the shortage of donor tissue and the requirement for immunosuppression to prevent rejection of the transplanted tissue (Jacobson & Tzanakakis, 2018). Following islet transplantation, insulin independence has been achieved for up to 5 years (Jin & Kim, 2017), suggesting that interventions using insulin-producing cells are a viable approach for *in vivo* control of blood glucose for diabetes. However, the severe shortage of islets available for transplantation indicates the need for a renewable source of functional β-cells. Human pluripotent stem cells (hPSCs), including embryonic (hESCs) and induced pluripotent cells (hiPSCs), can serve as a starting material for diabetes β-cell replacement therapy given their capacity for extensive expansion and potential to be differentiated to pancreatic cells.

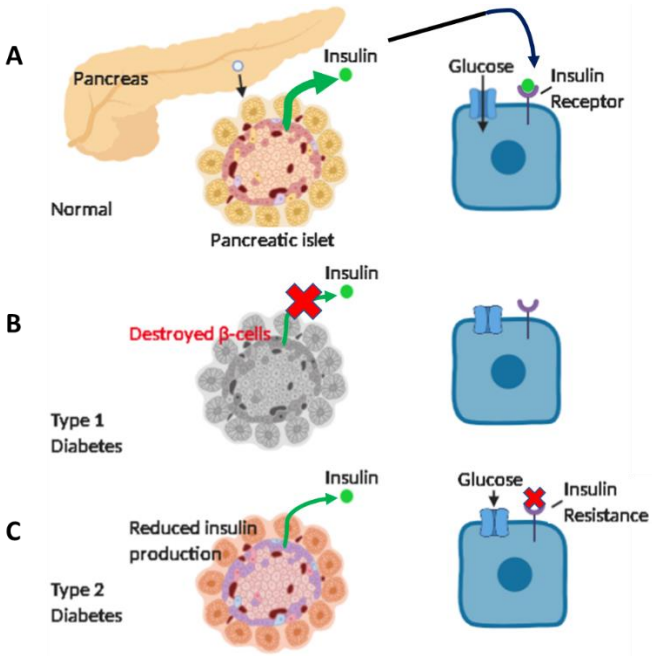

Figure 1-1. Schematic of diabetes pathologies: A) Normal, B) Type 1 Diabetes (T1D), C) Type 2 Diabetes (T2D). Created in Biorender.

1.1 Pancreatic Development

Over the past decade, significant progress has been made in coaxing hPSCs towards pancreatic β-cells similar to native islet cells. Nevertheless, the generation of fully functional insulin-producing cells resembling mature adult β-cells remains a challenge. Generally, differentiation protocols mimic embryonic development and pancreatic organogenesis. There are reviews on pancreas development informed principally by studies on animal models (Edlund, 2002; G. Nair & Hebrok, 2015), while those on human embryonic pancreatic tissue (Jennings, Berry, Strutt, Gerrard, & Hanley, 2015) are limited. Here a simplified description of the formation of pancreas in *vivo* is provided and major instructive cell signals for differentiation are highlighted.

Definitive endoderm (DE) and mesoderm develop from the epiblast during gastrulation (Figure 1-2, Part A) (Jacobson & Tzanakakis, 2017). The DE then folds into the primitive gut tube, which is segmented into foregut, midgut, and hindgut in an anterior-posterior orientation and

surrounded by mesenchyme and the notochord. The foregut is the source of cells for the respiratory system and digestive tract, for example the lung, esophagus, thyroid, stomach, liver, and pancreas, whereas the midgut and hindgut become the small intestine and colon. Signals, such as fibroblast growth factor 4 (FGF4) and retinoic acid (RA), mediate the commitment of foregut endoderm to pancreatic anlage (Martin et al., 2005; Wells & Melton, 2000). Then two distinct areas arise, the ventral and dorsal anlagen, which later fuse. The notochord secretes activin and FGF2, which suppress sonic hedgehog (Shh) signaling in the patterning of the pancreatic endoderm (Figure 1-2, Part B). This was shown in chick embryos and led to the appearance of PDX1 positive (pancreatic and duodenal homeobox 1, $PDX1^{+}$) epithelium (Hebrok, Kim, & Melton, 1998; Hebrok, Kim, St-Jacques, McMahon, & Melton, 2000), whose expansion is mediated by mesenchymal factors. In addition, epidermal growth factor (EGF) stimulates the proliferation of early pancreatic progenitor cells but inhibits endocrine differentiation. Similarly, FGF ligands targeting the FGF receptor 2B (FGF1, FGF7 and FGF10) most likely act as mitogens of progenitor cells in the developing pancreas, which is consistent with the role of FGF10 in mice (Ye, Duvillie, & Scharfmann, 2005). WNT signaling also appears to promote the proliferation of human pancreatic progenitors (Figure 1-2, Part B) (Bonfanti et al., 2015; Cebola et al., 2015) analogous to its role in mice (Rodriguez-Seguel et al., 2013). Less understood are the roles of Notch, RA, and bone morphogenetic protein (BMP) signaling in human pancreas development (Figure 1-2, Part C). Specifically, experiments in mice have shown Notch signaling is activated by FGF10 and Notch effects the expansion of undifferentiated pancreatic progenitor cells expressing *Pdx1* and *Nkx6–1* (Miralles, Lamotte, Couton, & Joshi, 2006). These cells give rise to the endocrine and exocrine sections of the pancreas; here we will focus on the endocrine.

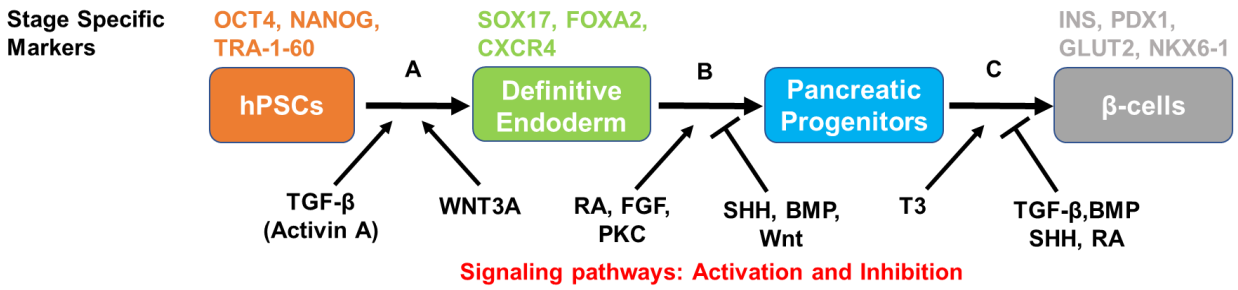

Figure 1-2. Schematic of pancreas development with stage specific markers and the signaling pathways that were activated (↑) or inhibited (⊤).

Expression of Neurogenin 3 (NGN3, a transcription factor) increases along with the appearance of human fetal β-cells (Jennings et al., 2013), peaks near the end of the first trimester and disappears after week 35 in human fetuses (Salisbury et al., 2014). Other transcription factors, such as PDX1, NKX6–1, PAX6, NEUROD1, and NKX2–2, are expressed by endocrine cells starting at 8 weeks (Figure 1-2, Pancreatic progenitors) (Jennings et al., 2015). Then epithelial progenitor cells migrate into the mesenchyme and form islets consisting of alpha (α), β, delta (δ), pancreatic polypeptide (PP), and epsilon (ε) cells, which produce glucagon (GCG), insulin (INS), somatostatin (SST), PP, and ghrelin (GHRL), respectively (Jacobson & Tzanakakis, 2017). For the β-cell insulin synthesis pathway, preproinsulin, which contains the C-peptide in its sequence, is translocated into the endoplasmic reticulum (ER) where a signal sequence is cleaved-off creating proinsulin (Figure 1-3). Then proinsulin is packaged into vesicles in the Golgi apparatus where C-peptide is removed, producing the insulin molecule. For this reason, C-peptide is often measured since it is equimolar to endogenously synthesized insulin. The capacity of β-cells for insulin secretion can be tested using secretagogues, some examples of which are listed in Table 1 and a schematic of the signaling involved in insulin release (Figure 1-4) (McCluskey et al., 2011).

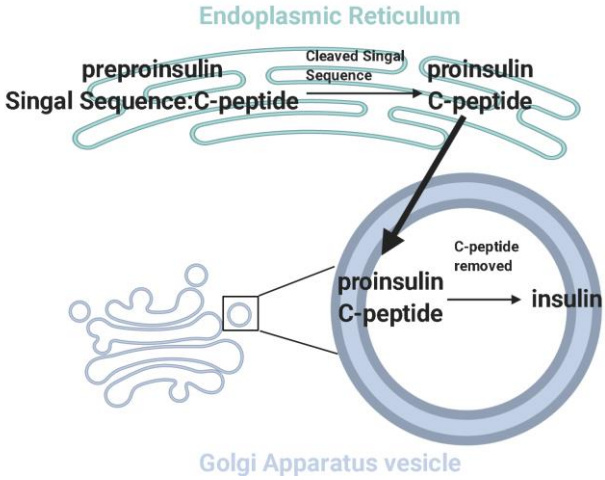

Figure 1-3. Schematic of the preproinsulin to insulin processing. Created in Biorender.

Human PSC-derived β-cells are compared to human primary β-cells to determine their functionality. Several assays are used, including quantitative polymerase chain reaction (qPCR), enzyme-linked immunosorbent assay (ELISA), immunostaining, electron microscopy, analysis of metabolic function, radioimmunoassay, flow cytometry, and karyotyping. qPCR evaluates gene expression and surveys genes such as *MAFA* (transcription factor that activates insulin gene expression), prohormone convertase 1/3 and 2 (*PC1/3* and *PC2*, which process proinsulin), Glucose transporter 1 or 2 (*GLUT-1* or *GLUT-2*, cell glucose uptake), glucokinase (regulates carbohydrate metabolism), K_{ATP} channel complex (sulfonylurea receptor (*Sur1*) and potassium channel (*Kir6.2*), necessary for insulin secretion), L-type Ca^{2+} channel (*Cav1.1*, *Cav1.2*, *Cav1.3, and Cav1.4*, regulates insulin release), and genes necessary for pancreatic cell differentiation (including *PDX1, NKX6-1, NKX2.2, Ngn3, PAX6, MAFB,* and *NEUROD1*). ELISA is performed to analyze insulin levels in cell culture medium or serum, which would indicate that the cells are secreting insulin. Immunostaining allows identification of cells positive for C-peptide, proinsulin, insulin, and protein expression of genes examined by qPCR (see above), and negative for GCG, SST, GHRL, and PP. Electron microscopy is used to examine insulin secretory granules with the

mature insulin granules having a dark center (crystallized insulin) encompassed by a pale halo. Cell glucose uptake is investigated by measuring uptake of a non-metabolizable radioactive analogue of glucose (3-O-methyl-d-[1-^{3}H]glucose) and glucokinase activity is evaluated by determining the rate that one mole of glucose 6-phosphate is formed from glucose and ATP per minute at 37°C. D-glucose labeled with tritium (D-[5-^{3}H(N)]) is used for measuring oxidative glucose metabolism (McCluskey et al., 2011). Ultimately, the functionality of hPSC-derived β-cells is determined by their ability to reverse experimental diabetes in rodents, caused by streptozotocin (STZ), which destroys rodent β-cells, and have glucose-stimulated insulin secretion (GSIS) like depicted in Figure 1-4, so that the cells can be implanted as a treatment for diabetes.

Role	Reagent
Membrane depolarization	Potassium chloride (KCl), leucine, α-ketoisocaproate (KIC), arginine, and cholecystokinin-8 (CCK-8)
Opens K_{ATP} channels	Tolbutamide and glibenclamide (sulfonylureas), diazoxide
Increases the production of cyclic adenosine monophosphate (cAMP) and levels of cytosolic calcium (Ca^{2+})	Glucose-dependent insulinotropic hormone (GIP), glucagon-like peptide-1 (GLP-1)
Increases Ca^{2+} uptake	Alanine
Blocks voltage-dependent Ca^{2+} channels	Verapamil, diltiazem
Activators of protein kinase and adenylate cyclase, which help turn ATP to cAMP	3-isobutyl-1-methylxanthine (IBMX), forskolin, phorbol ester phorbol 12-myristate 13-acetate (PMA)

Table 1. Secretagogues for β-cell insulin secretion machinery.

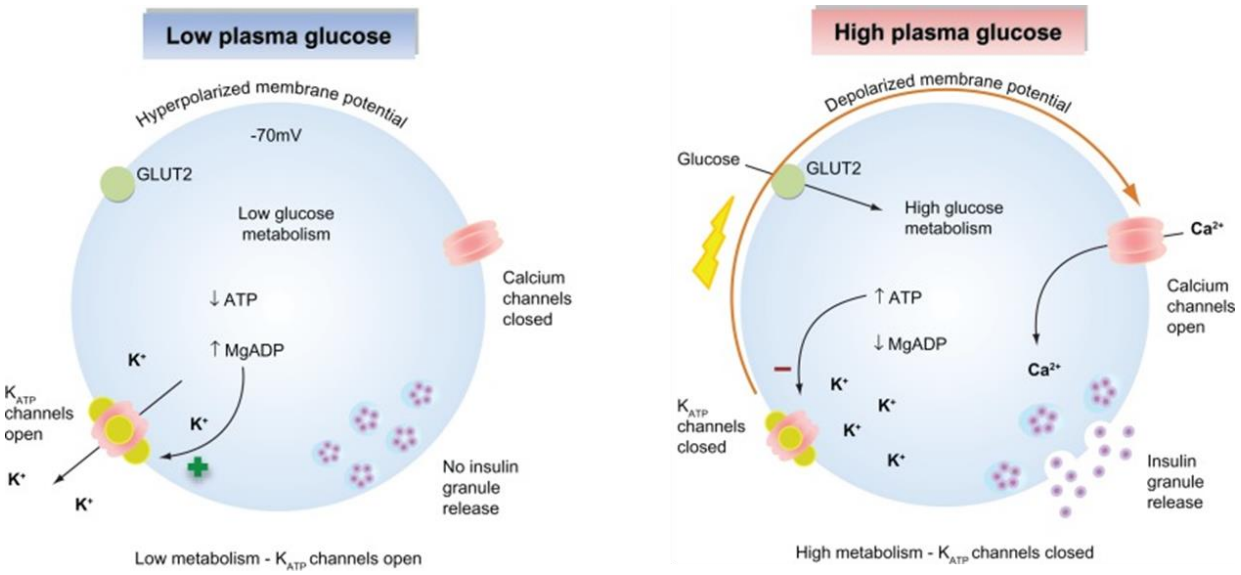

Figure 1-4. Schematic of β-cell insulin release (Lang & Light, 2010).

Overall, most of what we know about pancreatic development comes from animal studies, but there are significant differences between animal and human pancreatic development (Balboa & Otonkoski, 2015; G. Nair & Hebrok, 2015; Wilson, Scheel, & German, 2003). Some of the differences include islet function and architecture and for mice, delayed emergence of crucial differentiation markers in islet development. Specifically for the cytoarchitecture, in mice α- and δ- cells surround β-cells, while in humans β- and α-cells are distributed throughout the islet, in mice the islet is 80% beta cells and 60% in humans, and mice extracellular matrix composition is laminins 411 and 511 and only 511/521 in humans. In development, the timing of the expression of PDX1, GATA4, NKX2.2, and NGN3 is different in mice and humans. Furthermore, mice have synchronized oscillation in response to glucose, whereas humans do not, and mice have higher respiration uncoupling (Balboa & Otonkoski, 2015). Thus, better understanding of human pancreas formation *in vivo* will be essential for developing efficient methods of *in vitro* pancreatogenic differentiation of hPSCs to functional islet cells. hPSC pancreatic differentiation has focused on producing insulin-expressing β-like cells. However other endocrine cell types,

especially α-cells, are important because they work with β-cells to maintain blood glucose homeostasis. Nevertheless, achieving GSIS for β-cells derived *in vitro* should be attained first before emphasis is put on other endocrine cell types.

1.2 hPSC differentiation toward pancreatic β-cells

Pancreatogenic differentiation was first performed with mouse embryonic stem cells (mESCs) using factors such as serum, dimethyl sulfoxide (DMSO), and nicotinamide (Jacobson & Tzanakakis, 2017). These methods were also applied to hESCs (Xu et al., 2006), but the differentiation efficiency was low possibly due to the manifold effects of the factors. This led to the exploration of methods mimicking pancreas development. D'Amour et al. (D'Amour et al., 2006) differentiated hESCs to cells expressing markers of DE, primitive gut tube, posterior foregut, pancreatic endoderm, endocrine precursors, and then hormone-expressing endocrine cells using a 5-step process (Table 4). Although an average of 7% of resulting cells expressed insulin, most of the cells were multihormonal expressing INS, GCG, and/or SST at day 16 of differentiation as assessed by flow cytometry. Pancreatic cells are normally monohormonal as mentioned above with INS, GCG, and SST being exclusive to β-, α-, and δ-cells, respectively. Differentiated hPSCs had a substantially higher levels of proinsulin but an average C-peptide expression of 64% vs 97% for primary adult human islets. A two- to six-fold increase in C-peptide was seen in response to KCl. INS^+ cells had 14 to 208 pmol insulin/μg DNA, which is comparable to 58–310 pmol insulin/μg DNA for primary adult human islet. In addition, the cells appeared to have functional ATP-sensitive potassium (K_{ATP}) channels because tolbutamide treatment resulted in a 3- to 7-fold increase in C-peptide release. Furthermore, the cells had secretory granules, some of which had clear halos surrounding dense cores, a feature typical of human β-cells (D'Amour et

al., 2006). Although this protocol was a huge step forward, glucose induced C-peptide release was minimal, cell proinsulin content was too high, many of the cells were polyhormonal, and the overall differentiation efficiency was low (~7%). These problems suggest issues with glucose sensing, processing, and insulin secretion machinery of the cells. The characteristic of the cells responding to tolbutamide, but not to glucose is typical of the fetal pancreas (Jeon, Correa-Medina, Ricordi, Edlund, & Diez, 2009; Riedel et al., 2012; Rorsman et al., 1989). Whether these multihormonal cells can become monohormonal is unclear. However, direct lineage tracing demonstrated that mature murine α- and β-cells result from independent lineages that never co-express INS and GCG (Herrera, Nepote, & Delacour, 2002).

In a subsequent study the hPSC-derived pancreatic progenitor cells were implanted into mice. The cells underwent maturation *in vivo* and low serum levels of human C-peptide were observed in response to glucose thirty days and three months post-implantation (Kroon et al., 2008). Also, the matured hESC-derived cells had monohormonal expression of INS, GCG, SST, PP, and GHRL, expression of the transcription factor MAFA, and co-localization of a proinsulin enzyme in INS^+ cells. In addition, they were able to rescue mice from diabetes induced by STZ. However only two cell lines (CyT49 and CyT203 hESCs) were used for this study with varying committed progeny, suggesting that differentiation of each cell line would require optimization.

Similar to the above study, Rezania et al. differentiated cells to pancreatic endoderm progeny expressing PDX1/NKX6–1 in a planar culture and then seeded as clusters for air-liquid interface (ALI) cultivation (Table 4) (Rezania et al., 2014). Cells in ALI cultures exhibited upregulation of *NGN3*, *INS*, and *GCG* transcripts with ~50% being INS^+ and most cells co-expressed PDX1, NKX6–1, and MAFA. These cells had delayed, gradual, and low insulin release when subjected to perifusion, in comparison to human islets, and only a third of the cells responded

to a GLP-1 analog or KCl. This suggests the presence of functioning voltage-gated Ca^{2+} channels, but the cells had slow Ca^{2+} kinetics indicating defects in glucose sensing/metabolism, insulin secretion machinery, and/or the functionality of K_{ATP} channels. Problems in insulin secretion may be related to an insufficient quantity of easily releasable membrane docked insulin vesicles or defective vesicle trafficking and exocytosis. The amount of membrane-docked insulin vesicles can be quantified by imaging, while experiments with K_{ATP} channels blockers (e.g. tolbutamide) can be performed to address whether K_{ATP} channels are functional. Nevertheless, ALI culture is not scalable and cells expressed significantly lower MAFA in comparison to human islet cells. In addition, both aforementioned studies produce multihormonal C-peptide$^+$ cells that are lacking NKX6–1 expression. This could result from differentiation of PDX1$^+$ cells which do not express NKX6–1. This may be avoided by removing BMP inhibitors (e.g. Noggin) during *in vitro* differentiation (Jacobson & Tzanakakis, 2017). For example, highly efficient generation of PDX1$^+$/NKX6–1$^+$ cells and further differentiation to 23% C-peptide$^+$ cells were demonstrated, but the inclusion of Noggin led to C-peptide$^+$/GCG$^+$ endocrine cells. In addition, transplantation of PDX1$^+$/NKX6-1$^+$ cells into diabetic mice resulted in significant reduction of blood glucose levels.

In another report, cells were generated with GSIS by mimicking pancreas development to NKX6–1$^+$/PDX1$^+$ and then implanting the cells into mice (Kroon et al., 2008). Cells were coaxed by employing previously published protocols and implanted in mice, resulting in functional β-cells and polyhormonal cells which reached maximal insulin secretion after 3–4 months. This success prompted research into increasing the efficiency of hPSC *in vitro* differentiation to NKX6–1$^{+/}$PDX1$^+$ cells by adding different components such as betacellulin, triiodothyronine, γ-Secretase Inhibitor XXI (XXI), a transforming growth factor-β (TGF-β) type I receptor kinase (ALK5) inhibitor, and N-acetyl cysteine (Rezania et al., 2014). The NKX6–1$^+$/PDX1$^+$ cells were then

differentiated to β-cell-like cells (SC-β-cells) in two to three weeks with ~33% NKX6–1^{+}/C-peptide^{+}. SC-β-cells released insulin with a comparable stimulation index (ratio of insulin secretion at 20 to 2 mM glucose) to that of primary human adult islets, i.e. 2.2 ± 0.3 vs. 2.1 ± 0.9, respectively, after 2–3 successive glucose challenges. SC-β-cells secreted 1.6 ± 0.2 μIU/10^3 cells insulin in response to 20 mM glucose (vs. 3.6 ± 0.7 human islets) and their total insulin content was 240 ± 50 μIU vs. 200 ± 40 μIU/10^3 cells compared to that of human adult islets. Only a small percent of the C-peptide^{+} cells co-expressed GCG (7.7 ± 0.7%) and SST (4.7 ± 0.1%) and human insulin was detected in mice two weeks post-implantation. This is a significantly shorter time frame than 40 days (Rezania et al., 2014) and 30 days (Kroon et al., 2008) for previous studies. Furthermore, *in vivo* matured SC-β-cells restored normoglycemia for longer than four months in mice. Another advancement of this protocol was the differentiation of hPSC aggregates in 500-mL spinner flasks (Table 4) (Pagliuca et al., 2014). Although the yield of differentiated cells compared to the initial cell number was not reported and differentiation was not xenofree, this work demonstrated the feasibility of scalable production of β-cells.

A further advancement to the field was a study by Nair et al. reporting ~55% C-peptide^{+} cells in 20 days in planar aggregate culture with a hESC cell line with a GFP sequence inserted in the INS locus (Table 4). GFP^{+} cells (also INS^{+}) were sorted and reaggregated for further maturation after which ~85% of the cells co-expressed C-peptide and NKX6-1. Perifusion analysis showed similar C-peptide release for derived cells and human islets, although calcium signaling was blunted in comparison to human islets. One of the most important discoveries in this work is that the mitochondrial cristae were denser and more tightly folded in derived cells, which was similar to human islets. This finding is believed to account for the greater maturity of the cells.

Furthermore, after transplantation in mice, human insulin was detected in serum after 3 days, which is earlier than observed in other protocols (G. G. Nair et al., 2019).

Despite recent advances in the hPSC differentiation to insulin-producing, several challenges remain to derive insulin-producing cells from hPSCs comparable to native β-cells. Cell line variability indicates a need for protocol optimization specific to the hESC or hiPSC line used and *in vivo* maturation is still necessary to achieve GSIS. However, the factors that promote the *in vivo* maturation are unknown. In addition, the current differentiation protocols rely on xenogenic components limiting their use for therapy-grade β-cells.

1.3 Xenofree differentiation to Definitive Endoderm

As mentioned above, the first stage of differentiation to pancreatic cells is the definitive endoderm (DE). Xenofree differentiation protocols are important for bioprocesses that are compliant with good manufacturing practices (GMP). As a result, two studies have been published recently for the xenofree DE differentiation of hPSC in static cultures (Diekmann et al., 2019) and SSBs (Sahabian et al., 2019) (Table 6). Diekmann et al. did not utilize stirring, leading to oversized clusters (some ~500 μm) (Diekmann et al., 2019), exhibiting diffusion limitations. Moreover, the proposed system is not scalable, limiting its use for producing therapeutically relevant quantities of cells. Sahabian et al. used a commercially available kit and a custom differentiation medium, which includes xenogeneic Knockout Serum (Sahabian et al., 2019). Use of a commercially available kit limits the flexibility of optimization for different hPSC lines, increases the overall cost of production, and hampers process scale-up or scale-out. The need to adapt differentiation protocols for each cell line has been documented due to the variation in the signaling activity of canonical Wnt and TGF-β pathways, which drive DE commitment, seen in different cell lines

(Blauwkamp, Nigam, Ardehali, Weissman, & Nusse, 2012; Kattman et al., 2011; Ramos-Mejia et al., 2010). In addition, pH and dissolved oxygen (DO) were monitored in the study but were not controlled (Sahabian et al., 2019); such regulation may result in potential gains in differentiation efficiency.

1.4 Scalability of hPSC culture

In addition to the need for a better understanding of *in vivo* pancreatic development and xenofree differentiation, the development of scalable bioprocesses for clinical grade β-cells for diabetes therapies is essential. It is estimated that a dose of ~10^9 β-cells is necessary for diabetes treatment per patient (Lock & Tzanakakis, 2007). Cells may be produced in a scale-out manner as multiple small batches with each batch corresponding to a different patient (patient-specific) with starting cells derived from an individual's hiPSCs. Alternatively, production in a scaled-up platform will be for a large batch of pancreatic islet cells for delivery to multiple patients with human leukocyte antigens (HLA) matching, immunosuppression, or after cell encapsulation.

Nonetheless, monolayer methods are not easily scalable, so 3D cultivation systems are attractive. Differentiation to β-like cells has been demonstrated in spinner flasks (Pagliuca et al., 2014), but this system lacks online monitoring and feedback control of culture conditions. On the other hand, automated stirred suspension bioreactors (SSBs), which are the workhorse of the biopharmaceutical industry, allow the continuous monitoring and control of critical parameters such as pH, DO, concentration of nutrients and metabolites, and feeding. This can ensure the reproducibility and control of the expansion and directed differentiation. However, the dynamic bioreactor milieu is markedly different from the environment in static cultures and its effect(s) on the pancreatic specification of hPSCs has yet to be determined.

1.5 Expansion of pluripotent stem cells

1.5.1 Stem cell culture media and coatings

Specific factors are necessary for maintaining hPSC pluripotency. In addition, hPSCs were originally cultured on mouse embryonic feeders, which provided signals necessary for the maintenance of pluripotency. However, as people moved away from feeders the composition of the medium needed to change to supply the nutrients that the feeder would help supply otherwise. As a result, there are several media available for pluripotent, feeder-free stem cell culture some that are made commercially with proprietary compositions, while other media have defined composition (Table 7). Most pluripotency media are now chemically defined, but some contain components, such as non-recombinant serum albumin (e.g. mTeSR1^{TM}), which are derived from animals. The use of non-xenofree components limit these media's clinical use. The use of a small number of defined medium components, for example essential 8 (E8) has only eight ingredients, reduces lot-to-lot variability and allows for medium customization based on cell line and culture use. Consequently, a smaller number of defined components is preferable, but the exact compounds and their concentrations in various hPSC culture media remain proprietary, hindering efforts for cell line and system culture standardization and optimization. Newer xenofree commercially available pluripotency media include heat stable recombinant human basic FGF (FGF2), since normal FGF2 is only stable for 24 h at 37ºC (G. Chen, Gulbranson, Yu, Hou, & Thomson, 2012), and better buffering capacity, so that medium only needs to be changed every two days instead of every day. This advancement reduces the volume of medium used which lowers the overall cost of culture but also increases the build-up of metabolic by-products.

The feeder-free alternatives for culture surface coatings include Matrigel (mouse sarcoma extract with undefined composition) and xenofree recombinant human laminin-511/521 or human

vitronectin. On the other hand, human collagen can be used in aggregate culture to encourage aggregate formation.

1.5.2 Feeding strategies

Several feeding strategies exist for SSB cultivation of cells. These include batch, perfusion, and fed batch. Most studies on hPSC cultivation in bioreactors use batch mode operation (Table 8), where medium is replaced through partial or whole exchanges of spent medium. While batch feeding is straightforward, the cells can experience significant fluctuations in pH/DO (if they are not controlled by the SSB), osmolarity, concentration of metabolites (e.g. glucose, glutamine, lactate, glutamate), and growth factors after medium change. Control of pH and DO mitigate some of these changes but overall, the effect of these fluctuations is unknown. Fed-batch is another feeding strategy, where fresh medium, sometimes concentrated medium, enters the SSB continuously or intermittently. However, since medium is not changed there is an accumulation of metabolic by-products which can inhibit the growth rate of hPSCs and potentially lead to aberrant differentiation.

Perfusion processes have also been used, which is the continuous exchange of medium in the bioreactor. The benefits of this method are that there is no accumulation of cellular byproducts and the cells are exposed to limited fluctuations in pH, nutrients, factors, and DO. A cell retention system (e.g. filter, settling cone) is necessary to minimize cell loss although clogging of the retention device may happen. Kropp et al. showed that hPSCs perfusion cultivation resulted in higher cell densities (Kropp et al., 2016), suggesting this as a preferred feeding strategy.

1.5.3 Stem cell expansion systems

Differentiation of hPSCs, which is linked to reduced or no proliferation, is typically preceded by expansion. hPSC bioprocesses for the production of therapeutics generally involve two stages: (i) Expansion of hPSCs while preserving their pluripotency; and once a prescribed cell quantity or aggregate size is reached, the cells are subjected to (ii) Differentiation toward a desired cell or tissue type. From a bioprocess economics viewpoint, integration of these two steps is desirable.

There are large-scale adherent, two-dimensional (2D) culture systems (Figure 1-5), including (A) roller bottles, (B) Pall Corporation Xpansion® Multiplate Bioreactor System, (C)Nunc™ Cell Factory™ Systems, (D) Corning® CellSTACK® Chambers, (E) HYPERstack®, and (F) CellCube®, which have been used in the biopharmaceutical industry, but SSBs remain ubiquitous. This is because static culture modalities have several limitations, including difficulties in monitoring and controlling culture parameters (e.g. pH, temperature, DO), being labor intensive and featuring inherently lower surface-to-culture volume ratios compared to SSBs. In addition, concentration gradients are more pronounced in 2D cultures, contributing to significant batch-to-batch variability and adversely affecting cell growth and other specific cell characteristics. hPSCs can be cultured in SSBs as aggregates, after encapsulation (e.g. alginate beads or biomatrices) or adherent on microcarriers. Here we will focus on aggregate expansion and differentiation because of its scalability and ease of culture.

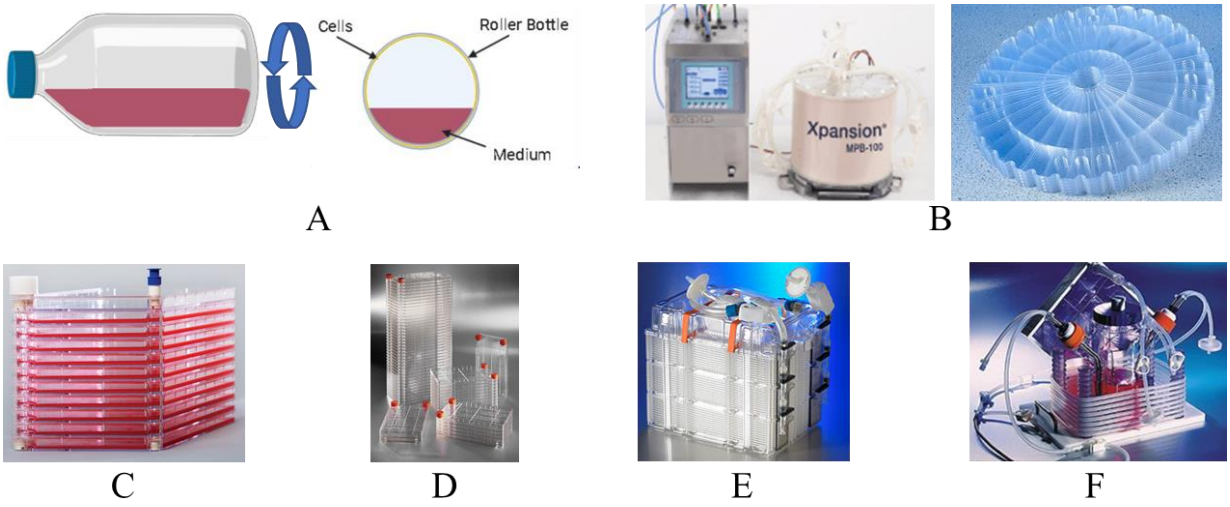

Figure 1-5. Examples of large-scale adherent, two-dimensional (2D) culture systems: A) Roller bottle (created in Biorender), B) Pall Corporation Xpansion® Multiplate Bioreactor System, C) Nunc™ Cell Factory™ Systems, D) Corning® CellSTACK® Chambers, E) HYPERstack, F) CellCube.

Several studies have expanded hPSC as aggregates in SSBs (Table 8) (Elanzew, Sommer, Pusch-Klein, Brustle, & Haupt, 2015; Kropp et al., 2016; Kwok et al., 2017; Olmer et al., 2012; Serra et al., 2010) using A) DASbox Mini, B) Mobius 3L, and C) Biolevitator systems (Figure 1-6). Both hiPSCs and hESC cell lines were utilized with perfusion, batch, or fed batch feeding and the fold increase for seven days was between four and ten with higher fold increase for perfusion systems. pH and DO were not regulated in any of these studies. As a result, both decreased during culture until medium was changed. Example of the fluctuations of pH and DO of two of these systems has been shown (Kropp et al., 2016; Olmer et al., 2012). In our system pH and DO remain relatively constant (Figure 1-7). Control of pH is important because deviations from neutral pH alter stem cell metabolism and proliferation, genomic stability, and potentially the proclivity for lineage commitment (Wilmes et al., 2017; Jacobs et al., 2016). In addition, higher pO_2 levels favor the differentiation of explant pancreatic endoderm progenitors (Heinis et al.,

2010) and hiPSCs to islet cells (Hakim et al., 2014). Hence, the monitoring and regulation of the cultivation milieu, as realized in automated SSBs, becomes critical for enhancing the performance and robustness of hPSC therapeutics manufacturing.

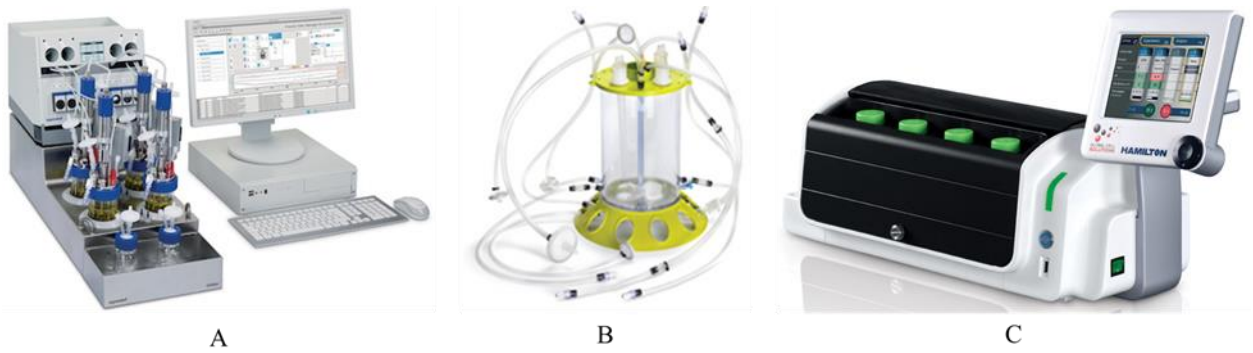

Figure 1-6. Examples of bioreactor system: A) DASbox® Mini, B) Mobius® 3L, C) BioLevitator™.

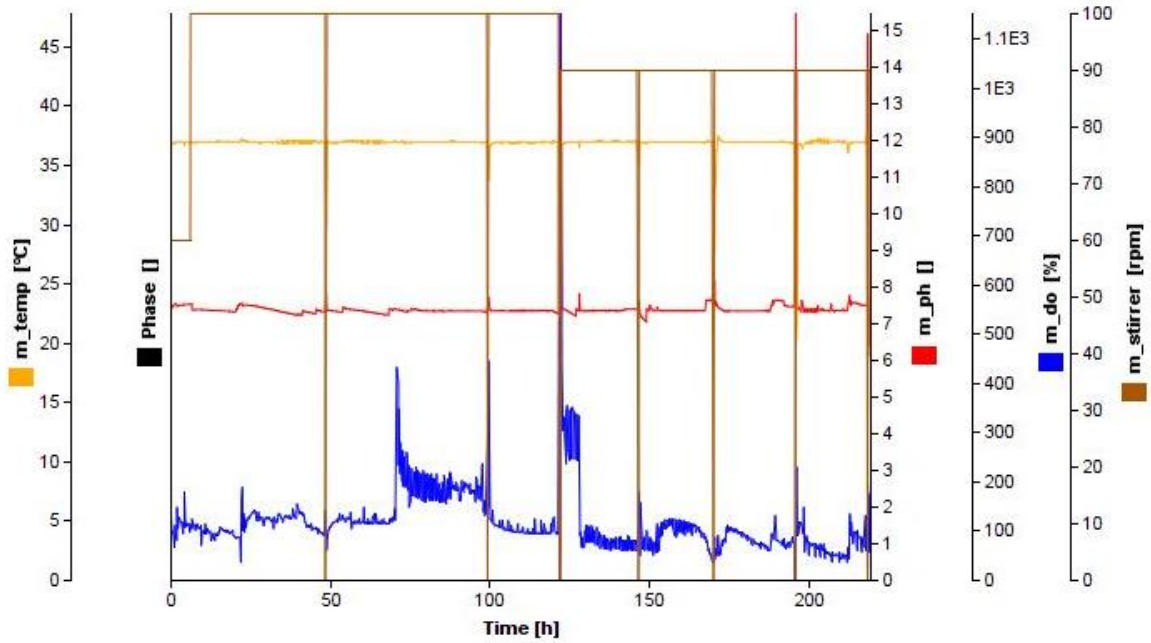

Figure 1-7. Example of control of agitation (m_stirrer), temperature (m_temp), pH (m_ph), and dissolved oxygen (m_do) by our bioreactor my-Control. Decrease to zero stirring rate is during medium changes.

1.6 hPSC metabolism

hPSCs depend on glycolysis for energy, producing pyruvate from glucose. In order for glycolysis to continue, pyruvate can be converted in lactic acid to form nicotinamide adenine dinucleotide $(NAD)^+$ (Figure 1-8) (Varum et al., 2011). In contrast to oxidative phosphorylation (OxPhos), which involves the mitochondrial tricarboxylic acid (TCA, aka Kreb) cycle, glycolysis is characterized by low ATP production efficiency (4 molecules of ATP per glucose molecule). Glycolysis happens in the cytosol, causing an accumulation of lactic acid and reducing intracellular pH (Figure 1-8). Monocarboxylate transporters (MCTs) are a family of H^+-coupled plasma membrane transporters that transfer molecules with one carboxylate group (monocarboxylates, such as lactate and pyruvate), across biological membranes. Lactate is exported out of the cell into the medium by MCT3 and MCT4. On the other hand, MCT1 and MCT2 mediate the uptake of lactate by cells. In comparison, MCT1 and MCT2 have a high affinity (Michaelis Constant, $K_m \approx$ 1–3 mM) for lactate, while MCT3 and MCT4 have a low affinity ($K_m \approx$ 6 mM and $K_m \approx$ 30 mM respectively) (Adijanto & Philp, 2012). Expression of these transports in hPSC could provide insight in to lactate metabolism.

The protein that inhibits the TCA cycle in hPSCs is the mitochondrial uncoupling protein 2 (UCP2), which exists in high levels, leading to the production of lactate from pyruvate as described above. After differentiation, UCP2 levels decrease leading to a reduction in the lactate production and an increase in OxPhos (Shyh-Chang, Zheng, Locasale, & Cantley, 2011). A switch from glycolysis to OxPhos has also been shown in hiPSCs cultured in mini bioreactors with a feeding strategy change from repeated batch feeding to perfusion. Perfusion yielded 47% higher cell numbers compared to batch, indicating the importance of metabolism for biomanufacturing (Kempf et al., 2014; Kropp et al., 2016).

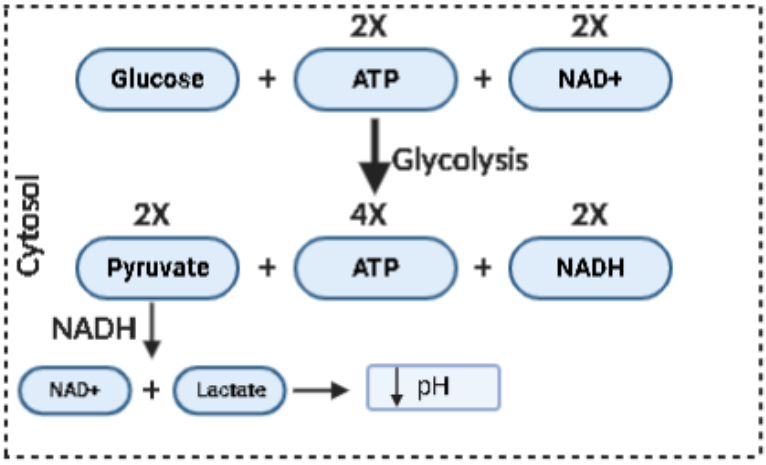

Figure 1-8. Diagram demonstrating glycolysis and lactate production which leads to medium acidification (decrease (↓) pH). Created in Biorender.

1.7 Effects of lactate

Understanding the production of lactate by hPSC is important for biomanufacturing. Lactate and its lowering pH effect have been shown to slow hPSC growth rate and decrease pluripotency (X. Chen et al., 2010; Horiguchi, Urabe, Kimura, & Sakai, 2018; Jacobs et al., 2016; W. Liu et al., 2018; Nath, Nagamori, Horie, & Kino-Oka, 2017; Wilmes et al., 2017). In addition, Silva et al. examined two hESC lines and found higher lactate production to glucose consumption fraction in bioreactor culture compared to 2D (Silva et al., 2015). The function of MCTs as it relates to lactate has only been explored in human peritoneal mesothelial cells. Knockdown of MCT1 (lactate uptake into the cell) partially rescued the decreased cell numbers and increase in cell death and apoptosis cause by high lactate concentrations (40 mM). On the other hand, MCT4 (lactate extrusion) knockdown did not change the effects of lactate (Kuma et al., 2017). Horiguchi et al.(Horiguchi et al., 2018) and Nath et al. (Nath et al., 2017) showed that growth rate decreases with increasing concentration of exogenous lactate in hiPSC monolayers and controlled pH. Also, Chen et al. showed that lactate above 1 g/L had decreased hPSC growth rate and 2 g/L lactate have

25% less cells than 1 g/L and specific growth rate was 0.45 vs 0.2 h^{-1} for 1 vs 5 g/L lactate in static suspension hESC microcarrier culture (X. Chen et al., 2010).

In terms of lactate's effect on expression of pluripotency markers, Nath et al. showed that OCT4 expression did not change, but that TRA-1-60 expression was 50.1 ± 3.0% for 1.0 g/L lactic acid compared to 62.6 ± 6.0% for the control ($p<0.01$) (Nath et al., 2017). Chen et al. also showed an effect on TRA-1-60, serial passages for three weeks in a lactate concentration of 1 g/L or 2 g/L (~9 and 18 mM, respectively) caused a decrease in TRA-1-60 expression from 88% to 75% and 60-66%, respectively (X. Chen et al., 2010). Nonetheless, control of pH was not specified by Chen et al. when the effect of lactate on pluripotency was studied. The differences in these finding could be explained by TRA-1-60 being a surface marker, while OCT4 (POU5F1) is intracellular, TRA-1-60 expression may be more affected by culture environment.

In addition to lactate's effect on growth rate and pluripotency, lactate at 15 mM caused a total DNA damage increase of 88.4% compared to 0 mM in hESCs in 2D culture. They also suggest that the increase of cells in G_1 and the slowing of the S phase are a consequence of higher lactate concentrations that resulted from high density culture. There however was not a loss of pluripotency or an increase in cell death (Jacobs et al., 2016). The change in G_1 and S phase would explain an increase in growth rate that others have seen.

Ideally it would be possible to control lactate production rates, especially because lactate production is higher in hPSCs than other cell types (Varum et al., 2011). This could potentially be done by selecting cells with lower inherent production rates, although this process could not be done for patient-specific hiPSCs. For example, Chen et al. showed that HES-3 hESCs produce less lactate than HES-2 hESCs in 2D and microcarrier culture. In addition, they showed that that using medium with 1-1.5 g/L of glucose instead of 3 g/L had a 10% decrease in lactate levels during 7-

10 days of culture, a pH of 6.7 vs 6.5, and 40% increase in cell density (X. Chen et al., 2010). This suggests that limiting glucose availability can regulate lactate production. In a bioreactor system glucose availability can be automated with glucose being added when pH (due to lactate) decreases. Furthermore, culture of H9 and IMR90 on polyethylene terephthalate (PET) had less lactate production in comparison to tissue culture plastic (Hai, Shin, Bi, Ye, & Jin, 2018).

Currently lactate levels are not monitored online. To better understand the variables that effect lactate production, having a lactate sensor would be beneficial. However, the technology for online sensing lactate concentration needed for biomanufacturing does not yet exist to our knowledge, even though several studies have been published on lactate sensors for sweat (Abrar, Dong, Lee, & Kim, 2016; Lin, Muthukumar, & Prasad, 2020; Payne, Zamarayeva, Pister, Yamamoto, & Arias, 2019; Promphet et al., 2019) or cell culture medium (Hashemzadeh, Omidi, & Rafii-Tabar, 2019) with an acceptable lactate detection range (at least 0-25 mM). These studies suggest that a better understanding of lactate metabolism is needed if we hope to reduce the effects of lactate on hPSC culture.

1.8 Motivation for the present study

There is no reported protocol for a custom xenofree medium for the differentiation of aggregates to DE in non-static culture. A tunable medium would allow cell line optimization, which has been shown to be necessary (1.3). In addition, the use of a controlled SSB for this differentiation has yet to be described. Control of pH and DO is necessary to limit batch-to-batch variability, which provides a more consistent product, a goal that is highly sought after in industry. Also, it mitigates and the negative effects of low DO or pH (1.5.3). Current systems for hPSC SSB expansion have relatively low fold increases and no control of pH or DO (1.5.3). These systems

are scalable, but better rates of expansion would be beneficial for creating the 10^8-10^9 cells needed per patient for cell therapies. However, while growing cells in high density in an SSB, lactate can accumulate, which has been shown to slow growth rate (1.7), an undesirable consequence during expansion. As a result, it would be advantageous to better understand the effects of lactate on hPSC aggregate culture. In addition, despite the large volume of research on differentiating hPSCs to β-like cells (1.2), there are no reports of insulin expressing cells differentiated in an SSB, which would also allow monitoring and control of multiple culture parameters. Furthermore, β-like cells, which were matured *in vitro* and produced detectable insulin in mouse serum in only a few days (1.2), were generated in planar suspension culture, which is not scalable. Overall, there is much improvement to be made on hPSC expansion and differentiation toward β-like cells.

2 Materials and Methods

2.1 Human pluripotent stem cell culture

H9 hESCs and IMR90 clone #4 (IMR90-4; henceforth IMR90) hiPSCs (WiCell, Madison, WI) were maintained as colonies in StemMACS iPS-Brew XF medium (cat. no. 130-104-368, Miltenyi Biotec, Cambridge, MA), E8 Flex medium (cat. no. A2858501, ThermoFisher Scientific, Waltham, MA), or in-house made E8 medium (DMEM/F12 (cat. no. 12500062 Thermo), 64 mg/L L-ascorbic acid 2-phosphate magnesium (cat. no. A8960-5G), 14 µg/L sodium selenium (S5261-10G), 19.4 mg/L insulin (I3536-100MG), 543 mg/L sodium bicarbonate (cat. no. S5761-500G), 10.7 mg/L transferrin (cat. no. T0665-50MG), 15 mM HEPES (cat. no. 54457-10G-F) (all from Millipore-Sigma, Burlington, MA), 100 µg/L FGF2 (cat. no. 100-18B), and 2 µg/L TGF-β1 (cat. no. 100-21C) (both from PeproTech, Rocky Hill, NJ) on dishes coated with Matrigel (cat. no. 354230, Corning, Corning, NY).

For cell seeding, hPSC colonies were harvested after treatment with 10 µM ROCK inhibitor Y-27632 (ROCKi, cat. no. 10005583, Cayman Chemical, Ann Arbor, Michigan) for 1 h then Accumax (cat. no. AM105, Innovative Cell Technologies, Inc., San Diego, CA) for 10 min. The cell number was determined by counting with a hemocytometer after staining with Trypan Blue (cat. no. 25900CI, Corning).

2.2 Definitive endoderm differentiation in multi-well plates

hPSCs were seeded as described above at 10^6 live cells/mL in 5.5 mL day 0 medium (Figure 2-1**,** Section I.a, ‘priming’ D0 medium: DMEM/F12 (cat. no. 12500062), GlutaMAX (cat. no. 35050061), non-essential amino acids (NEAA, 100x, cat. no. 11140050), KnockOut Serum Replacement (KSR, cat. no. 10828028) or CTS KSR XenoFree medium (cat. no. 12618012) (all

from ThermoFisher Scientific, Waltham, MA), sodium bicarbonate (cat. no. S5761) and β-mercaptoethanol (cat. no. ES007E) (both from Millipore-Sigma, Burlington, MA), 10 µM ROCKi, 10 ng/mL recombinant human activin A (cat. no. PHC9561, Thermo) and 10 ng/mL recombinant human heregulin-β1 (cat. no. 100-03, PeproTech, Rocky Hill, NJ) in 6-well suspension plates (cat. no. 657185, Greiner Bio-One, Kremsmünster, Austria) on an orbital shaker set to 100 rpm. Differentiation was carried out as reported by Nair et al. (Nair et al., 2019) with modifications including the use of CHIR99021 trihydrochloride (CHIR; cat. no. 495310, Tocris Bioscience, Bristol, UK) instead of WNT3A, 1% CTS B-27 Supplement XenoFree (cat. no. A1486701, Thermo) for xenofree differentiation (instead of fetal bovine serum), extended treatment with differentiation medium (Table 2 and Table 3), and xenofree insulin-selenium-transferrin (ITS, cat. no. 41400045, Thermo) (Figure 2-1, Section I.b).

Differentiation was also carried out with aggregates formed in the same way as above in D0 priming medium (Figure 2-1, Section I.a) with differentiation medium as described (Zhu et al., 2016). Briefly, MCDB 131 (cat. no. 10372019, Thermo), 1.5 g/L sodium bicarbonate, 1x GlutaMAX, 10 mM glucose (cat. no. G8270, Millipore-Sigma), 0.5% bovine serum albumin (BSA, cat. no. BP1605100, Thermo) for the basal medium and 100 ng/mL Myostatin (GDF8, cat. no. 12000, PeproTech) for all three days and 3 µM CHIR for day 1, 0.3 µM for day 2, and no CHIR for day 3 (Figure 2-1, Section I.b).

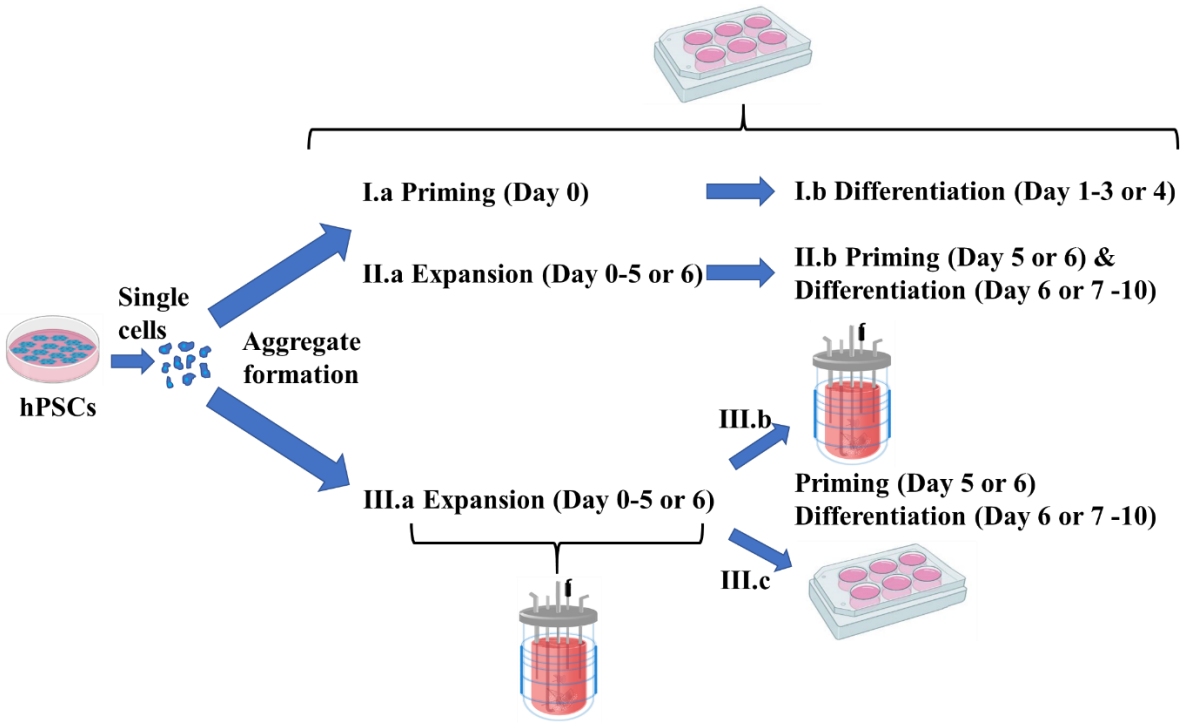

Figure 2-1. Schematic of the experimental strategies for DE differentiation of hPSCs in multi-well plates and an automated bioreactor. I: multi-well differentiation; II: multi-well with expansion and differentiation. III: bioreactor with expansion and differentiation. Some pictures created in Biorender.

AW Protocol					
Priming	**Differentiation** **Basal medium: RPMI + 0.2% FBS + 100 ng/mL Activin A + 1x GlutaMAX**				**SOX17$^+$/FOXA2$^+$ (%±SD)**
DMEM/F12 + 20% KSR†+1x NEAA† +1x βME†+ 1x GlutaMAX+ 10 ng/mL heregulin-β1+ 10 ng/mL activin A	D1-2: 3 µM CHIR 0.02% ITS		D3: 0.3 µM CHIR 0.05% ITS	D4: 0 µM CHIR 0.05% ITS	H9 hESCs	87.5±8.8
	D1: 3 µM CHIR 0.02% ITS	D2: 0.3 µM CHIR 0.05% ITS	D3: 0 µM CHIR 0.05% ITS		IMR90 hiPSCs	80.2±9.2

† KSR: KnockOut Serum Replacement, NEAA: non-essential amino acids, βME : β-mercaptoethanol, ITS: insulin-transferrin-selenium

Table 2. AW protocol for DE differentiation of H9 and IMR90 hPSCs.

xfAW Protocol						
Priming	**Differentiation** **Basal medium: RPMI + 1% xfB27 + 100 ng/mL Activin A + 1x GlutaMAX**					**SOX17⁺/FOXA2⁺ (%±SD)**
DMEM/F12 + 20% xfKSR‡+1x NEAA‡ +1x βME‡+ 1x GlutaMAX+ 10 ng/mL heregulin-β1+ 10 ng/mL activin A	D1-2: 3 µM CHIR 0.02% ITS		D3: 0.3 µM CHIR 0.05% ITS	D4: 0 µM CHIR 0.05% ITS	H9 hESCs	72.5±2.6%
	D1: 3 µM CHIR 0.02% ITS	D2: 0.3 µM CHIR 0.05% ITS	D3: 0 µM CHIR 0.05% ITS		IMR90 hiPSCs	82.5±4.9%

‡ xfKSR: KnockOut Serum Replacement XenoFree, NEAA: non-essential amino acids, βME : β-mercaptoethanol, ITS: insulin-transferrin-selenium

Table 3. xfAW protocol for DE differentiation of H9 and IMR90 hPSCs.

2.3 Bioreactor cultivation

After harvesting as described above and centrifugation, cells were resuspended in 2 mL of StemMACS iPS-Brew XF medium (expansion medium) and 100 µl of animal origin-free coating matrix (cat. no. R011K, Thermo) was added. Then, the suspension was gently mixed with a 5 mL pipet every 2 min for 15 min. The cells were seeded into the bioreactor (Figure 2-1, Section III.a, 250 mL with my-Control biocontroller; Applikon Biotechnology, Delft, Netherlands) at a density of $2x10^5$ cells/mL in expansion medium and 10 µM ROCKi supplemented with 0.2% Pluronic F-68 (cat. no. 24040032, Thermo) and 1x penicillin/streptomycin (P/S, cat. no. 30002CI, Corning). For comparison, multi-well plate cultures were seeded simultaneously at the same density with 5.5 mL medium per well (Figure 2-1**,** Section II.a). All media were supplemented with Pluronic and P/S for expansion and differentiation. For pH control in the bioreactor, 0.5 M HCl and NaOH solutions were used with the pH set to be maintained at 7.4±0.2 for expansion (due to the buffer capability of the expansion medium) and 7.2±0.2 for differentiation. For DO control, oxygen levels were kept constant at the initial value with headspace aeration. The impeller speed was gradually increased from 60 rpm to 100 rpm. The medium was changed every two days, for both the well and bioreactor, until the initiation of differentiation (Figure 2-1, Section II.b and III.b). For bioreactor medium change, agitation was halted and the aggregates were allowed to settle for 2

min before pumping out all but 10 mL medium to retain the aggregates, before adding fresh medium. The culture was sampled through a port and placed in a 24-well plate for imaging before cell counting.

On day 5 or 6 of expansion (Figure 2-1, Section III.b; H9: 5 days and IMR90: 6 days), medium was replaced with D0 medium. Then, medium was replaced daily with differentiation medium as in the well differentiation culture (IMR90: 3 days and H9: 4 days, Table 3), except for the addition of Pluronic and penicillin/streptomycin (P/S). For a well differentiation comparison to the bioreactor, H9 pluripotent aggregates were removed from the bioreactor after expansion and placed in 6-well suspension plates at the same density as the bioreactor in 5.5 mL and priming and differentiation was performed as described above (Figure 2-1, Section III.c; Table 3).

2.4 Cell Seeding for lactate experiments

For monolayer culture H9 cells were seeded at $0.8x10^4$ cells/cm^2 and IMR0 cells at $1.1x10^4$ cells/cm^2 on Matrigel coated 6 cm dishes (Cat No. 628160, Greiner Bio-One, Kremsmünster, Austria) in E8 flex or StemMACS™ with 10 µM ROCK. For aggregate culture, H9 or IMR90 cells were seeded at $0.2x10^6$ cells/mL in 5.5 mL E8 flex or StemMACS™ with 10 µM ROCK in 6-well suspension plates (Cat. No. 657185, Greiner Bio-One) on an orbital shaker set to 100 rpm. After 24 h, the media was replaced with E8 flex or StemMACS™ with either 0, 2.5, or 5 g/L L-Lactic acid sodium salt (Cat. no. AC439220100, ACROS Organics™, Waltham, MA) and pH was adjusted with NaOH with media changes every two days for the remainder of the culture. For aggregates, the medium was changed by aspirating the medium surrounding the circular-shaped aggregate cluster that accumulates in the center of the well.

2.5 INS GFP cell line cultivation

Culture methods are the same as in the paper by Nair et al. (G. G. Nair et al., 2019). Briefly, MELl *INS*$^{GFP/W}$ hESC were obtained from Matthias Hebrok (University of California, San Francisco) and propagated on mouse embryonic fibroblasts as single cells with in-house hESC medium. Cells were passaged and harvested with TrypLE (cat. no. 12563011, Thermo). Before seeding, 100 µl of coating matrix was added as mentioned above. Medium was supplemented with 1X P/S and 0.2% Pluronic for all the days culture. Cells were then seeded in spinner flask at 1x10^6 cells/mL in D0 medium (priming) at 45 rpm, after one day the aggregates were settled and resuspended in medium to a density of 1x10^6 cells/mL (since not all cells form aggregates). Then the aggregates were cultured for 3 days in D0 medium before following the protocol with Nair et al. differentiation protocol (Table 4) for twenty days (G. G. Nair et al., 2019). Medium was changed by letting aggregates settle to the bottom, removal of the spent medium, and replaced with fresh differentiation medium. Aggregates were removed by a pipette, imaged, and counted with a hemocytometer as mentioned. For the bioreactor, cells were seeded at 1x10^6 cells/mL in D0 medium and 60 rpm which was gradually increased to 100 rpm by day 1 at which time differentiation was initiated with the same protocol as Nair et al. (G. G. Nair et al., 2019) except with 3 µM CHIR instead of WNT3A. pH was controlled with the automatic addition of 0.5 M HCl or NaOH. Medium was exchanged by stopping the agitation, letting the aggregates, pumping the spent medium out, and pumping medium in through a sterilizing filter. Aggregates were removed with a sampling port.

2.6 Aggregate size distribution

Images of harvested aggregates were taken with an inverted microscope (Leica DM IL LED, Leica Microsystems, Buffalo Grove, IL) connected to a camera (Leica DFC3000G). Average aggregate size was calculated using ImageJ (NIH, Bethesda, MD) as described (Wu, Rostami, Cadavid Olaya, & Tzanakakis, 2014).

2.7 Flow cytometry

Cells/aggregates were treated with Accumax for 10 min or until aggregates were single cells and dispersed cells were centrifuged at 500xg for 5 min. The pellet was resuspended in phosphate buffered saline (PBS) before fixing the cells with 4% paraformaldehyde (cat. no. A11313, Alfa Aesar, Tewksbury, MA) in PBS for 10 min. After washing with PBS, the cells were resuspended in 1x permeabilization buffer (cat. no. 00833356, Thermo), spun down and suspended in CAS-Block Histochemical Reagent (cat. no. 008120, Thermo), 0.1% Triton X-100 (cat. no. 327371000, Thermo), 10% normal donkey serum (cat. no. 017000121, Jackson ImmunoResearch, West Grove, PA), and 10% BSA. Cells were incubated with antibodies overnight: SOX17 (cat. no. 562205), FOXA2 (cat. no. 561589), PDX-1 (cat. no. 562161), NKX6-1 (cat. no. 563338) (all from BD Biosciences, San Jose, CA), NANOG (cat. no. 130117377), OCT3/4 (OCT4; cat. no. 130-123-257), TRA-1-60 (cat. no. 130-106-872) (all from Miltenyi Biotec). For nuclei staining Hoechst 33342 (cat. no. H3570, Thermo) was used. After which they were washed three times before analysis. Stained samples and corresponding isotype controls were processed on an Attune NxT flow cytometer (Thermo) and the results were analyzed with FCS Express software (v. 6, De Novo Software, Glendale, CA). Cells were designated as positive for a marker if their emitted fluorescence was >98% of the isotype control histogram.

2.8 Immunostaining

Aggregates were fixed with 4% paraformaldehyde in PBS for 30 min. For intracellular markers, aggregates were suspended in the same blocking and permeabilization solution as for flow cytometry, for surface markers the triton was removed. After the aggregates were suspended, antibodies were added at the right dilution. Cells were incubated with antibodies overnight: FOXA2 (cat. no. sc-9187, Santa Cruz, Dallas, TX), SOX17 (cat. no. AF1924, R&D System, Minneapolis, MN), NANOG (cat. no. AF1997, R&D System), and OCT4 (cat. no. sc-5279, Santa Cruz). After three washes with PBS, cells were incubated with a donkey anti-goat/mouse/rabbit secondary antibody conjugated to Alexa 488/647 or rhodamine red (cat. no. 705-545-003, 715-605-150, 711-295-152, Jackson Immunoresearch) for 2 h at room temperature. Nuclear DNA was stained with Hoechst 33342 (cat. no. H1399, Thermo). After incubation, samples were washed with PBS three times. Images were acquired with a Leica TCS SPE confocal microscope (Leica Microsystems Inc.) and quantitative analysis was performed with the Leica LAS X software.

2.9 Quantitative Polymerase Chain Reaction (qPCR)

Cells were suspended in TRIzol (Cat. No. 15596018, Thermo), 1 mL per 10^5-10^7 cells and the RNA was extracted based on the manufacturer's instructions. Reverse transcription (RT) was performed using oligo(dT)18 primers (Cat. No. SO132, Thermo), ImPromII reverse transcriptase (cat. no A3802, Promega, Madison, WI), and Recombinant RNasin ribonuclease inhibitor (Cat. No. N2515, Promega, Madison, WI). Quantitative PCR (qPCR) was performed on a StepOne Plus qPCR thermocycler (Thermo) using PowerUp SYBR Green Master Mix (Cat. No. A25776, Thermo) under the following conditions: denaturation and polymerase activation at 95°C for 10 min; amplification for 40 cycles at 95°C for 15 s and 60°C for 60 s; melt curve at 95°C for 15

s, 60°C for 1 min, and 95°C for 15 s. All reactions were run in triplicates and amplification specificity was verified by the melting curve method and gel electrophoresis of qPCR products. Relative gene expression was calculated by normalizing to the expression of endogenous *β-actin (ACTB)*, using the $\Delta\Delta C_T$ method (Livak & Schmittgen, 2001).

2.10 Lactate measurement

Lactate levels were determined from medium samples using EnzyChrom™ D-Lactate Assay Kit (cat. no. EDLC-100, BioAssay Systems, Hayward, CA). Fluorescence was determined using a microplate reader.

2.11 Statistical Analysis

Data are expressed as mean±standard deviation (SD), unless otherwise stated, from at least triplicates. Analysis of variance (ANOVA) and Dunnett's *post hoc* test were performed using Prism (v. 8, GraphPad Software, La Jolla, CA). Values of $p<0.05$ were considered as significant.

3 Planar Suspension Differentiation of hPSCs to Definitive Endoderm

3.1 Introduction

This chapter contains results from the adaptation of the definitive endoderm (DE) stage differentiation protocol from Nair et al. (G. G. Nair et al., 2019) that used the MELl *INS*$^{GFP/W}$ human embryonic stem cell line (MELl) (Basford et al., 2012) cultured as multilayered single cell seeded on mouse embryonic feeder layer, to a hiPSC (IMR90) and a hESC (H9) line. IMR90 and H9 are cultured as colonies on Matrigel and require ROCKi for seeding, while MEL1 does not. These different culture methods and the genetic engineering of MEL1 cells mean that the IMR90 and H9 require optimization of the protocol for achieving a high efficiency for DE differentiation. After formation of the aggregates in Knockout serum (KSR) and low concentration of activin A and heregulin β1, incubation with activin A and inhibition of glycogen synthase kinase 3 (GSK-3, with CHIR) was utilized for specification to DE. In comparison to the Nair et al. protocol, CHIR was used instead of WNT3A and application was prolonged and the days of differentiation with activin A were extended by one day for IMR90 and two days for H9. CHIR is a small molecule which is more stable than WNT3A and has less lot-to-lot variability. The CHIR regimen used was similar to the DE stage protocol from Zhu et al. (Zhu et al., 2016). The Zhu protocol was initially tried since it worked well in monolayer but not was successful in aggregates due to cluster disintegration and cell death. The protocol developed in our study as described below led to successful differentiation of one hiPSC line (IMR90) and one hESC (H9) to DE (both ~88% SOX17^{+}/FOXA2^{+}, Figure 3-3).

The protocol then needed to be further adapted to be xenofree in line with future clinical applications. KSR and the FBS utilized in our initial protocol are of animal origin, so these were traded for a xenofree version of knockout serum replacement (xfKSR) and xenofree B27 (xfB27).

xfB27 was originally used as a supplement for neuronal cells, but has since been used for xenofree DE differentiation (Diekmann et al., 2019). Once the correct concentrations of xfKSR and xfB27 were found, cells were effectively differentiated to >70% cells expressing DE markers (Figure 3-6). Since DE is the first step toward differentiation hPSC to pancreas, liver, and lungs, having a high-efficiency, xenofree differentiation protocol allowing for cell line-specific tuning is vital for hPSC-based manufacturing of cellular therapeutics.

3.2 Results

3.2.1 Differentiation of hPSCs to DE cells in multi-well plates

IMR90 or hESC cells were initially seeded as single cells in pluripotency medium with ROCKi in suspension plates on the orbital shaker at $1x10^6$ cells/mL. Aggregates spontaneously formed due to the centripetal force. The planar suspension differentiation of hiPSC (IMR90) and hESC (H9) was first attempted with the DE stage of the protocol from Zhu et al. (Table 6) (Zhu et al., 2016), which yielded 87.81±1.17% $FOXA2^+$ and 74.29±2.65% $SOX17^+$ for H9 and 90.78±4.02% $FOXA2^+$ and 89.56±2.85% $SOX17^+$ for IMR90 in monolayer culture. This protocol resulted in cluster disintegration and substantial drop in viability, in line with a previous study (H. Wang, Luo, Yao, Lehman, & Wang, 2015). Extending the length of time that the aggregates were in suspension culture in pluripotency medium from 1-4 days did not fully alleviate the cell death and the aggregate that remained were fragmented. Therefore, cells were seeded in D0 (‘priming’) medium to form aggregates under orbital shaking then differentiated as Nair et al. reported (Table 6, Figure 2-1, Section I.a-b) (G. G. Nair et al., 2019). However, neither hPSC line appreciably expressed DE markers at day 3 or 4 (<1%, data not shown). Next, after seeding with D0 medium,

aggregates were differentiated as above with the Zhu DE stage protocol (Zhu et al., 2016) (Table 6) Figure 2-1, Section I.a-b). Substantial loss of cluster integrity was observed (

Figure **3-1**A, left), despite >80% of IMR90 cells differentiating by day 3 and >65% of H9 cells by day 4 being $SOX17^{+}/FOXA2^{+}$ (one day extension of the protocol for H9,

Figure **3-1**B). Moreover, continued culture in basal medium caused their complete breakdown making further differentiation impossible.

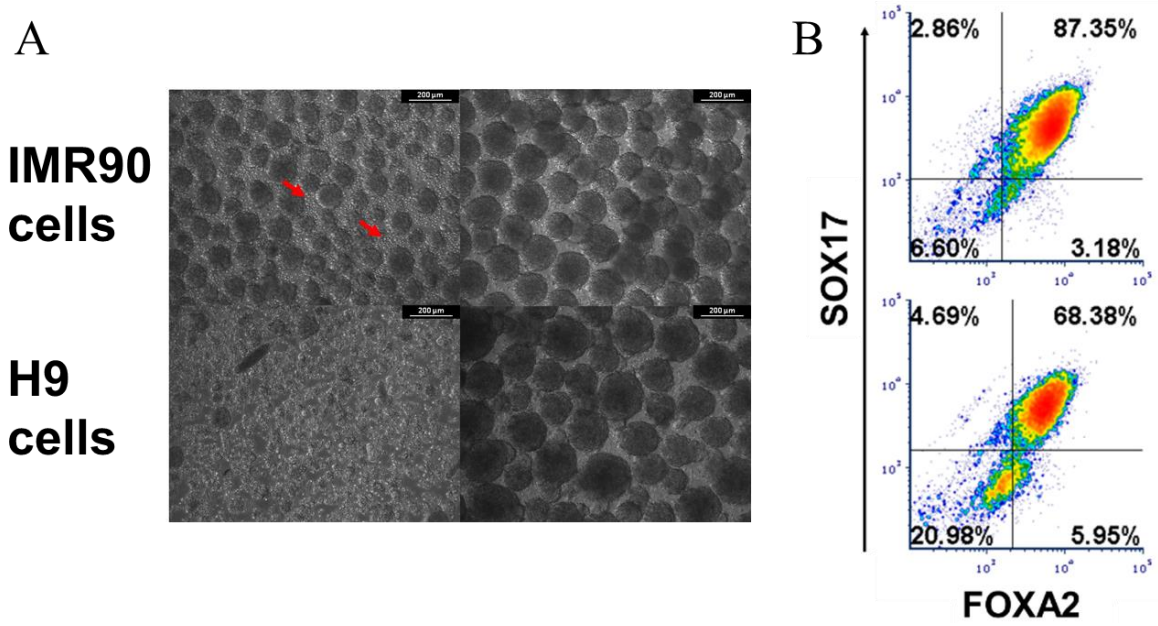

Figure 3-1. A) Micrographs of aggregates differentiated with GDF8/CHIR/BSA (left, (Zhu et al., 2016)) or with AW protocol (right) at the final day of DE differentiation. Arrows indicate lysed cells. Scale bars: 200 μm. B) Representative flow cytometry density plots of $SOX17^{+}/FOXA2^{+}$ cells at the final day of DE differentiation for IMR90 hiPSCs (top) and H9 hESCs (bottom) treated with GDF8 for DE differentiation after priming step.

Consequently, cells were seeded in D0 media followed by 3 days of differentiation with 100 ng/mL activin A and CHIR (day 1: 3 μM, day 2: 0.3 μM) (Figure 2-1**,** Section I.a-b). This protocol is a combination of the basal medium from Nair's protocol (G. G. Nair et al., 2019), which has less activin A cell death, and the Zhu CHIR differentiation regimen (Zhu et al., 2016) with activin

A instead of myostatin. CHIR is a small molecule, so it is more stable (no lot-to-lot variability) and less expensive in comparison to WNT3A (which was used for the Nair et al. DE stage differentiation) so it has an economical benefit as well as ease of use since agitation could be detrimental to the activity of growth factors. With this protocol H9 cells produced <2% $SOX17^+/FOXA2^+$ cells at day 3 (Figure 3-2A). Even an extra day of activin only increased $SOX17^+/FOXA2^+$ cells to ~30% (Figure 3-2A).

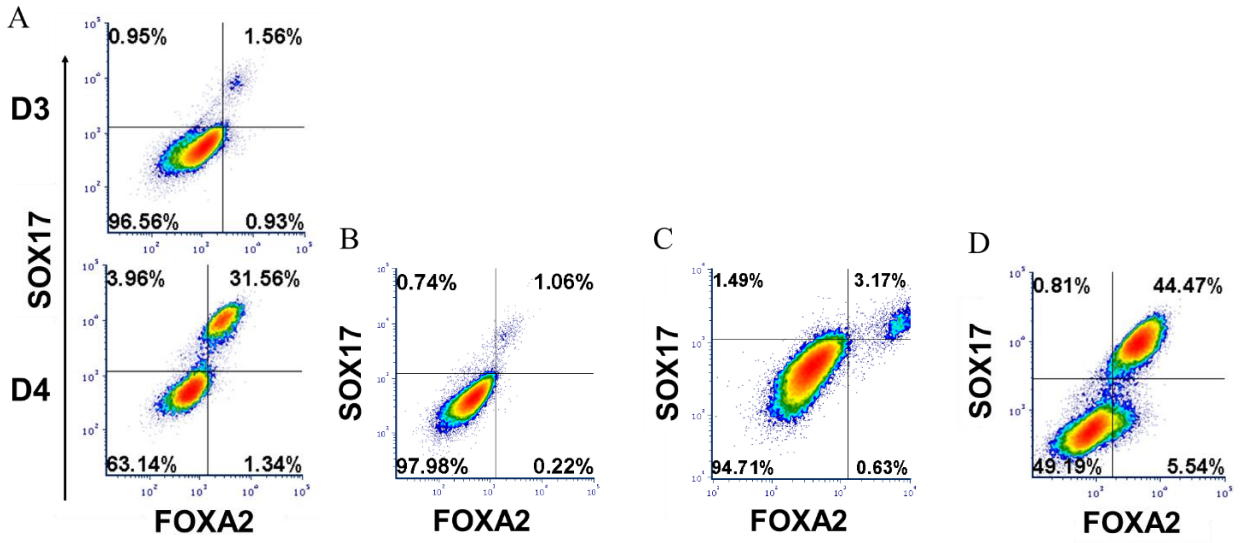

Figure 3-2. Representative flow cytometry density plots of $SOX17^+/FOXA2^+$ cells from H9 planar aggregates subjected to the initial trial DE protocols A) 3, .3 µM CHIR (day 1-2), flow from day 3 and 4, B) 50 ng/mL WNT3A (day 1), flow of day 4 C) 25 ng/mL WNT3A and 1.5 µM CHIR (day 1), 2.5 ng/mL WNT3A and .15 µM CHIR (day 2) , flow of day 4 D) 3 µM CHIR (2 days), .3 µM CHIR (day 1-3) flow of day 3.

To this end, varying concentrations of canonical Wnt stimuli (Wnt3a or CHIR) and as well as activin A application lengths were tested for the DE conversion of H9 cells (Table 9**;** Figure 2-1**,** Section I.a-b), given the variability among cell lines (Siller et al., 2016). Furthermore, Lian et al. reported that H9 hESCs have low endogenous Wnt signaling (Lian et al., 2012). Thus, extending the CHIR application for H9 differentiation to days 1-2: 3 µM, day 3: 0.3 µM, day 4: 0 µM (with

four days of 100 ng/mL activin A), led to greater fractions of DE cells (Table 2). 87.52±8.84 $SOX17^+/FOXA2^+$ cells at day 4 (Figure 3-3) and intact aggregates (

Figure **3-1**, bottom right; Figure 3-4). Treating the cells with other combinations of CHIR concentrations (Figure 3-2A), a combination of CHIR and WNT3A (Figure 3-2C), or WNT3A alone (Figure 3-2B), or <4 days of activin A (Figure 3-2D) resulted in substantially lower fractions (<50%) of DE cells.

On the other hand, when IMR90 cells were seeded in priming media followed by 3 days of differentiation with 100 ng/mL activin A and CHIR (day 1: 3 μM, day 2: 0.3 μM) (Table 2**;** Figure 2-1**,** Section I.a-b), they gave rise to 80.19±9.25% $SOX17^+/FOXA2^+$ cells at day 3 (Figure 3-3) and intact aggregates (

Figure **3-1**, top right; Figure 3-4). The two different protocols for each IMR90 (D0+3 days of differentiation) and H9 (D0+4days of differentiation) are called AW protocol (Table 2; Figure 2-1, Section I.a-b) because of the activation with activin A and the Wnt stimuli (AW).

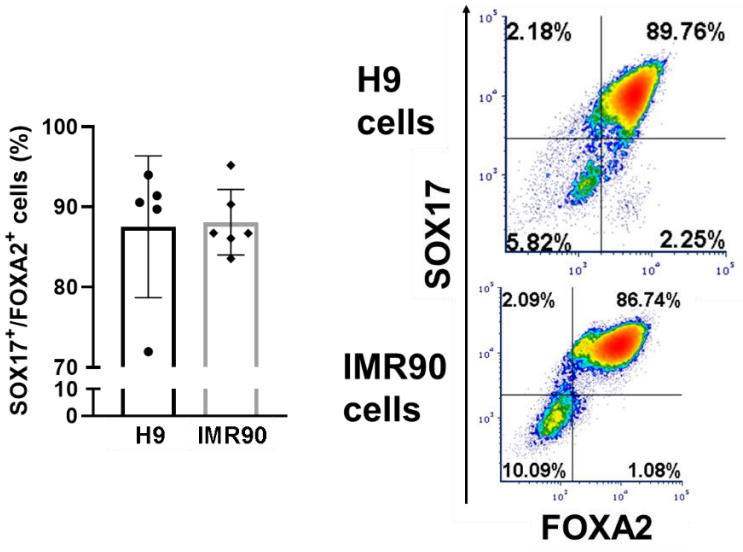

Figure 3-3. Flow cytometry analysis of SOX17+/FOXA2+ cells from IMR90 and H9 planar aggregates with AW protocol at the final day of DE differentiation. Results are shown as mean±SD along with representative density plots.

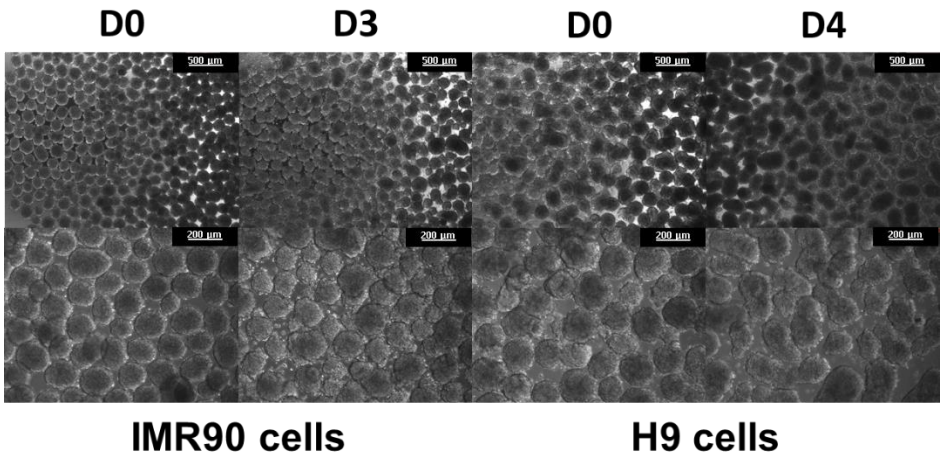

Figure 3-4. Representative images of IMR90 and H9 aggregates on days 0 (D0) and final day of AW DE differentiation (Day 3 (D3) or Day 4 (D4)). Scale bars: 500 µm (top row), 200 µm (bottom row).

Taken together, the data show that hPSCs can be coaxed to DE cells with activin A and exogenous activation of the canonical Wnt pathway (CHIR) after a day of priming. However, it indicates that each cell line requires optimization and that some cell lines require longer differentiation protocols to achieve the same level of differentiation and knowledge of each cell line endogenous expression of factors would be beneficial. These finding are important for applying planar aggregate suspension DE differentiation to other cell lines.

3.2.2 Xenofree differentiation in multi-well plates

The presence of animal components, such as FBS and KSR, limits the use of differentiated hPSC progeny for clinical applications. Thus, our focus shifted toward replacing xenogeneic elements in the AW protocol. Xenofree KSR (xfKSR) and xenofree B-27 (xfB27) were used in place of KSR and FBS in D0 medium and day 1-4, respectively. The use of B27 was reported for hPSC aggregate differentiation to DE cells (Diekmann et al., 2019; Norrman, Strombeck, Semb, & Stahlberg, 2013)) and a modified B27 form called NeuroCult has been used for later stages of

pancreatic differentiation (Nair et al., 2019). Thus, 30% and 20% xfKSR for D0 and 1% or 2% xfB27 for the differentiation was tested. (Figure 3-5, Table 10). The differentiation DE was comparable between 20% and 30% xfKSR, so 20% was chosen since xfKSR is expensive, and 1% xfB27 had superior differentiation to 2% so that was selected. Consequently, the AW protocols with 20% xfKSR and 1% xfB27 was coined 'xfAW' (Table 3).

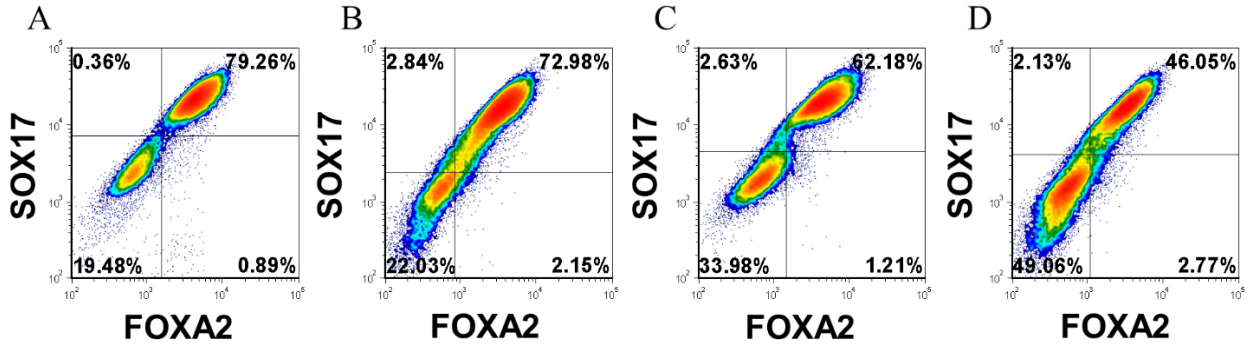

Figure 3-5. Representative flow cytometry density plot of SOX17$^+$/FOXA2$^+$ cells from IMR90 planar aggregates with trial xenofree protocols at the final day of DE differentiation. A) 1% xfB27 and 30% xfKSR. B) 1% xfB27 and 20% xfKSR. C) 2% xfB27 and 20% xfKSR. D) 1% xfB27 and 30% xfKSR. xfB27: xenofree B27 supplement, xfKSR: Xenofree KnockOut Serum Replacement.

Inducing DE differentiation of H9 hESCs with xfAW (Table 3) resulted in 72.49±2.59% vs 87.52±8.84% SOX17$^+$/FOXA2$^+$ cells for the AW method at day 4 (p=0.0169; Figure 3-6; Figure 2-1, Section I.a-b). IMR90 cells gave rise to similar fractions of SOX17$^+$/FOXA2$^+$ cells (p=0.99) with either the xfAW (82.53±5.07%, Table 3) or AW method (80.19±9.25%**Table 2**) (Figure 3-6; Figure 2-1, Section I.a-b). Differentiation was confirmed by immunocytochemistry (Figure 3-7). Conversely, only small fractions of cells were NANOG$^+$/OCT4$^+$ for H9 and IMR90 for AW (<6%, Figure 3-6) and their expression was further suppressed in xfAW-treated cells compared to AW (<4%) (Figure 3-6). The cell aggregates retained their structural integrity and normal morphology throughout differentiation (Figure 3-8), which includes no formation of cysts or dark spots forming in the aggregate which indicates abnormal differentiation. The aggregate cluster size leveled off

after day 2 and reached 196±27 µm on day 3 (vs. 196±34 µm for AW) for IMR90 and 163±6 µm (vs. 168±22 µm for AW) on day 4 for H9 (Figure 3-8B and C). These results demonstrate that robust DE differentiation can be achieved under xenofree conditions in planar suspension aggregate culture with the xfAW formulation described here. Establishing xenofree orbital shaking aggregate differentiation is the first step to differentiation in an SSB since it is small scale, where the process can be optimized. However, the next step is utilization of an SSB for the expansion and differentiation of hPSCs to meet clinical needs.

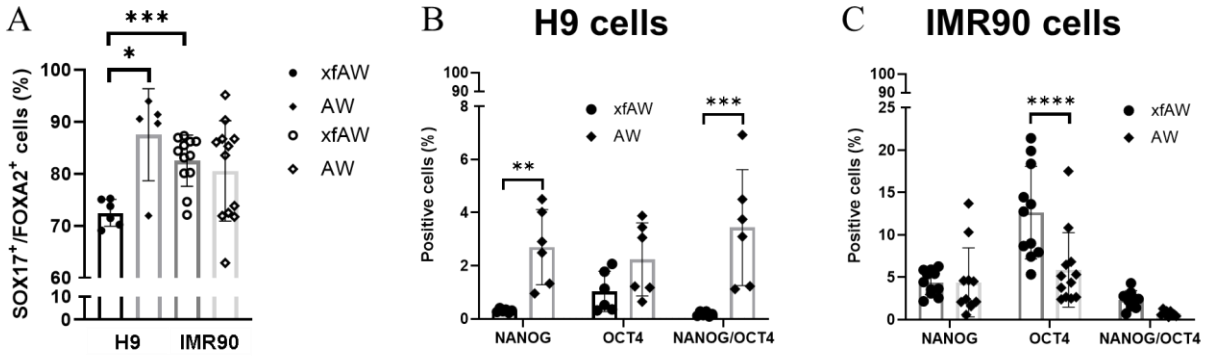

Figure 3-6. Flow cytometry analysis of IMR90 and H9 cells following xfAW and AW differentiation in 6-well plate planar cultures. A) DE markers. B) Pluripotency markers of H9 cells. C) Pluripotency markers of IMR90 cells. *p≤ 0.05, **p ≤ 0.01, *** p ≤ 0.001, ****p ≤ 0.0001. Results are shown as mean±SD.

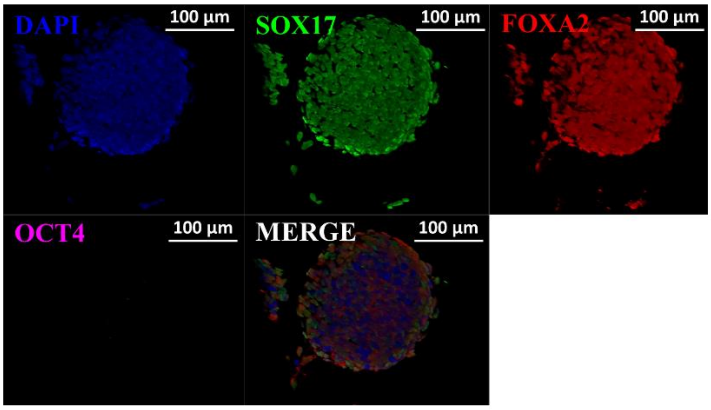

Figure 3-7. Representative immunocytochemistry of IMR90 aggregate after xfAW differentiation DAPI (blue), SOX17 (green), FOXA2 (red), OCT4 (no staining), and MERGE. Scale bars: 100 µm.

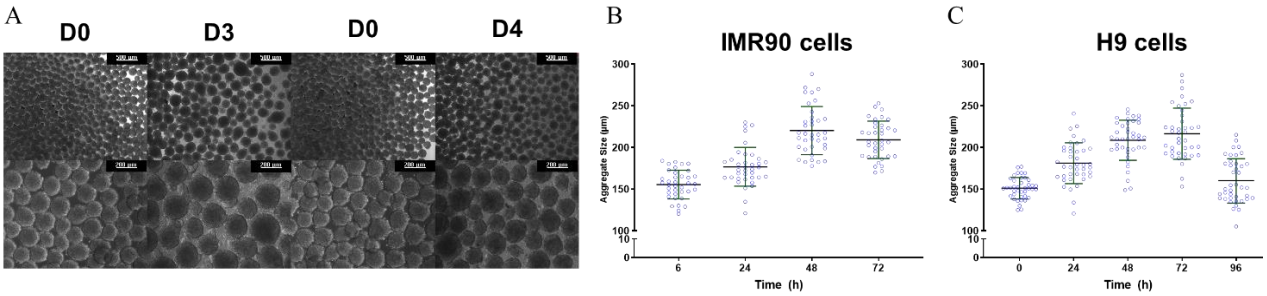

Figure 3-8. A) Representative images of IMR90 and H9 hPSC aggregates at day 0 (D0) and 3 (D3) or 4 (D4) of the xfAW protocol. Scale bars: 500 µm (top row), 200 µm (bottom row). B) and C) Representative cell aggregate sizes over the course of xfAW differentiation. B) IMR90 cells. C) H9 cells. Results are shown as mean±SD.

3.3 Discussion

Scalable xenofree differentiation to desired cell types is required for cell therapies, which generally need 10^8-10^9 cells per patient. For hPSCs this differentiation is typically carried out in aggregates. In this chapter we demonstrated the specification of two widely used hPSC lines, H9 (hESC line) and IMR90 (hiPSC line), to DE cells, which are progenitors to cells in the pancreas, liver, and lungs.

The protocol we developed was an adaptation of the DE differentiation stage from Nair et al. (G. G. Nair et al., 2019) and Zhu et al. (Zhu et al., 2016) termed AW. Our cultures were suspended hPSC aggregates in planar suspension (same as Nair et al) and the protocol were modified for different cell lines and then into a xenofree protocol (xfAW). Cells were directed to DE with similar efficiency under the AW and xfAW protocols for IMR90 and H9 (Figure 3-6).

One of the benefits of this protocol is that the formulation can be optimized as we demonstrated with H9 and IMR90. On the other hand, commercially available xenofree DE kits are optimized for cells maintained on specific expansion media, which is indicated on the kit websites and was also confirmed in another study (Diekmann et al., 2019). These kits however

offer no flexibility for cell line-specific optimization and scale-up. Furthermore, our cost analysis indicates that the xfAW method is more economical and could be even cheaper if components were purchased in larger quantities.

The xenofree DE differentiation has been recently reported. As we mentioned in 1.3, Diekmann et al. used B27 for a xenofree formulation. They developed this modified xenofree B27 by excluding two of its animal-derived components. However, they employed static culture, which lead to oversized clusters (some ~500 μm). These cultures have oxygen and nutrient diffusion limitation because they are >200-300 μm and static culture usually leads to concentration gradients. The estimated yield of DE cells (2.8-5.6x10^6 DE cells/well (6-well plate, Table 11) for HES3 hESCs) (Diekmann et al., 2019), was comparable to that in our study (6.4x10^6 and 7.2x10^6 DE cells/well for IMR90 and H9 hPSCs (Table 12), respectively). A more precise value for their yield could not be calculated because their seeding value was not specified, just 1-2x10^6 cells per well, and seeding volume and cells/mL was not reported so we could only calculated cells/well. Generally, a shift away from supplements such as B27 supplement that were employed in our and Diekmann et al.'s studies as well as xfKSR would be preferable since they are comprised of factors with pleiotropic effects and/or hard-to-predict impacts on the specification outcome. For instance, triiodothyronine, which is contained in B27, is used for inducing hPSC-derived pancreatic progenitors toward islet cells (Aguayo-Mazzucato et al., 2015; G. G. Nair et al., 2019), promoting maturation of cardiomyocytes (Burridge, Holmstrom, & Wu, 2015), and increasing the efficiency of differentiation to photoreceptor precursor cells (Yanai, Laver, Joe, & Gregory-Evans, 2016).

Extending the application of activin/CHIR to differentiating H9 cells by a day was necessary to obtain fractions of DE cells compared to those derived from IMR90 cells. This finding agrees with the known variability among hPSC lines (Siller et al., 2016) and it particularly points

to the disparate endogenous Wnt/β-catenin signaling (Blauwkamp et al., 2012; Kurek et al., 2015; Moya, Cutts, Gaasterland, Willert, & Brafman, 2014). H9 cells exhibit low endogenous canonical Wnt signaling activity (Lian et al., 2012), which is consistent with their need for extended CHIR incubation to achieve DE compared to IMR90 cells. In addition, hPSC lines have differences in endogenous transforming growth factor beta (TGF-β)/activin/Nodal signaling (Kattman et al., 2011; Ramos-Mejia et al., 2010), which could explain the longer activin A treatment needed for H9 cells. Perhaps, a better understanding of the native activity of major signaling pathways in different cell lines would be appropriate for maximizing the efficiency of subsequent stages of commitment.

These differences in signaling pathways that effects the efficiency of differentiation, indicating the need to optimize the differentiation protocol for each hPSC line. Since identifying the necessary components to increase efficiency takes time, it would slow the adaption of the protocol for a new cell line, thus increasing the cost and potentially production time. A potential way to alleviate line variability could be priming the cells with component that would make the cells amenable for differentiation toward the desired lineage. Russ et al. (Russ et al., 2015) and Nair et al. (G. G. Nair et al., 2019) treated the hPSC cells with low concentrations of heregulin-β1 and activin A (10 ng/mL) for a day before starting differentiation, a procedure which we also utilized and consider a priming step. Previously, heregulin-β1, aka neuregulin-1, has been shown to help promote cell growth and pluripotency as well as enhance single cells hPSC plating efficiency in combination FGF2 (Marinho, Chailangkarn, & Muotri, 2015) and with activin A and FGF2 was used for long-term growth of hESC lines (L. Wang et al., 2007). In our single cell aggregate seeding, the inclusion of activin A and heregulin-β1 seems to promote the formation of aggregates as excluding them causes less aggregates to form and the aggregates disintegrate after

further culture, indicating they are not as robust. Others have used other methods of priming to increase the efficiency of DE differentiation and/or decrease the length or concentration of activin A (Diekmann, Lenzen, & Naujok, 2015); (Guo, Mao, He, Liu, & Ming, 2014).

Overall, the creation of the AW protocol and xfAW (xenofree version) for hiPSC (IMR90) and hESC (H9) planar suspension aggregates was demonstrated with >70% of cells expressing DE markers. This small-scale suspension 6-well plate format is great for optimizing cell line specific protocols before scaling up to SSB systems.

4 Expansion of hPSC aggregates in an automated bioreactor

4.1 Introduction

This chapter contains results from expansion of hPSCs as pluripotent aggregates in an automated, controlled SSB. In-house-made essential 8 (E8) medium or commercially available StemMACS medium were used to maintain the hPSC in a pluripotent state while increasing their cell number. IMR90 (hiPSC) and H9 (hESC) cells were seeded into the SSB as single cells from monolayer colony cultures. Since 10^8-10^9 cells are necessary for cell therapies, SSB are a great culture modality for expansion because monolayer cultures have concentration gradients, require large surface area, and are not scalable. On the other hand, SSB can be scaled-up, are available as a single-use disposable or autoclavable system, have pH and dissolved oxygen control, are easy to sample, and cell retention systems exist for perfusion feeding (which has been shown to have better fold increases than batch method (1.5.2). However, some of the disadvantages are that the long-term impact of culturing hPSCs in SSB is unknown, there are high capital costs, the shear from the agitation can lead to cell differentiation and/or cell death, and SSBs requires specific expertise for operation. Despite this, SSB remain a great option for the expansion and differentiation of hPSC as well as being the current workhorse of the biotechnology industry, which would make its implantation for hPSC manufacture smoother since facilities already exist.

Conditions for yielding hPSCs were optimized, including the agitation rate, frequency of medium changes, and length of culture. We found that use of a commercially available pluripotency medium that has heat-stable recombinant FGF2 and enhanced buffering capabilities allows medium changes every other day while maintaining cell pluripotency, decreasing the medium usage and thus the cost of operation. The accumulation of lactate in the bioreactor was noted and the effect of exogenous lactate was explored. Using StemMACS medium we achieved

>80% of the IMR90 and H9 cells to be positive for OCT4 (a pluripotency marker) after six and five days, respectively, with a 10- and 13-fold increase in cell numbers. Furthermore, we demonstrate that the growth rate is slowed by an exogenous lactate concentration of 5 g/L (~35 mM) in two types of commercially available xenofree media (E8 Flex and StemMACS™ iPS-Brew XF). This suggests that the lactate levels we reach in SSB culture has a negative impact on fold increase. However, intracellular expression of pluripotency markers is not affected by exogenous lactate at the levels we tested.

4.2 Results

4.2.1 Expansion of hPSCs in the bioreactor

For bioreactor expansion, hPSC seeding was initiated by agitation at 60 rpm (low speed) to promote clustering without damaging the cells and the inclusion of ROCKi, which promotes the survival of hPSC single cells. pH was set to 7.4±0.2 and DO was maintained by controlling headspace aeration. Then, stirring rate was gradually increased to and kept at 100 rpm after 24 h. Either E8 medium made in-house or commercially available (StemMACS) pluripotency medium was used.

4.2.1.1 Expansion with Essential 8 medium

H9 and IMR90 aggregates were grown for eight days with in-house formulated E8 medium. After eight days of culture, H9 cells had a fold increase of ~55 and IMR90 of ~17, both with a viability >85% for the duration of the culture (Figure 4-1A and B). Aggregates maintained a normal morphology (Figure 4-2). Since aggregates remained <150 µm (Figure 4-1C and D), no oxygen or nutrient diffusion limitations is expected since that usually is common for clusters larger

than 200-300 µm. Lactate concentration increased reciprocally to glucose decrease, as expected glucose concentration increased after the medium changed and the lactate decreased (Figure 4-3A). Return to initial glucose or lactate levels was not seen because only half of the medium was changed. H9 pluripotency ($NANOG^+/OCT4^+$) began at 86.86±.34% remained similar at day 5 but decreased to 52.58±.91% by day 8 (Figure 4-3B). Approximately 50% of cells expressing pluripotent markers was also confirmed by immunostaining (Figure 4-4).

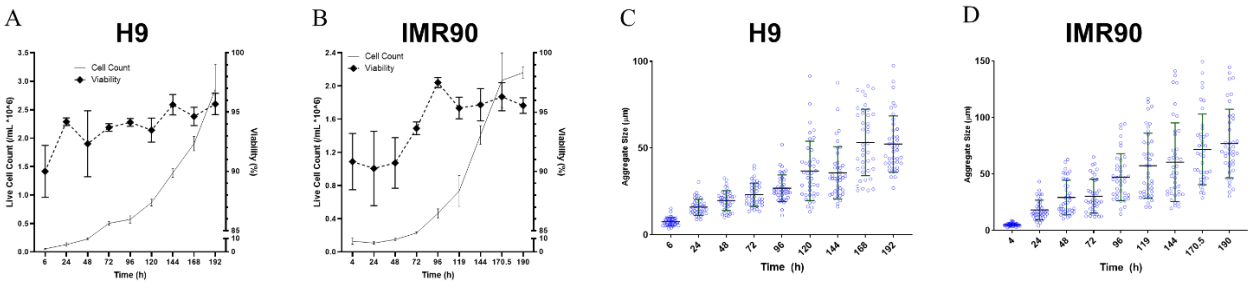

Figure 4-1. A) and B) Live cell concentration (cells/mL) and viability (%) for expansion in the bioreactor with essential 8 (E8) medium, H9 and IMR90. C) and D) Aggregate size analysis of IMR90 and H9 cells propagated in bioreactor cultures with essential 8 (E8) medium, H9 and IMR90. Results are shown as mean±SD.

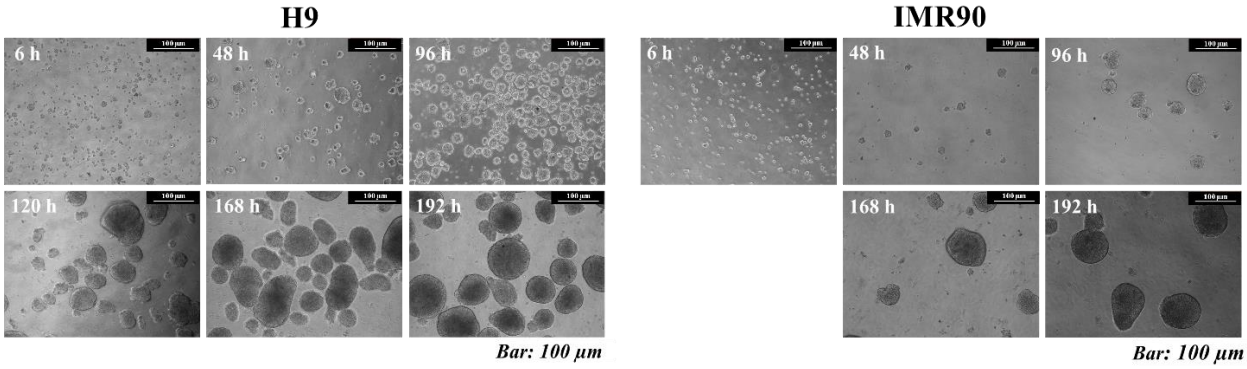

Figure 4-2. Representative images of IMR90 and H9 hPSC aggregates 6 to 192 h in the bioreactor with essential 8 (E8) medium. Scale bars: 100 µm.

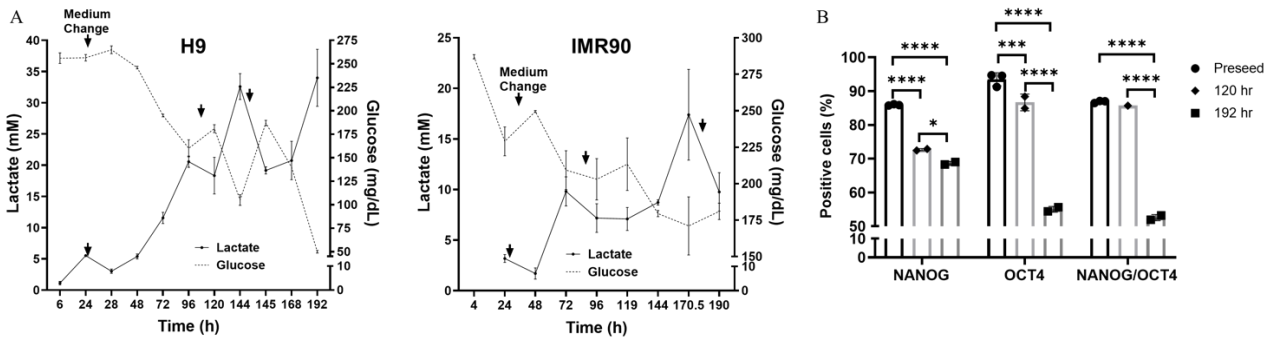

Figure 4-3. A) Lactate and glucose concentrations for H9 and IMR90 aggregates over the course of bioreactor culture with essential 8 (E8) medium. Arrows indicate medium changes. B) Flow cytometry analysis of H9 cells for pluripotency marker expression during bioreactor expansion with essential 8 (E8) medium. *p ≤ 0.05, *** p ≤ 0.001, ****p ≤ 0.0001. Results are shown as mean±SD.

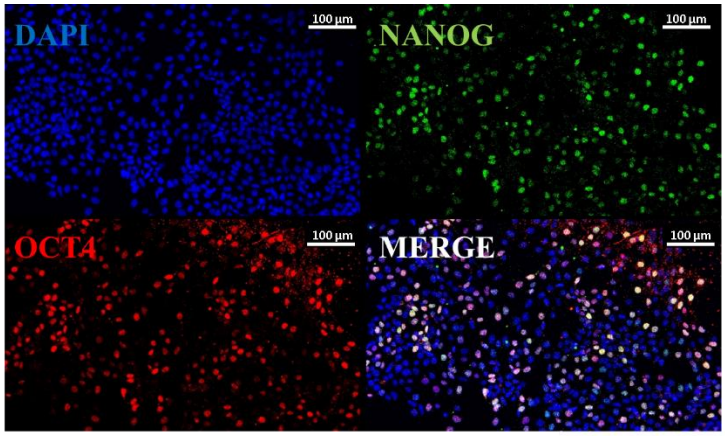

Figure 4-4. Immunocytochemistry of pluripotent markers (NANOG and OCT4) and nucleus staining (DAPI) of cells seeded as single cells in a monolayer and grown for 3 days after bioreactor culture with essential 8 (E8) medium. Scale bars: 100 µm.

4.2.1.2 Expansion with StemMACS Medium

Since commercially-available medium is known to contain FGF2 (which is necessary to maintain hPSC pluripotency) that is stable for two days and enhanced buffering to combat the effects of pH change in culture, we switched from in-house E8 medium. H9 and IMR90 cells were grown until the aggregates reached 120-200 µm diameter (H9: 192.57±72.60 µm; IMR90: 179.07±57.56 µm; Figure 4-5B), a size similar to aggregates formed in 6-well cultures for

differentiation (3.2.2) that also does not limit mass transfer. Therefore, H9 were expanded in the bioreactor for 5 days, while IMR90 were cultured for 6 days due to their slower growth (Figure 4-5A; $t_{D\ IMR90}$ = 38.5 h, $t_{D\ H9}$ = 29.4 h, t_D: doubling time). The fold increase for H9 was 13 (5 days) and 10 (6 days) for IMR90 (Figure 4-5A). The cells maintained the expression of pluripotency markers at >70% $OCT4^+/NANOG^+$ (Figure 4-5C). It should be noted that OCT4 expression persisted more readily than that of NANOG during the culture.

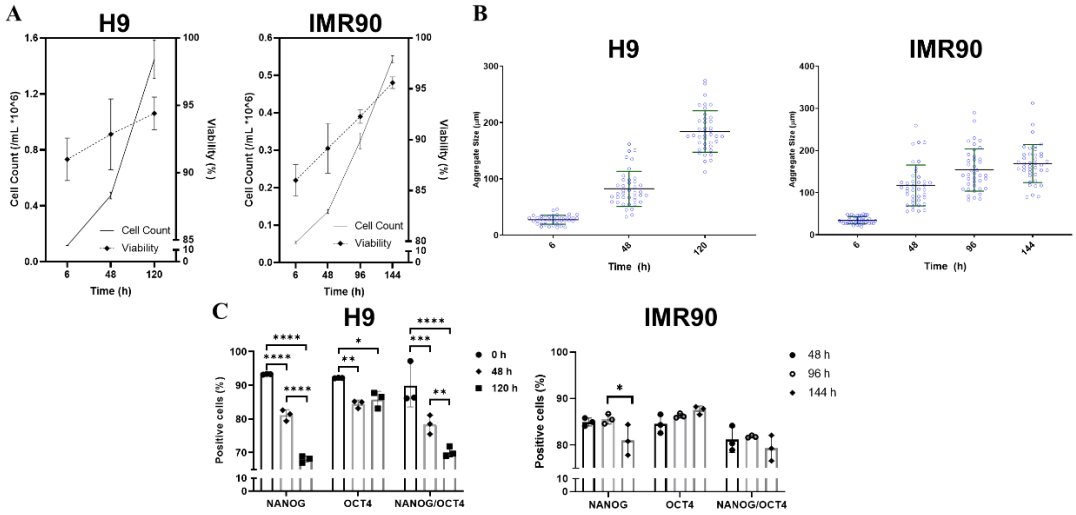

Figure 4-5. IMR90 and H9 bioreactor expansion in StemMACS A) Live cell concentration (cells/mL) and viability (%). B) Aggregate size analysis. C) Flow cytometry analysis for pluripotency marker expression. *p≤ 0.05, **p ≤ 0.01, *** p ≤ 0.001, ****p ≤ 0.0001. Results are shown as mean±SD.

Three separate bioreactor runs for the expansion of H9 were compared and cell counts (Figure 4-6A) and aggregate sizes (Figure 4-6B) were similar over the 5 days of culture. In addition, two out of the three runs had a significant drop in pluripotency by day 5 (Figure 4-6C). These results suggest that the process is reproducible for hESCs of different passage numbers.

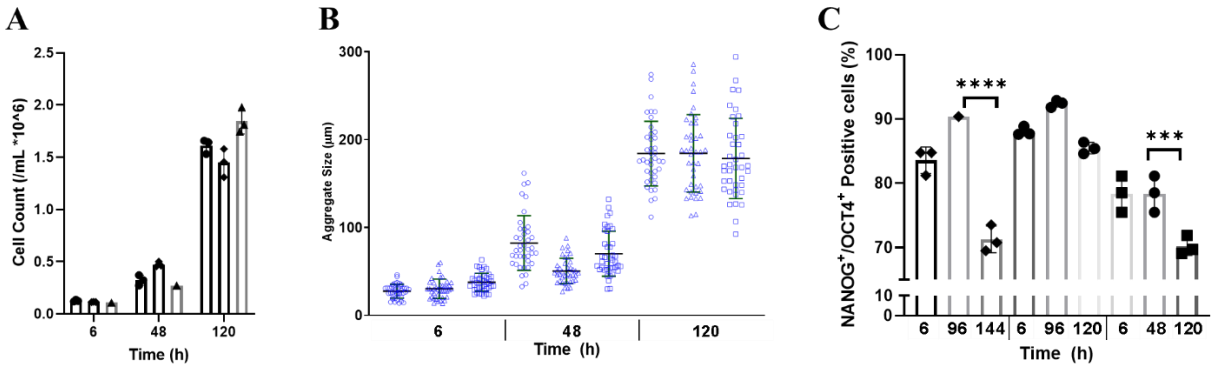

Figure 4-6. Comparison between three H9 bioreactor expansion runs in StemMACs medium (A) Live cell concentration (cells/mL) and viability (%). (B) Aggregate size analysis. C) Flow cytometry analysis for pluripotency marker expression. *** $p \leq 0.001$, ****$p \leq 0.0001$. All results are shown as mean±SD.

4.2.2 Effect of exogenous lactate on monolayer and suspension aggregate culture

IMR90 and H9 cells were seeded as single cells for either monolayer or aggregate culture, then exogenous sodium lactate was added for a final concentration of 0 g/L, 2.5 g/L, and 5 g/L and pH was adjusted to the pH of the 0 g/L (7.2-7.6) and cultured for 6 days. No significant decreases were seen in the expression of pluripotent markers intracellular marker $NANOG^+/OCT4^+$ when 0 g/L is compared to 2.5 and 5 g/L for IMR90 and H9 aggregate or monolayer culture in E8 Flex media as well as aggregate culture in StemMACs (Figure 4-7). The expression of NANOG and OCT4 was also found to be similar between exogenous lactate concentration using qPCR. On the other hand, the growth rate of cells exposed to exogenous lactate was less than that without lactate. This observation was also corroborated by aggregate size data, which showed that higher concentrations of lactate had smaller aggregate sizes after the 6 days of culture (an effect was even seen for 5 g/L by day 2) (Figure 4-8).

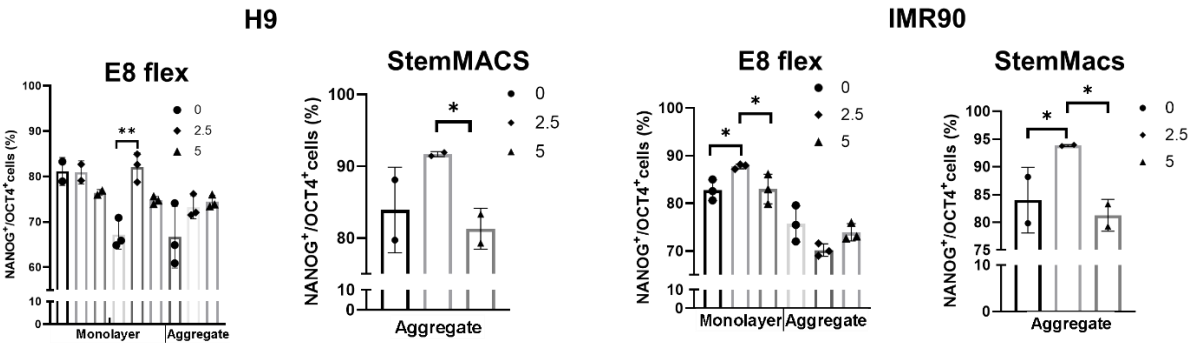

Figure 4-7. Flow cytometry analysis for pluripotency marker expression ($NANOG^+/OCT4^+$ co-expressing cells) of IMR90 cells cultured as monolayer or aggregates in E8 Flex or StemMACs medium after six days with different concentration of sodium lactate (0, 2.5, 5 g/L). *p≤ 0.05, **p ≤ 0.01. Results are shown as mean±SD.

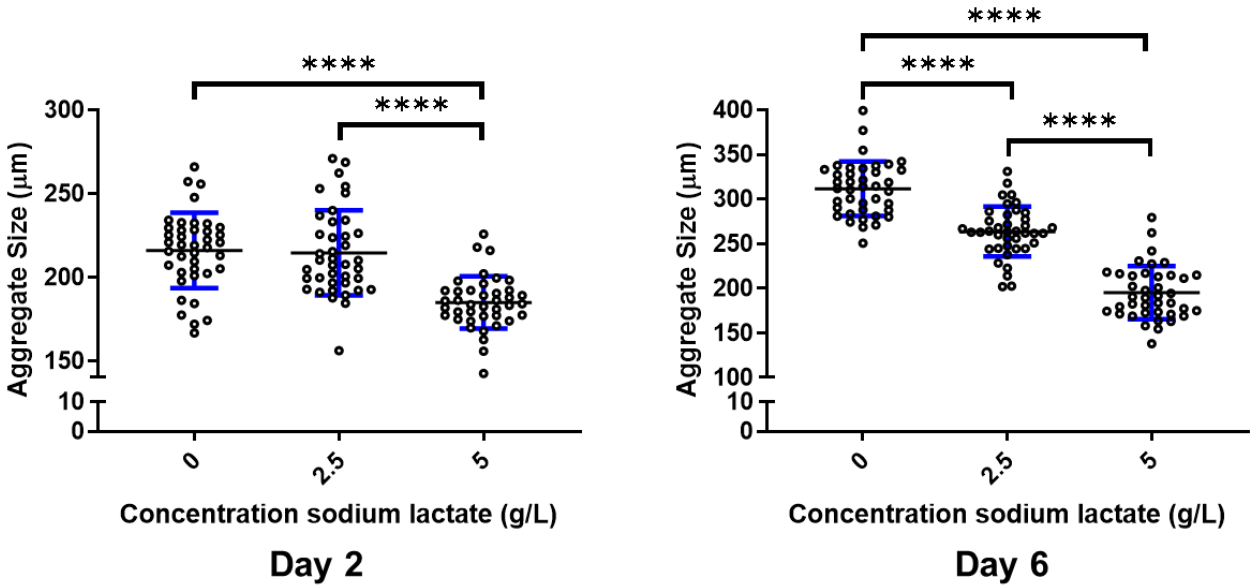

Figure 4-8. Aggregate size analysis of IMR90 at day 2 and 6 of culture with 0, 2.5, and 5 g/L sodium lactate in StemMACS medium. Results are shown as mean±SD.

4.3 Discussion

Scalable xenofree expansion of hPSC is important for the realization of cell therapies where 10^8-10^9 cells per patient are needed for treatment. For hPSC differentiations the efficiency can be relatively low, for example for pancreatic differentiation C-peptide$^+$ cells ~55% (G. G. Nair et al., 2019), ~33% (Pagliuca et al., 2014), and ~50% (Rezania et al., 2014), indicating the need for ever

more cells to achieve the necessary cell number for treatment. Other studies on the expansion of hPSCs as aggregates have demonstrated a fold increase from 4-10 over seven culture days but have not controlled pH or DO (Elanzew et al., 2015; Kropp et al., 2016; Kwok et al., 2017; Olmer et al., 2012). In our experiments for E8 medium, H9 cells had a ~55-fold increase vs. ~17-fold for IMR90 in 8 days. When StemMACS medium was used H9 cells grew 13-fold (5 days) whereas IMR90 expanded by 10-fold (6 days). The noted increases were comparable or greater than those reported in other studies (Elanzew et al., 2015; Kropp et al., 2016; Kwok et al., 2017; Olmer et al., 2012), all of which used hiPSCs. Elanew et al. utilized the same hESC line used here (H9) and a hiPSC (iLB-C-31f-r1). The reported maximal fold increase was ~5 for four days, less than the fold increase we achieve in five or six days.

In this experiment we control pH and DO, which helps to keep the culture conditions consistent potentially limiting batch-to-batch variability. Oxygen and nutrient diffusion are a function of the cluster size, which is influenced by cell seeding density and SSB agitation. Aggregates in the bioreactor exhibit a high aggregate size variability but are on average below an oxygen limiting threshold (<200-300 μm) (Wu et al., 2014). Aggregate size is important because it can impact differentiation (Chen et al., 2015). To avoid high shear, we had a low stirring rate initially, which helped promoted cell aggregation and prevent cell death. Then, agitation was increased so aggregates remained suspended and did not agglomerate.

pH control is important for hPSC function. For example, a 6.8 pH in hiPSCs cultures inhibited glycolysis, prolonged the G_0/G_1 phases, and attenuated cell proliferation (Wilmes et al., 2017). Conversely, addition of sodium bicarbonate (a buffer) led to greater glycolysis rates. In addition, low pH contributes to DNA damage and genomic instability in high-density hESC cultures (Jacobs et al., 2016). These studies in addition to hPSCs being metabolically glycolytic

with considerable production of lactate, which lowers pH, mean that pH control is necessary for cell expansion.

The switch from in-house made E8 medium to commercially available media was made because of their inclusion of a recombinant FGF2 that is stable for more than 24 h at 37ºC. In the future, it would be beneficial to formulate E8 medium in-house with the same heat stable FGF2 since it is now commercially available. That way the medium is customizable and specific factors can be added depending on the cell line or density. In addition, in-house medium formulation can be more cost effective.

We demonstrated that hPSC growth rate decreases with increasing concentration of exogenous lactate (while controlling for pH) in both monolayer and aggregate culture. This finding is corroborated by Horiguchi et al. who used 0-25 mM lactate (Horiguchi et al., 2018) and Nath et al., 0-2.5 g/L lactate, both studies were with hiPSC monolayers and equilibrated pH. Nath et al. demonstrated that lactate concentration >1.5 g/L had an inhibitory effect on growth (Nath et al., 2017). Chen et al. also showed that hESCs with lactate >1 g/L had a decreased growth rate, treatment with 2 g/L lactate yielded 25% less cells than 1 g/L, and growth rate was .45 vs .2 h^{-1} for 1 and 5 g/L lactate, respectively, in static suspension microcarrier culture (X. Chen et al., 2010). Therefore, the results in our cell lines in monolayer and aggregates are similar to what has been seen and these effects would translate to aggregate culture in the bioreactor, which can exceed 5 g/L.

Our results indicate that there was no difference in the expression of two intracellular (NANOG and OCT4) pluripotency markers when the cells were treated with lactate for six days in monolayers or aggregates. This agrees with Nath et al. for OCT4 expression with exogenous lactate (Nath et al., 2017). We also found that a pluripotency surface marker (TRA-1-60) was not

affected by 6 days of lactate in aggregate culture. As mentioned before Chen et al. showed a decrease in TRA-1-60 expression with lactate (X. Chen et al., 2010), however whether pH was adjusted after the addition of lactate was not reported, so these results cannot be solely contributed to lactate. Conversely, Nath et al. did adjust pH and still saw a decrease in TRA-1-60 expression (Nath et al., 2017), this can potentially be explained by that fact that some cell lines may differentiate more readily due to stress or because they medium we used has extra buffering capacity. In addition, the G_1 increase and the slowing of the S phase (cell cycle phases) of cells exposed to lactate (Jacobs et al., 2016) could explain the decrease in growth rate that we and others have seen.

One of the largest contrasts to the other studies that have looked at effects of lactate is our use of stabilized medium. This is because E8 Flex and StemMACS have extra buffering capacity and a more heat stable form of FGF2. As a result, media only needs to be changed every two days because it buffers pH and the heat stable FGF2 helps maintain pluripotency. Liu et al. explored the effect that high density (HD) E8-conditioned medium (medium that the cells had been cultured in) with sodium bicarbonate ($NaHCO_3$) had on low density (LD) cells. In comparison to the HD control, addition of $NaHCO_3$ increased cell survival with concentrations above 5 mM having more cells per surface area of culture after 48 h of HD medium. Twenty mM $NaHCO_3$ caused less apoptosis (programmed cell death), although not comparable to LD. In addition, $NaHCO_3$ decreased the percent of apoptotic cells and resulted in more cells in the S phase (DNA replication phase). Comparable effects were seen for HEPES and sodium phosphate, both of which are buffers (W. Liu et al., 2018). This study suggests that the extra buffering capacity is essential for evaluating the effect of lactate on the culture by lessening the impact of pH change.

Ideally it would be possible to control lactate production rates. This would be especially helpful because lactate production is higher in hPSCs than other cell types leading to greater accumulation during culture (Varum et al., 2011). This could potentially be done by selecting cells with lower inherent production rates if patient-specific hiPSCs are not needed. For example, Chen et al. showed that HES-3 produce less lactate than HES-2 (hESCs) (X. Chen et al., 2010). In addition, they showed that that using medium with 1-1.5 g/L of glucose instead of 3 g/L led to a 10% decrease in lactate levels during 7-10 days of culture, a pH of 6.7 vs 6.5, and 40% increase in cell density (X. Chen et al., 2010). This suggests that limiting glucose availability can limit lactate production. In a bioreactor system this can be automated with glucose being added when pH (due to lactate) decreases. A similar system, called high-end pH-controlled delivery of glucose (HIPDOG) is used for Chinese hamster ovary (CHO) cells and it suppresses lactate accumulation in CHO bioreactors (Gagnon et al., 2011), suggesting that application of this method could help although the effects of hPSC metabolism for glucose limiting are not well understood. Furthermore, as mentioned in the background (1.7) lactate levels are currently not monitored online. However, if these probes could be developed, medium could be changed when lactate levels exceed values that cause growth inhibition. Thus, higher fold increases can be achieved for hPSC expansion.

5 Scalable differentiation of hPSCs toward insulin expressing cells

5.1 Introduction

In this chapter we adapted the protocol reported by Nair et al. (G. G. Nair et al., 2019) for spinner flask culture then in an SSB. A spinner flask was first used because it is a stirred suspension culture and can be used to optimize certain parameters before employing an SSB since several spinners can be run simultaneously. Adjustments were made for agitation-based cultures, such as increasing the length of priming for spinner flask, using CHIR instead of WNT3A in the first stage of differentiation for both the spinner and SSB, and adjusting agitation rate. Culture in the SSB included control of pH and maintenance of DO, which is the first time this type of system has been used for differentiation to insulin expressing cells.

In the previous chapter, we discussed the expansion of H9 and IMR90 cells in an SSB in StemMACs medium (4.2.1.2). After the cells were expanded, the aggregates were switched to differentiation, including the priming step, with the xenofree protocol developed in 3.2.2. The bioreactor expansion and differentiation were compared to expansion and differentiation in 6-well plates as well as differentiation in 6-well plates after SSB expansion. The SSB yielded up to 89% $FOXA2^{+}/SOX17^{+}$ cells or ~8 DE cells per hPSC seeded. DE differentiation was consistently more efficient in the bioreactor compared to planar cultures, suggesting that scalable SSBs can be utilized for the xenofree manufacturing of DE cells.

5.2 Results

5.2.1 Scalable Differentiation of hPSCs Toward Insulin-expressing Cells

The same seeding density was used for seeding of the spinner flask as the Nair et al. protocol (G. G. Nair et al., 2019), however aggregates did not form as readily as in the orbital shaking 6-well plates. Instead of centripetal forces bringing the aggregates together as in the 6-well plate, the agitation of the spinner flask causes shear to which minimizes aggregation. A lower agitation rate was employed for the first day to facilitate aggregate formation and xenofree collagen coating matrix was added before seeding to increase cell-to-cell adhesion. However, aggregates in the spinner flask remained smaller than multi-well plate cultures after one day of priming medium and the density of aggregates was <1 million cells/mL subsequent to aggregate settling which is part of the Nair protocol. Consequently, after day one the aggregate cell number was counted and the medium is adjusted for the density to be 1 million cells/mL. Then, the aggregates were cultured for two more days in priming medium (D0) to allow the aggregates to grow in size before differentiation is initiated. In the spinner flask, ~85% of the cells were $SOX17^{+}/FOXA2^{+}$ (Figure 5-1), which is similar to the percentage for 6-well plate differentiation. These results are corroborated by the increase in gene expression of FOXA2, SOX17, and CXCR4 and a decrease of OCT4 and NANOG (pluripotency markers) for aggregates in the spinner flask when compared to a no-growth factor control. The gene expression was also similar to expression in the well (Figure 5-2). Aggregates maintained a normal morphology and were <200 μm which is below diffusion limitations Figure 5-1).

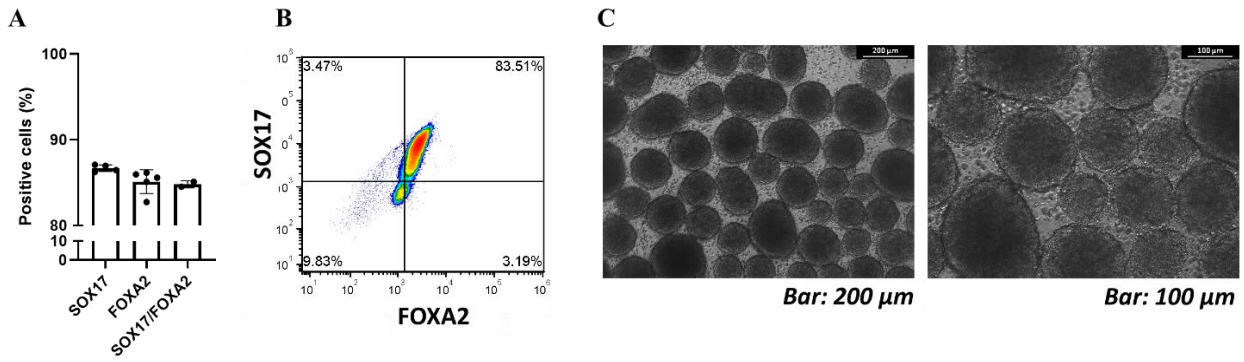

Figure 5-1. Spinner flask culture: A) Flow cytometry analysis of SOX17$^+$/FOXA2$^+$ cells at DE. Results are shown as mean±SD. B) Representative density plot. C) Representative images of aggregate at DE. Scale bars: 200 and 500 µm.

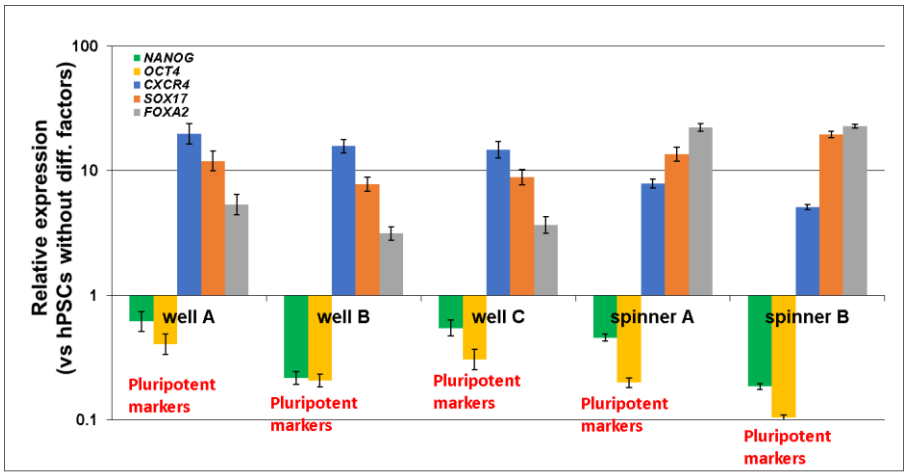

Figure 5-2. Relative expression of pluripotency and DE markers compared to control without differentiation factors.

For differentiation in the SSB, extra days of culture in priming medium was not necessary for aggregates to be the desired size for differentiation. Therefore, the same length of priming (one day) as for the 6-well plate was used in the SSB, however a slow initial agitation rate and the incubation with collagen coating matrix was still necessary. In the SSB, ~75% of cells became SOX17$^+$/FOXA2$^+$ (Figure 5-3A), however when compared to 6-well plate it is lower ($p<0.05$). This can be explained by the variability in aggregate size which is significantly larger (Standard deviation: 52 µm) for the SSB compared to well (12 µm) and spinner (32 µm) (Figure 5-4). In addition, while the aggregates sizes for well and spinner flask are similar to those for IMR90 and

H9 in 3.2.2, the SSB aggregate size is significantly larger (on average 200 µm) (Figure 5-4). On the other hand, when gene expression is compared between well, spinner flask, and SSB relative expression is higher in the SSB (Figure 5-4), indicating that it could achieve better differentiation if the aggregate size was decreased and the distribution was narrowed.

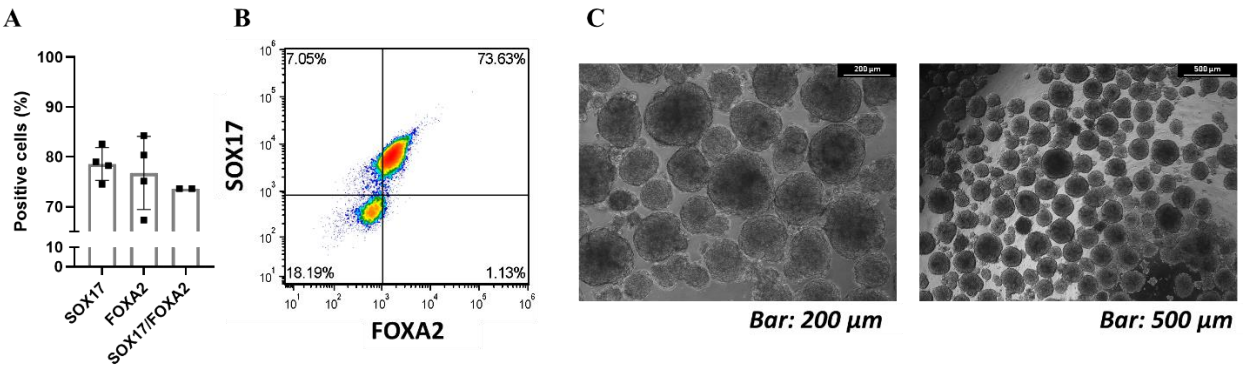

Figure 5-3. SSB culture A) Flow cytometry analysis of $SOX17^{+}/FOXA2^{+}$ cells at DE. Results are shown as mean±SD. B) Representative density plot. C) Representative images of aggregate at DE. Scale Bars: 200 and 500 µm.

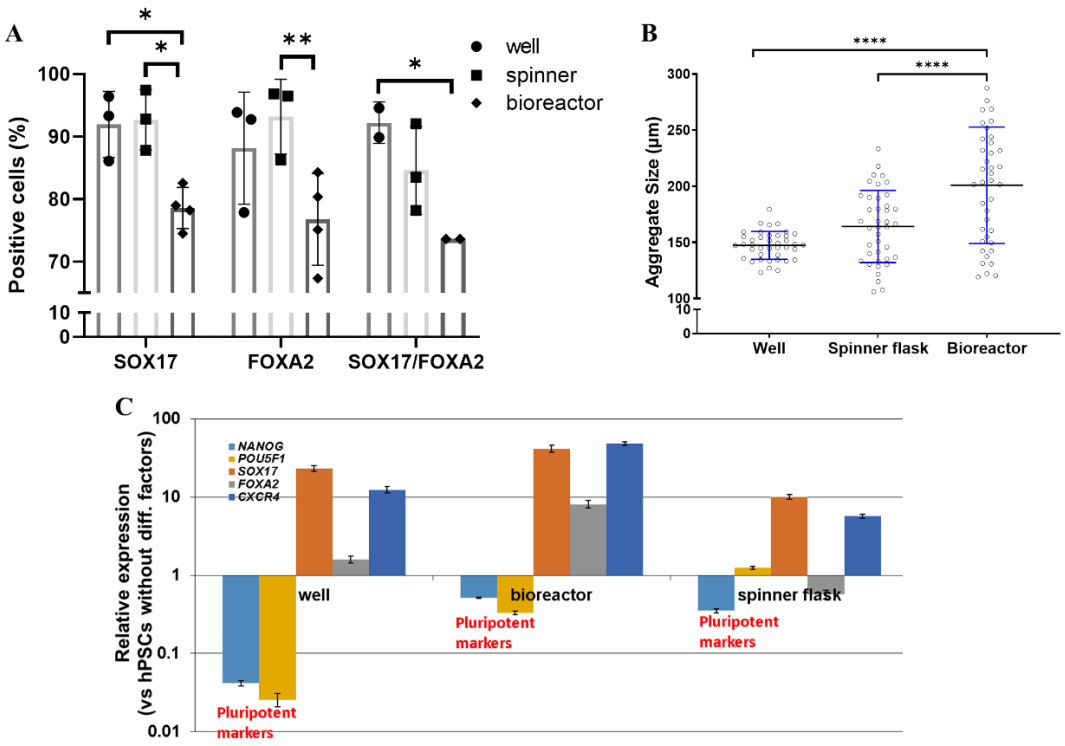

Figure 5-4. Comparison between well, SSB, and spinner flask culture. A) Flow cytometry analysis of $SOX17^{+}/FOXA2^{+}$ cells at DE. B) Aggregate size analysis. C) Relative expression of pluripotent and DE markers compared to control without differentiation factors. Results are shown as mean±SD. *p≤ 0.05, **p ≤ 0.01, ****p ≤ 0.0001.

Initially when differentiation was continued past the DE stage in the spinner flask, cysts/cavities formed in the aggregates starting at day 5 (Figure 5-5). The presence of cavities/cysts at this stage is linked to unsuccessful differentiation. However, this problem was remedied by adjusting the cell density to 1 million cells/mL as mentioned above. Aggregate size peaked at day 3 then steadily decreased until the end of culture on day 19, without ever exceeding a diffusion-limiting threshold (<250 µm) (Figure 5-6A). Morphology remained normal for most aggregates (Figure 5-6B). A range of expression for NKX6-1, PDX1, and GFP in the spinner was noted for different cell passage numbers, an observation which was confirmed by Nair et al. (G. G. Nair et al., 2019). Concurrent expression of NKX6-1, PDX1, and GFP (INS) was detected in aggregates from day 12 through 25 (Figure 5-7A). To explore the effects of aggregate density on expression of β-like pancreatic markers, $1x10^6$ and $2x10^6$ cells/mL were tested. There was very low expression in the culture with $2x10^6$ cells/mL (<5% for all markers) as compared to the one with 10^6 cell/mL, which had good expression (up to ~20% PDX1, 50% NKX6.1, 15% GFP) (Figure 5-7B).

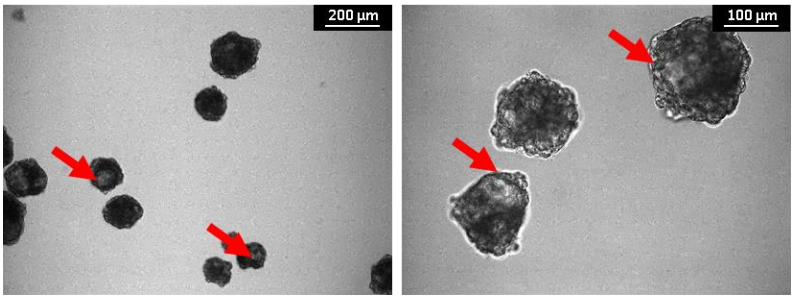

Figure 5-5. Representative images of aggregates on day 5 of culture with cysts/cavities. Scale bars: 200 µm (left) and 100 µm (right).

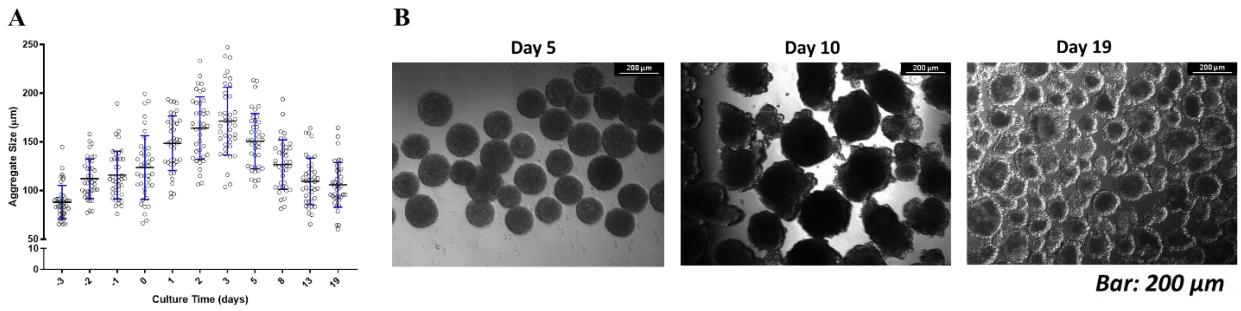

Figure 5-6. Spinner flask culture. A) Aggregate size analysis. Results are shown as mean±SD. B) Representative images of aggregates over the length of culture. Scale bars: 200 µm.

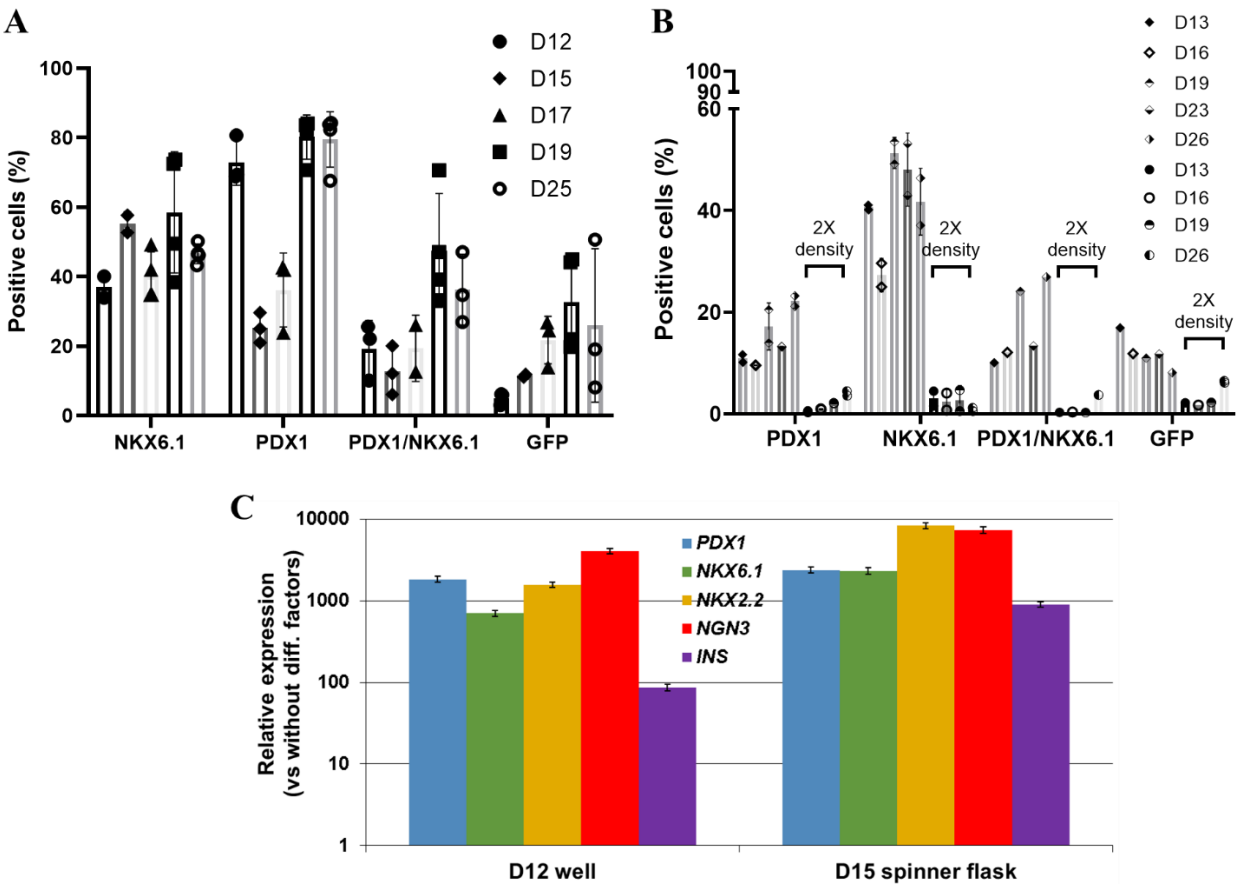

Figure 5-7. Spinner flask culture, 25 days (D25) A) Flow cytometry analysis of pancreatic markers. B) Flow cytometry analysis of pancreatic markers at one and two (2X) million cells/mL density. C) Relative expression of pancreatic compared to control without differentiation factors for well culture day 12 (D12) and spinner flask culture day 15 (D15). Results are shown as mean±SD.

When gene expression levels are compared between well and spinner flask cultures there appears to be a delay in the emergence of pancreatic markers. For example, a day 12 well culture is similar to day 15 spinner flask culture (Figure 5-7C), despite the priming steps not contributing to the differentiation day count. Unlike the aggregate sizes for the spinner flask, the cluster diameter in SSB culture increase from day 0 to day 2 then levels off for the duration of the culture, even up to 30 days (Figure 5-8A). In addition, GFP expression is apparent in certain aggregates but not in others (Figure 5-8B), once again pointing to the importance of aggregate size for successful differentiation. Expression of pancreatic markers in the SSB also appears to be delayed since peak expression of NKX6-1 was achieved at day 27, whereas GFP peaked at day 34 (Figure 5-9). This is also supported by gene expression differences between well and SSB cultures (Figure 5-9B). While cells in spinner flasks and wells have comparable levels of PDX1 expression, the corresponding expression in SSBs is significantly lower suggesting that bioreactor culture needs to be further optimized.

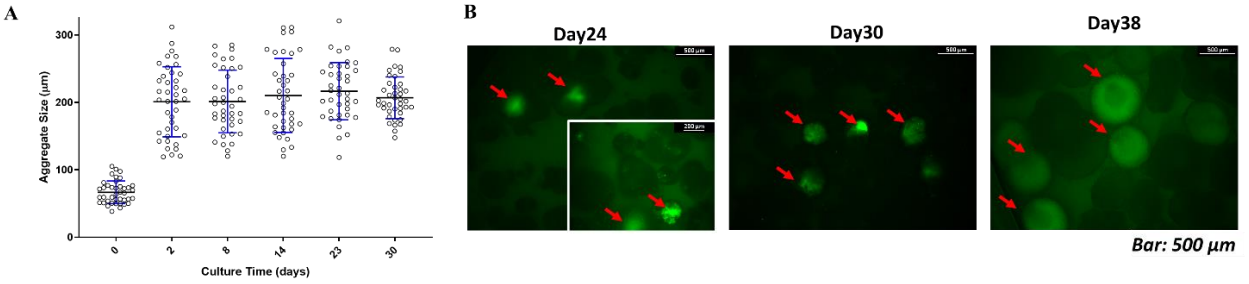

Figure 5-8. SSB culture. A) Aggregate size analysis. Results are shown as mean±SD. B) Representative images of GFP expression by aggregates toward the end of culture. Scale bars: 500 µm, Inset bar: 200 µm.

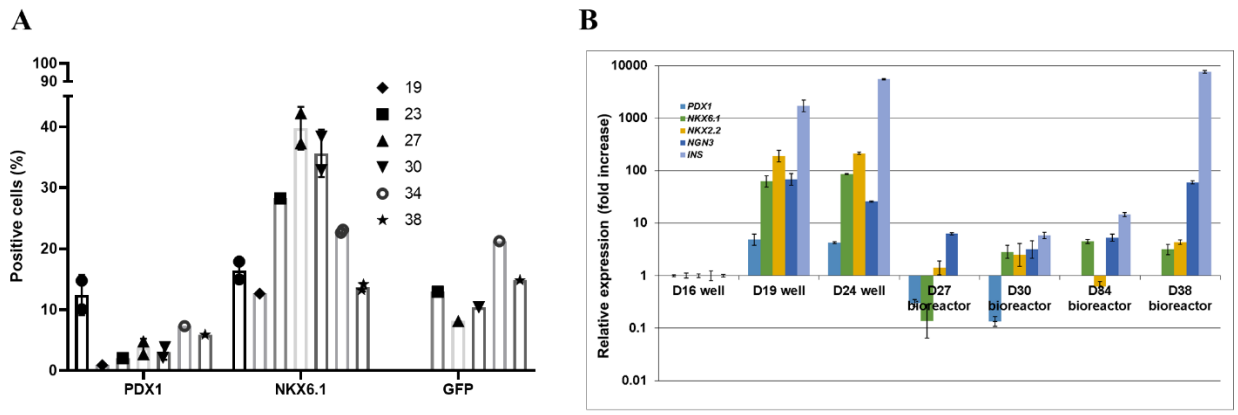

Figure 5-9. SSB culture. A) Flow cytometry analysis of pancreatic markers day 19-38. B) Relative expression of pancreatic markers day 19-24 for well and day 27-38 for SSB compared to expression at well (planar) cultures day 16 (D16). Results are shown as mean±SD.

5.2.2 Scalable Xenofree Differentiation of hPSCs To Definitive Endoderm

The H9 and IMR90 aggregates that were expanded in an SSB in the previous chapter (4.2.1.2) were then differentiated to DE in the xenofree protocol (Table 3) from 383.2.2 in the SSB also with pH (7.2±0.2) and DO control (Figure 1-7). The cell concentration continued to rise during priming and differentiation and viability remained above 85% (Figure 5-10A). This is to be expected because although DE cells are not as proliferative as hPSC it is not until the final day of differentiation that the percent of DE are significant, so the $NANOG^+/OCT4^+$ continue to rapidly proliferate until they become DE cells. Differentiation resulted in 69.4±2.8% and 89.1±4.2% $FOXA2^+/SOX17^+$ cells for H9 and IMR90 cultures, respectively (Figure 5-10B). This corresponds to $0.81x10^6$ IMR90 and $1.66x10^6$ H9 DE cells/mL in SSB culture (Table 12). Conversely, the percent of $NANOG^+/OCT4^+$ cells decreased as expected (<5%) after differentiation (Figure 5-10B). Aggregates maintained structural integrity and morphology during expansion and DE differentiation, which is important for successful differentiation (Figure 5-10C).

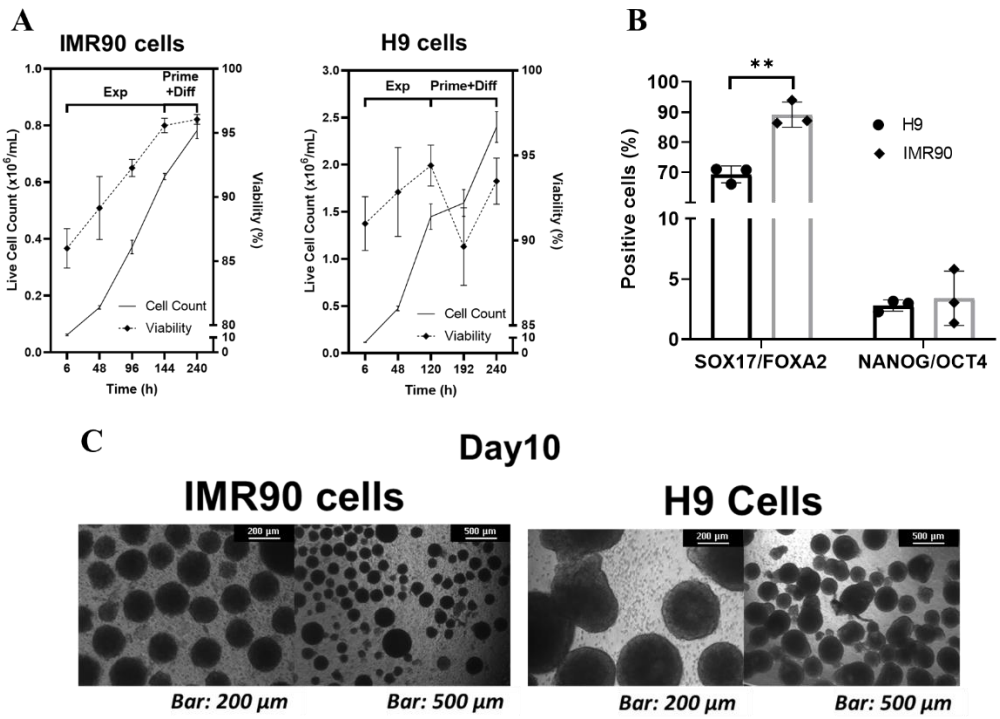

Figure 5-10. IMR90 and H9 DE differentiation in SSB A) Live cell concentration (cells/mL) and viability (%). B) Flow cytometry analysis for DE markers ($SOX17^+/FOXA2^+$) and pluripotency marker ($NANOG^+/OCT4^+$) expression. **$p \leq 0.01$. Results are shown as mean±SD. C) Representative images of aggregates at the last day of culture (Day 10). Scale bars: 200 µm and 500 µm.

In order to compare results in the SSB we simultaneously seeded cells in 6-well plates (planar) for a parallel expansion and differentiation with the same media (Figure 2-1, Section II.a-b and III.a-b). 60.1±0.16% $FOXA2^+/SOX17^+$ cells arose in H9 planar cultures vs. 69.4±2.8% in the SSB (p=0.0143; Figure 5-11A) and 66.8±1.6% % $FOXA2^+/SOX17^+$ for planar IMR90 vs 89.1±4.2% % in the SSB (p=0.0059; Figure 5-11A) at the final day of differentiation. Negligible (<0.15%) FOXA2/SOX17 expression was detected in control cultures without differentiation factors (Figure 5-12). It is important to note that the greater percent of DE cells in the SSB compared to planar cultures cannot be ascribed to differences in the populations of pluripotent cells ($NANOG^+/OCT4^+$) before initiation of differentiation because both cultures had a similar percent of hPSCs at the end of the expansion (Figure 5-11D).

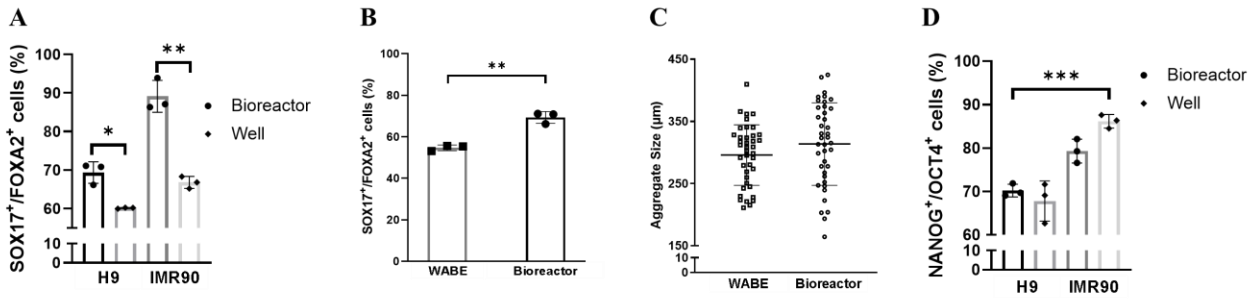

Figure 5-11. A) Flow cytometry analysis of hPSCs in the bioreactor compared to the well after expansion and xfAW differentiation. *p≤ 0.05 and **p ≤ 0.01. B) Flow cytometry analysis of cells expanded in the bioreactor and differentiated in 6-well plates (well after bioreactor expansion: WABE) compared to expansion and differentiation in the bioreactor. **p ≤ 0.01. (C) Aggregate size analysis for bioreactor and WABE H9 cell aggregates at 240 h. (D) Pluripotency marker expression after expansion (and before priming/differentiation) as determined by flow cytometry for the well and bioreactor. *** p ≤ 0.001. All results are shown as mean±SD.

In addition, to determine if the cells that were expanded in the bioreactor were still able to differentiate to DE, aggregates were transferred from the bioreactor to 6-well suspension plates and differentiated with the xfAW protocol (Figure 2-1, Section III.c). H9s yielded 54.67±1.37% $FOXA2^+/SOX17^+$ cells (Figure 5-11B), which was significantly lower ($p<10^{-4}$) than the percent of DE cells that the SSB differentiation produced (Figure 2-1, Section III.b), despite equivalent aggregate sizes (Figure 5-11C).

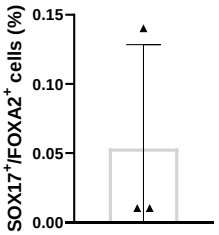

Figure 5-12. Flow cytometry analysis of H9 cells at the final day of DE differentiation treated with the same basal media but no activin A and CHIR. Results are shown as mean±SD.

5.3 Discussion

The fraction of INS GFP$^+$ cells in the spinner flask is ~32%. This is equivalent to that reported by Pagliuca et al. (Pagliuca et al., 2014), but still less than ~55% achieved in planar culture (G. G. Nair et al., 2019). As demonstrated in Figure 5-7C, pancreatic gene expression is delayed in spinner flasks in comparison to multi-well plate cultures. This could explain the fewer GFP$^+$ cells we observed in this study. Consequently, the spinner flask system should be optimized to realize similar expression levels as in planar culture.

Pancreatic differentiation in the SSB produces even less GFP$^+$ than spinner, suggesting that the conditions implemented for SSB cultivation are less ideal for the protocol we are using for differentiation. Similar to the spinner flask culture, SSB gene expression is delayed (5.2.1) so the system needs to be future optimized. Nonetheless, the SSB provides the unique ability to control pH, DO, and other parameters. This will be beneficial for the differentiation of aggregates to INS-expressing cells, and a system that is scalable, providing the means to generate enough cells to be used for therapies.

Furthermore, although the aggregate size differences between planar and spinner was not significant, the standard deviation was larger for spinner. On the other hand, in comparison to planar and spinner, the SSB aggregate sizes are statistically different. As mentioned previously aggregate size effects differentiation. There are a few methods for controlling aggregate size, including the AggreWell system and others of forced cellular aggregation (Hookway, Butts, Lee, Tang, & McDevitt, 2016; Pesl et al., 2014; Spelke, Ortmann, Khademhosseini, Ferreira, & Karp, 2011). However, this limits the scalability of the process. Using a mesh to select aggregates based on a narrow size range is also possible; however, this reduces the efficiency of aggregate formation for a given seeding density because a lot of aggregates are removed. It is possible to optimize the

agitation regimen further to make the aggregate size distribution more uniform. In addition, we currently use collagen to help the aggregates form, but this causes uneven agglomeration. Including one to two days of culture in maintenance medium before priming may be sufficient for the cells to form aggregates within a target size range without the use of collagen. Furthermore, the bioreactor system we use has an area of low agitation under the impeller as well as multiple probes and a sampling port that influence the liquid flow pattern making a higher agitation rate necessary, but potentially detrimental for cell viability and aggregate formation.

The xfAW method, developed in section 1.3, was applied to hPSC aggregates in a controlled, instrumented SSB after expansion in the same vessel. Differentiation in the bioreactor was shown to yield more $FOXA2^{+}/SOX17^{+}$ cells than in planar culture (Figure 2-1), supporting the use of SSBs for hPSC therapies. As mentioned in 1.3 xenofree differentiation of hPSCs to DE in 150-mL bioreactor cultures has been recently reported (Sahabian et al., 2019). The average yield of hiPSC-derived DE cells with custom and commercially available medium was ~$0.75x10^6$ DE cells/mL (Table 12), which is comparable with the results described here for our IMR90 hiPSC line (~$0.70x10^6$ DE cells/mL, Table 12), despite them using a different line (MHHi001-A). We also demonstrated differentiation with a hESC line (H9), which had 1.66 DE cells/mL, while they only use one hiPSC line. In addition, they monitored pH, which decrease to 6.58 by day 3 of culture, a number that has been shown to be detrimental to hPSCs (1.7), and DO decreased to 38%, whereas we maintained pH and DO at the initial values before culture. Beyond, the potential of the absolute values of the pH and DO in their experiment being harmful to the cells, cells experience shock with concentration changes due to medium replacement which can be alleviated by SSB control.

6 Conclusions and Future Work

6.1 Impact of Work

In this thesis a protocol was developed for the xenofree (xfAW) differentiation of hiPSC (IMR90) and hESC (H9) planar suspension aggregates to definitive endoderm (DE). Up to 87% of cells co-expressed $FOXA2^+/SOX17^+$ (DE markers). The findings confirm that a xenofree protocol, which is preferred for production of therapeutic cells, can successfully replace a xenogenic one. In addition, H9 and IMR90 are widely used hPSC lines, further supporting the applicability of this protocol for further differentiation to pancreas, liver, and lung cells.

Then we propagated IMR90 and H9 as pluripotent cells in a stirred suspension bioreactor (SSB), while monitoring and controlling pH and DO. Control of these parameters during human pluripotent stem cell (hPSC) expansion has not been reported yet. We used two xenofree pluripotency media, one custom-made and another that is commercially available, demonstrating that this process works for different types of medium and cell lines. In commercially available medium, cultures had a 10- or 12-fold increase in cell number over six or five days, IMR90 and H9 respectively, with high expression of pluripotency markers (>85% $OCT4^+$) and viability (>85%). Studies focusing on hPSC expansion in SSBs have only seen expansion ≤10 for seven days of culture (Kropp et al., 2016; Kwok et al., 2017; Olmer et al., 2012) or ~5 for 4 days of culture (Elanzew et al., 2015). The yield from IMR90 and H9 is $0.55\text{-}1.5 \times 10^6$ cells/mL. SSB (maximum 250 mL) expansion of cells for five or six days leads to the production of the amount of hPSCs that would necessary to produce $10^8\text{-}10^9$ cells/patient for cell therapy treatments currently being developed or used, even if a subpar efficiency of 50% for differentiated cells is achieved.

Accumulation of lactate was noted in the bioreactor during expansion. The negative effects of lactate on hPSC have been reported in adherent culture (X. Chen et al., 2010; Horiguchi et al., 2018; Jacobs et al., 2016; W. Liu et al., 2018; Nath et al., 2017; Wilmes et al., 2017). We confirmed that intracellular pluripotency markers are not affected by lactate but the growth rate was lower as others have shown. However, we also demonstrated this effect in aggregate culture, which is the method we use for expanding hPSCs in an SSB. Besides changing medium more regularly there is no known way to limit hPSC lactate accumulation and its decelerating effect on growth. As a result, a better understanding of hPSC lactate metabolism is necessary to achieve the higher density cultures of hPSC required cell therapies.

Next, we focused on the scale-up of the differentiation of MELl $INS^{GFP/W}$, an hESC cell line which expresses GFP when insulin is expressed, to β-cell-like cells of our collaborator (G. G. Nair et al., 2019) in stirred suspension. In a spinner flask we were able to achieve ~33% GFP^+, which is equivalent to the only other protocol (Pagliuca et al., 2014) that differentiated cells to β-cell-like cells in a scalable stirred suspension system. Subsequently, we differentiated the same cell line in an SSB with control over pH and DO, but no protocol optimization. Unfortunately, only 10-20% of the resulting cells were GFP^+, although there was an increase in the gene expression of insulin and other pancreatic markers. This implies that the protocol is causing an increase in the expression of the correct pancreatic markers but further tuning is necessary. The use of a SSB should be able to yield the amount of β-cells necessary for treating patients and the control of pH and DO should help limit batch-to-batch variability, delivering a better product.

Afterwards, we applied the xfAW protocol from the planar differentiation to generate cells co-expressing definitive endoderm markers ($FOXA2^+/SOX17^+$) in a scalable controlled SSB after xenofree expansion demonstrated in 4.2.1 in the same vessel. These cultures produced up to 89%

FOXA2^{+}/SOX17^{+} cells or ~ 8 DE cells per seeded hPSC. Furthermore, differentiation to DE was more efficient for IMR90 and H9 cells in the bioreactor compared to planar cultures. Overall, these results indicate a tunable protocol for different hPSC lines and that a scalable SSB can be used for xenofree manufacturing of DE cells. This thesis advances the development of bioprocesses for producing hPSC and pancreatic β-cell progeny, shines light on hPSC metabolism and its role in hPSC growth, and explores xenofree formulations for the derivation of human DE cell-based therapeutics for maladies such as diabetes and liver cirrhosis.

6.2 Future Work

6.2.1 Expansion of hPSC in an automated SSB

As mentioned in 4.2.1.2 there is a slight drop in pluripotency expression of H9 cells after five days of expansion. Retention of the maximum amount of pluripotency would be beneficial since these are the cells that differentiate to DE. Cell conditions that maintain pluripotency should be further explored or H9 cells should be differentiated at day 4 if the aggregate sizes are at the target (120-200 µm) for DE differentiation with ≥80% DE marker expression.

Our current SSB is an autoclavable system. However, the industry as a whole is moving toward single-use disposable systems. This is because no cleaning or sterilization is necessary, there is no downtime for sterilization (in our case, autoclaving), system configuration is easier to change, low maintenance/investment cost, and lower cross contamination between runs. Some of the downsides are potential for leeching from plastics that are touching fluid, differences in material caused by manufacturing, shelf life of disposable systems, and whether the supply has Food and Drug Administration (FDA) approval (necessary for clinical trials) (Schmidt, 2016). Despite these disadvantages, most companies are moving to disposable systems.

Our SSB studies are currently limited by our lab only having one SSB. As a result, three separate SSBs cannot be run simultaneously with different parameters to optimize a protocol or process. This is particular problematic because there are different differentiation outcomes based on passage number, specifically for pancreatic differentiation, and purity of hPSC seeding population. Going forward it would be advantageous to run experiments side-by-side, although capital costs limits application of this.

6.2.2 Lactate metabolism and effects on hPSCs

The results from experiments on the effects of lactate on hPSC are preliminary but demonstrate that the levels of lactate that are reached in the bioreactor adversely affect hPSCs. A better understanding of the lactate metabolism involving regulators such as MCTs and UCP2 will be beneficial. Experiments as those performed on other cell types (e.g. human peritoneal mesothelial cells with MCT knockdown (Kuma et al., 2017)) would be valuable to replicate on hPSCs so as to increase our understanding of the role of MCTs in an environment with elevated lactate. MCTs could also be overexpressed in hPSCs to establish if greater MCT expression would exacerbate the observed effects.

Another way to analyze metabolism is by using two-photon excited fluorescence (TPEF) combined with fluorescence lifetime imaging microscopy (FLIM). FLIM quantitates NAD Hydrogen (NADH, reduced form of NAD) and flavine adenine dinucleotide (FAD), which are metabolic coenzymes, using their autofluorescence (Z. Liu et al., 2018). Metabolic processes such as glycolysis/glutaminolysis, extrinsic and intrinsic mitochondrial uncoupling, and fatty acid oxidation and synthesis can be monitored with this system. Groups within Tufts have expertise in this type of imaging and have offered to help our lab conduct FLIM imaging studies on cultured

hPSCs. This type of analysis would reveal if there are metabolic differences between cells exposed to different lactate concentrations.

Bioreactor feeding strategies that minimize lactate accumulation, like perfusion, should also be considered. The higher cell density that has been seen in perfusion systems compared to batch (Kropp et al., 2016) could be a result of low lactate levels. Implementation of a perfusion system with our SSB could potentially alleviate the lactate accumulation. However, setup of perfusion requires a cell retention apparatus (1.5.2). In addition to clogging resulting from cell retention devices, aggregates can agglomerate during cell settling (e.g. in a cone) or filtering. Excessive agglomeration would be problematic for the efficient diffusion of nutrients and waste, maintenance of pluripotency, and differentiation efficiency. Furthermore, if the chosen cell retention system induces any further shear on the aggregates this could lower hPSC viability. More frequent whole- or half-medium changes is another way to improve lactate levels.

Beyond the cells' ability to remain pluripotent when exposed to lactate, their capacity for directed differentiation should be evaluated. After exposure to various amounts of lactate for six days, cells can be plated as monolayers at the same seeding density and be coaxed to DE, ectoderm, and mesoderm cells. Directly differentiating the aggregates is not an option because the aggregate size differences between aggregates treated with 0, 2.5, and 5 g/L lactate (4.2.2).

Cell cycle analysis can be useful to better understand the hPSC growth inhibition caused by lactate. Potential changes to the cell cycle have been demonstrated by Jacobs et al. who showed an increase of cells in G_1, decrease in the G_2/M fraction by 50%, and slowing of the S phase when monolayer hESCs were exposed to medium conditioned with high density culture, high lactate (15 mM) and low pH (6.9) (Jacobs et al., 2016). Being able to control variables and investigate only

the effect of lactate while analyzing cell cycle phases would be instrumental in learning if cell cycle changes are responsible for the observed lower growth rate.

6.2.3 MEL1 Differentiation toward insulin expressing cells

6.2.3.1 Optimization in a spinner and an SSB

The efficiency of MEL1 differentiation to insulin-expressing in a spinner flask is relatively low (~33%) and for an SSB it is very low (~10-20%) in comparison multi-well plate culture. As described in Section 5.5 these processes should be optimized. Factors for optimization include changing the agitation rate regimen, seeding density, overall cell density, length of each stage of expansion and differentiation, components used in differentiation, and aggregate size to see if it improves GFP^+ cell yield. In our laboratory we can run several spinner flasks simultaneously, so it will be possible to test several conditions at once. Running concurrent experiments is important because of yield differences that we and our collaborators (Hebrok lab, University of California, San Francisco) have seen during differentiation based on hESC passage number. In addition, there is inherent heterogeneity in stem cells. The final item to optimize is length of each stage and components, since this a lengthy process with many possibilities but direction can be taken from work by others (Pagliuca et al., 2014; Rezania et al., 2014) and signals involved in human embryonic pancreatic development. MEL1 $INS^{GFP/w}$ hESC adaptation to suspension culture for several passages (Amit et al., 2011) or growth as aggregates in medium that maintains pluripotency for a few days before the initiation of differentiation may be beneficial. Some cell lines have different sensitivities to shear (Leung, Chen, Choo, Reuveny, & Oh, 2011), so acclimatization to a stirred environment may be necessary for MEL1 cells.

In addition, activin A causes cell death when applied to cells so culturing aggregates for a long time before differentiating them may lead to more successful differentiation. This was achieved already by prolonging the priming step from one to three days in the spinner flask, possibly explaining the better differentiation in spinner. The initial experiments would be performed in spinner flasks for optimization, then attempted in the bioreactor.

6.2.3.2 6.2.3.2 Adaptation of MEL1 INS$^{GFP/W}$ differentiation to xenofree

After the successful establishment of a xenofree protocol for differentiating a hESC and hiPSC line to DE cells, a logical next step is to adapt the protocol developed by Nair et al. (G. G. Nair et al., 2019) to xenofree cultivation. As with our xfAW protocol, the 20% KSR in the priming step (Table 3) would be replaced with 20% xfKSR and the DE step, 0.2% FBS for 1% xfB27, but two days for DE will initially be tried instead of the three to four days we employed. For day 3-6 FBS (0.2% (day 3-4) and 0.4% (day 5-6)) will also be substituted with xfB27 and for day 6-21 the 1% B27 replaced with 1% xfB27. The heparin used for day 13-21 is derived from porcine intestinal mucosa (cat. no. H3149, Sigma), so this would need to be removed/replaced since it is animal-derived. Heparin is usually used as an anticoagulant and to stabilize growth factors (Ahmadian Baghbaderani et al., 2016), indicating it may be necessary. However, there is currently no cell-based production of recombinant human heparin (Weiss et al., 2020). On the other hand, Pagliuca et al. did not use heparin (Pagliuca et al., 2014), so it may be possible to replace it with recombinant human serum albumin (HSA), which prevents protein precipitation, in our protocol. Overall, there are only a few xenogenic components in the MEL1 differentiation protocol, making it less challenging to identify xenofree substitutes.

6.2.3.3 6.2.3.3 Fluorescence-activated cell sorting (FACS) of INS^+ cells from spinner

The next step after the establishment of insulin-expressing cells in a spinner flask is to use GFP expression to sort the cells as in Nair et al. (G. G. Nair et al., 2019). Fluorescence-activated cell sorting (FACS) can be used and the cells reaggregated for further maturation to determine if GFP^+ cells from the spinner flask function the same way as cells differentiated in planar culture. This can be performed even before the spinner differentiation is optimized as ~33% GFP^+ cells would be enough for seeding in AggreWells after sorting. There is a sorting FACS facility at the Tufts Medical Center and our collaborators have access to FACS so they can also perform these experiments. Subsequent to maturation the cells would be functionally evaluated as described in Nair et al. (G. G. Nair et al., 2019).

Table 4. hPSC differentiation to β-like cells

Differentiation Stage	Definitive Endoderm	Primitive gut tube	Posterior foregut	Pancreatic endoderm/ endocrine precursor	Hormone expressing endocrine cell
Growth factors/Small Molecules	Activin A: 100 ng/mL	CYC: .25 µM		DAPT: 1 µM	IGF1: 50 ng/mL
		FGF10: 50 ng/mL			HGF: 50 ng/mL
	Wnt 3a: 25 ng/mL (D0-1)		RA: 2 µM	Ex4: 50 ng/mL	
Medium & Supplements	RPMI + 0-.2% FBS	RPMI+2% FBS	DMEM+1% B27	DMEM+1% B27	CMRL+1% B27
Culture length (days)	2-4	2-4	2-4	2-3	3+
Culture Method	Monolayer differentiation on mouse embryonic feeder layer				
Reference	(D'Amour et al., 2006)				

For all abbreviations see the list of abbreviations and for a component's functional role see **Table 5**.

Differentiation Stage	Definitive Endoderm	Primitive gut tube	Early pancreatic progenitors	Pancreatic progenitors $PDX1^+/NKX6\text{-}1^+$	Endoderm $NKX6\text{-}1^+/C\text{-}peptide^+$	Stem-cell-derived β cells
Growth factors/Small Molecules	Activin A: 100 ng/mL	KGF: 50 ng/mL	KGF: 50 ng/mL		Alk5i II: 10 µM	
			SANT-1: 0.25 µM		T3: 1 µM	
	CHIR: 3µM (D0-1)		RA: 2 µM		RA: .1 µM	
			LDN: .2 µM (only D7)		SANT-1: 0.25 µM	
			PdBU: .5 µM (only D7-9)		XXI: 1 µM	
					Betacellulin: 20 ng/mL	
Medium*	S1	S2	S3		S5	S6
Culture length (days)	0-4	4-7	7-14		14-21	21-35
Culture Method	500 mL Spinner flask					
Reference	(Pagliuca et al., 2014)					

*S1 media: MCDB131 + 8mM D-(+)-Glucose+ 2.46 g/L $NaHCO_3$ + 2% FAF-BSA + ITS-X 1:50.000 + 2mM GlutaMax + 0.25mM Vitamin C + 1% P/S.
S2 media: MCDB131 + 8mM D-Glucose + 1.23 g/L $NaHCO_3$ + 2% FAF-BSA + ITS-X 1:50.000 + 2mM GlutaMax + 0.25mM Vitamin C + 1% P/S.
S3 media: MCDB131 + 8mM D-Glucose + 1.23 g/L $NaHCO_3$ + 2% FAF-BSA + ITS-X 1:200 + 2mM GlutaMax + 0.25mM Vitamin C + 1% P/S.
S5 media: MCDB131 + 20mM D-Glucose + 1.754 g/L $NaHCO_3$ + 2% FAF-BSA + ITS-X 1:200 + 2mM GlutaMax + 0.25mM Vitamin C + 1% P/S + Heparin 10µg/mL.
S6 media: CMRL 1066 Supplemented + 10% FBS + 1% P/S.

Differentiation Stage	Definitive Endoderm	Primitive gut tube	Posterior foregut	Pancreatic endoderm	Pancreatic endocrine precursors	Immature β cells	Maturing β cells
Growth factors/Small Molecules	GDF8: 100 ng/mL	KGF: 50 ng/mL	KGF: 50 ng/mL		$ZnSO_4$: 10 µM		
	MCX-928[i] or CHIR: 1, .1, 0 µM (D0-3)	Ascorbic Acid: 0.25 mM	SANT-1: 0.25 µM		SANT-1: 0.25 µM	XXI: .1 µM (D13-20 only)	Trolox: 10 µM
			RA: 1 µM	RA: .1 µM	RA 0.05 µM		*N*-Cys: 1 mM
			LDN: .1 µM	LDN: .2 µM	LDN .1 µM		R428: 2 µM
			TPB: .2 µM	TPB: .1 µM	Alk5i II: 10 µM		
					T3: 1 µM		
					Heparin: 10 µg/mL		
Medium[ii]	MCDB 131	MCDB 131	BLAR	BLAR	BLAR	BLAR	BLAR
Culture length (days)	0-3	3-5	5-7	7-10	10-13	For 7-15 days	For 7-15 days
Culture Method	Planar Culture (matrigel coated plates)				Air-liquid interface		
Reference	(Rezania et al., 2014)						

[i]For iPSC line, 1.5 μM MCX-928 D1
[ii]MCDB 131: medium with sodium bicarbonate (1.5 g/L), 1× GlutaMax, 10 mM final glucose concentration, 0.5% BSA
BLAR: medium with 2.5 g/L for S3-4 and 1.5 g/L for S5-7 sodium bicarbonate. 1× GlutaMax, 10 mM (S3-4) and 20 mM (S5-7) final glucose concentration, 2% BSA, 1:200 ITS-X. MCDB 131 could be substituted for BLAR media.

Differentiation Stage	Definitive Endoderm	Early Pancreatic Progenitor		PDX1$^+$/NKX6.1$^+$ progenitor cells	β-cell-like		
Growth factors/Small Molecules	GDF8: 100 ng/mL	KGF: 50 ng/mL		KGF: 2 ng/mL	$ZnSO_4$: 10 μM		
	CHIR D1: 3 μM D2: .3 μM D3: 0 μM	Ascorbic Acid: 0.25 mM			Heparin: 10 μg/mL		
			SANT-1: 0.25 μM		SANT-1: 0.25 μM	XXI: .1 μM	Trolox: 10 μM
			RA: 1 μM	RA: .1 μM	RA: 0.05 μM		*N*-Cys: 1 mM
			LDN: .1 μM	LDN: .2 μM	LDN: .1 μM		R428: 2 μM
		IWP-2: 1.25 μM	TPB: .2 μM	TPB: .1 μM	Alk5i II: 10 μM		
				IWP-2: 1.25 μM	T3: 1 μM		
Medium[‡]	S1	S1	S3		S5		
Culture length (days)	0-3	3-4	5-6	7-9	10-12	13-19	20-33
Culture Method	Planar Culture (matrigel coated plates)				Air-liquid interface		
Reference	(Zhu et al., 2016)						

[‡]S1: MCDB 131, sodium bicarbonate (1.5 g/L), 1× GlutaMax, 10 mM final glucose concentration, 0.5% BSA
S3: MCDB 131, sodium bicarbonate (2.5 g/L), 1× GlutaMax, 10 mM final glucose concentration, 2% BSA, ITS-X 1:200
S5: BLAR, sodium bicarbonate (1.5 g/L), 1× GlutaMax, 20 mM final glucose concentration, 2% BSA, ITS-X 1:200.

Differentiation Stage	Priming	Definitive Endoderm		Gut tube		Pancreatic foregut		Pancreatic progenitors	Immature β-like	
Growth factors/Small Molecules	Activin A: 10 ng/mL	Activin A: 100 ng/mL		KGF: 25 ng/mL		TTNPB: 3 nM		KGF: 50 ng/mL	ALKi II: 10 μm	T3: 1 μM
									XXI: 1 μm	Zinc sulfate: 10 μM
	Heregulin-β1: 10 ng/mL	WNT3a: 50 ng/mL		TGFbi IV: 2.5 μM			EGF: 50 ng/mL	EGF: 50 ng/mL	LDN: 500 nM	Heparin sulfate: 10 μg/mL
									N-acetyl cysteine: 1 mM	
									Vitamin C: 0.5 mM	
Medium & Components	DMEM/F12, 1x GlutaMAX, 1x NEAA, 20% KSR, 1x β-mercaptoethanol	RPMI, 0.2% FBS, 1:5000 ITS	RPMI, 0.2% FBS, 1:2000 ITS	RPMI, 0.2% FBS, 1:1000 ITS	RPMI, 0.4% FBS, 1:1000 ITS	DMEM, 25 mM glucose, 1:100 B27	DMEM, 25 mM glucose, 1:100 B27	DMEM, 25 mM glucose, 1:100 B27	DMEM, 25 mM glucose, 1:100 B27, 1:100 GlutaMax, 1:100 NEAA	
Culture length (days)	1	2	3	4	5-6	7-8	9	10-12	13-21	
Culture Method	6-well suspension plates with orbital shaking									
Reference	(G. G. Nair et al., 2019)									

After GFP sorting of INS$^+$ cells and reaggregation in Aggrewells

Differentiation Stage	β-cell maturation	
Growth factors/Small Molecules	ALKi II: 10 μm	Vitamin C: 0.5 mM
	T3: 1 μM	N-acetyl Cysteine: 1 mM
	Zinc sulfate: 10 μM	Heparin sulfate: 10 μg/mL
Medium & Components	CMRL, 1:100 B27 (or 10% FBS), 1:100 GlutaMax, 1:100 NEAA	
Culture length (days) and Method	Day 21-23/24 Aggrewells, Day 23/24-28 6-well suspension plates with orbital shaking	
Reference	(G. G. Nair et al., 2019)	

For all abbreviations see the list of abbreviations and for a component's functional role see **Table 5**.

Table 5. Differentiation components and their functional roles

Functional Role	Component
Antioxidant	N-acetyl cysteine (N-Cys)
AXL (tyrosine-protein kinase receptor) inhibition	R428
Bone morphogenetic protein inhibition	Dorsomorphin, Noggin, LDN193189
EGF family member	Betacellulin
Extracellular matrix production	Vitamin C
GLP-1 receptor agonist	Exendin-4
Glycogen synthase kinase 3 (GSK3) inhibition	Wnt3a, CHIR99021
Growth factors	KGF=FGF7, FGF10, bFGF=FGF2
γ-secretase/notch inhibition	XXI, DAPT[††]
Hedgehog signaling inhibition	KAAD-cyclopamine (CYC), SANT-1
Mitogen-activated protein kinase (MEK) inhibition	PD0325901
Phosphatidylinositol 3-kinase (PI-3K) inhibition	Activin A
Protein kinase C activation	Phorbol 12,13-dibutyrate (PdbU), TPB[†††], (−)-Indolactam V
Rock Inhibitor	Y267632
TGF-β type I receptor inhibition	Alk5i, SB431542, A8301
TGF-β family member	GDF8 aka Myostatin
Thyroid hormone	Triiodothyronine (T3)
Vitamins	Trolox (analog of vitamin E), Nicotinamide (vitamin B group), Vitamin C
Wnt inhibition	IWP-2

[†]XXI: γ-Secretase Inhibitor XXI

[††]DAPT: N-[(3,5-Difluorophenyl)acetyl]-L-alanyl-2-phenyl]glycine-1,1-dimethylethyl ester

[†††]TPB: ((2S,5S)-(*E*,*E*)-8-(5-(4-(trifluoromethyl)phenyl)-2,4-pentadienoylamino)benzolactam

Table 6. Protocols for Definitive Endoderm differentiation of hPSCs

Components	Basal Medium	Length (days)	Mode	Reference
Activin A: 100 ng/mL Mouse Wnt3a: 25 ng/mL (D0-1)	RPMI 0-.2% FBS	2-4	Monolayer differentiation on mouse embryonic feeder layer	(D'Amour et al., 2006)
Activin A: 100 ng/mL CHIR: 3 μM (D0-1)	S1a*	4	500 mL spinner flasks	(Pagliuca et al., 2014)
GDF8: 100 ng/mL MCX-928*** or CHIR: 1, .1, 0 μM (D0-3)	S1b**	3	Planar Culture (Matrigel-coated plates)	(Rezania et al., 2014)
GDF8: 100 ng/mL CHIR: 3, 0.3, 0 μM (D0-3)	S1b**	3	Planar Culture (Matrigel-coated plates)	(Zhu et al., 2016)
Activin A: 50 ng/mL CHIR: 1, 2.5, or 5 μM (D0-1)	Advanced RPMI 1640, MCDB 131, or RPMI 1640 .2% FCS, 1:100 mB27 or xfmB27	3/4	Static suspension 6-well plates	(Diekmann et al., 2019)
Activin A: 100 ng/mL CHIR: 3 μM (D0-1)	RPMI 1640 0.8% KSR (D1-2), 8% KSR (D2-3) STEMdiff™ Definitive Endoderm Kit	3	Shaking 125 mL Erlenmeyer flasks and 150-mL bioreactor	(Sahabian et al., 2019)
Activin A: 80 ng/mL D1-2: 50 ng/mL FGF2, 20 ng/mL BMP4, 3 μM CHIR	RPMI 1640**** .25% BSA D4: 0.5% KSR	4	Orbital shaking 6 well plate	(Yabe et al., 2019)
Activin A: 100 ng/mL CHIR: 3 μM (D0-1.5)	StemPro34 medium[i]	3	100-mL stirred bioreactor	(Mihara et al., 2017)
[ii]Activin A: 100 ng/mL human Wnt3a: 50 ng/mL (D1)	RPMI 0.2% FBS, ITS: 0.02% (D1), 0.05% (D2)	2	Orbital shaking 6 well plate	(G. G. Nair et al., 2019; Russ et al., 2015)
[ii]Activin A: 100 ng/mL Mouse Wnt3a: 50 ng/mL (D1)	RPMI .2% FBS, ITS: 1:5000	2	Orbital shaking 6-well plate	(Schulz et al., 2012)
[ii]Activin A: 100 ng/mL D1 or D1-2: 3 μM CHIR D3 or D4: .3 μM CHIR	RPMI 1X Xenofree B27 ITS: 0.02% D1, 0.05% D2-3/4	3/4	Orbital shaking 6-well plate 250 mL bioreactor	Our Protocol

*S1a media: MCDB131 (basal medium)+ 8mM D-(+)-Glucose+ 2.46 g/L $NaHCO_3$ + 2% Fatty Acid-free-Bovine Serum Albumin (BSA) + Insulin-Transferrin-Selenium-Ethanolamine (ITS-X) 1:50.000 + 2mM Glutamax + 0.25mM Vitamin C + 1% Penicillin-Streptomycin (P/S).
**S1b media: MCDB 131, sodium bicarbonate (1.5 g/L), 1× GlutaMax, 10 mM glucose, 0.5% BSA
***For iPSC line, 1.5 μM MCX-928 Day 1
****RPMI 1640 supplemented with: D1-4: 1x Non-Essential Amino Acid (NEAA), 0.055 mM 2-Mercaptoethanol, D1-4: 1 mM sodium pyruvate. For 454E2 (hiPS cell line), 1:100,000 ITS-X

[i]StemPro34 medium with 50 μg/mL ascorbic acid, 2 mM L-glutamine, and 400 μM 1-thioglycerol
[ii]Nair et al., Russ et al., and Schulz et al.:
Priming 1 day- Activin A: 10 ng/mL, Heregulin: 10 ng/mL, 20% Knockout Serum Replacement (KSR)/20% xenofree KSR (Our protocol), and DMEM/F12.
mB27: modified B27, xfmB27: xenofree mB27. KSR: Knockout Serum Replacement, xfKSR: xenofree KSR. BSA: bovine serum albumin, ITS: insulin-transferrin-selenium

Table 7. Xenofree and feeder-free human pluripotency medium

Medium	**Main components**	**Xenofree?**	**Reference**	**Catalog number**
Essential 8 (E8)	DMEM F-12, L-ascorbic acid, Selenium, Transferrin, $NaHCO_3$, Insulin, FGF2, TGFβ1	Yes	ThermoFisher Scientific	Essential 8: A1517001
			Stem Cell Technologies	TeSR™-E8: 05990
			(G. Chen et al., 2011)	Custom made
E8 Flex	Same as E8 but with heat-stable FGF2 and better buffering capacity	Yes	ThermoFisher Scientific	A2858501
TeSR	DMEM F-12, L-ascorbic acid, Selenium, Transferrin, $NaHCO_3$, Glutathione, L-Glutamine, Defined lipids, Thiamine, Trace elements B, Trace Elements C, β-Mercaptoethanol, Albumin (BSA), Insulin, FGF2, TGFβ1, Pipecolic acid, LiCl, GABA, H_2O	mTeSR1: No TeSR2: Yes mTeSR Plus: No	Stem Cell Technologies	1: 85850 TeSR2: 05860 Plus: 05825
StemMACS iPS-Brew XF	Proprietary composition with heat stable FGF2	Yes	Miltenyi Biotec	130-104-368

Table 8. hPSC bioreactor expansion studies

Culture System	**Cell line/s**	**Culture Volume (mL)**	**Media**	**Seeding Density (cells/mL)**	**Feeding Method**	**Culture Time (days)**	**Fold Increase**	**Ref**
DASbox Mini System	hCBiPS2, hHSC_F1285T_iPS2	100-125	mTeSR1, E8	$5x10^5$	Repeated batch, perfusion	7	Repeated batch: 4, Perfusion: 6	(Kropp et al., 2016)
DASbox Mini System	hCBiPSC2	10-125	mTeSR1	$5x10^5$	Repeated batch	7	4-6	(Olmer et al., 2012)
Mobius® 3L	AR1034ZIMA hiPSC clone 1, FS hiPSC clone 2	1000	mTeSR1	$2x10^5$	Repeated batch	7	10	(Kwok et al., 2017)
BioLevitator	iLB-C-31f-r1 (hiPSC), H9 (hESCs)	10-30	mTeSR1, E8	0.33-2.0x 10^5	Fed-batch	4	~5	(Elanzew et al., 2015)
Applikon	IMR90-4 (hiPSC), H9 (hESC)	30-100	E8, StemMACS iPS-Brew XF	$2.0x10^5$	Repeated batch	5-8	E8, 8 days: ~55 (H9), ~17 (IMR90) StemMACS: 10 (IMR90, 6 days), 12 (H9, 5 days)	Our study

All used a single cell seeding method and cells were cultured as aggregates

Table 9. Experimental protocols for testing different concentrations of canonical Wnt activation with CHIR and activin A application length for DE differentiation of H9 hESC aggregates.

Experimental DE Protocols				
Priming	**Differentiation** **Basal medium: RPMI + 0.2% FBS + 100 ng/mL activin A + 1x GlutaMAX**			
DMEM/F12 + 20% KSR† + 1x NEAA† + 1x βME† + 1x GlutaMAX + 10 ng/mL heregulin-β1 + 10 ng/mL activin A	D1-2: 3 μM CHIR D1: 0.02% ITS, D2: 0.05% ITS		D3: 0.3 μM CHIR 0.05% ITS	D4: 0 μM CHIR 0.05% ITS
	D1: 3 μM CHIR 0.02% ITS	D2: 0.3 μM CHIR 0.05% ITS	D3-4: 0 μM CHIR 0.05% ITS	
	D1: 50 ng/mL hWNT3A 0.02% ITS	D2: 0 ng/mL hWNT3A 0.05% ITS	D3-4: 0 ng/mL hWNT3A 0.05% ITS	
	D1: 50 ng/mL hWNT3A 1.5 μM CHIR 0.02% ITS	D2: .5 ng/mL hWNT3A .15 μM CHIR 0.05% ITS	D3-4: 0 ng/mL hWNT3A 0 μM CHIR 0.05% ITS	

† KSR: KnockOut Serum Replacement, NEAA: non-essential amino acids, βME : β-mercaptoethanol , ITS: insulin-transferrin-selenium

Table 10. Experimental protocols for testing different concentrations of xfKSR and xfB27 for DE differentiation of IMR90 aggregates.

Experimental Xenofree DE Protocols			
Priming	**Differentiation** **Basal medium: RPMI + 0.2% FBS + 100 ng/mL Activin A + 1x GlutaMAX**		
DMEM/F12 + 1x NEAA† + 1x βME†† + 1x GlutaMAX + 10 ng/mL heregulin-β1 + 10 ng/mL activin A	D1: 3 μM CHIR 0.02% ITS	D2: .3 μM CHIR 0.05% ITS	D3: 0 μM CHIR 0.05% ITS
20% xfKSR	1% XF B27		
20% xfKSR	2% XF B27		
30% xfKSR	1% XF B27		
30% xfKSR	2% XF B27		

†† xfKSR: Xenofree KnockOut Serum Replacement, NEAA: non-essential amino acids, βME : β-mercaptoethanol , ITS: insulin-transferrin-selenium

Table 11. Yield of DE cells/well reported here and by Diekmann et al. (Diekmann et al., 2019).

Xenogeneic-free differentiation in planar cultures			
Definitive endoderm ($x10^6$ cells/well)	**hPSC line**	**Culture System**	**Reference**
7.2††	H9 (hESC)	Orbital Shaker 6-well Suspension plate	Our Study
6.4††	IMR90 (hiPSC)		
2.8-5.6‡‡	HES3 (hESC)	Static Suspension 6-well plate	Diekmann et al.

†† Average of live cells/well times the average of the percent of $SOX17^+/FOXA2^+$ cells
‡‡ Calculated with 1x or $2x10^6$ cells per well seeding described by Diekmann et al. (Diekmann et al., 2019) (Methods, Differentiation experiments) and 3.75-fold increase (Figure 7C) and 75% $CXCR4^+$ cells (Figure 7A).

Table 12. Yield of DE cells/mL reported here with the xfAW protocol and by Sahabian et al. (Sahabian et al., 2019).

Xenogeneic-free differentiation in bioreactors		
Definitive endoderm ($x10^6$ cells/mL)	**hPSC line**	**Reference**
0.81§	IMR90 (hiPSC)	Our Study
1.66§	H9 (hESC)	
~0.75¶	MHHi001-A (hiPSC)	Sahabian et al.

§ Average of live cells/mL times the average of the percent of $SOX17^+/FOXA2^+$ cells
¶ Calculated from the average $1.12x10^8$ DE cells per 150 mL bioreactor culture reported by Sahabian et al. (Sahabian et al., 2019).

7 References

Abrar, M. A., Dong, Y., Lee, P. K., & Kim, W. S. (2016). Bendable Electro-chemical Lactate Sensor Printed with Silver Nano-particles. *Sci Rep, 6*, 30565. doi:10.1038/srep30565

Adijanto, J., & Philp, N. J. (2012). The SLC16A family of monocarboxylate transporters (MCTs)--physiology and function in cellular metabolism, pH homeostasis, and fluid transport. *Curr Top Membr, 70*, 275-311. doi:10.1016/B978-0-12-394316-3.00009-0

Aguayo-Mazzucato, C., DiIenno, A., Hollister-Lock, J., Cahill, C., Sharma, A., Weir, G., . . . Bonner-Weir, S. (2015). MAFA and T3 Drive Maturation of Both Fetal Human Islets and Insulin-Producing Cells Differentiated From hESC. *J Clin Endocrinol Metab, 100*(10), 3651-3659. doi:10.1210/jc.2015-2632

Ahmadian Baghbaderani, B., Tian, X., Scotty Cadet, J., Shah, K., Walde, A., Tran, H., . . . Fellner, T. (2016). A Newly Defined and Xeno-Free Culture Medium Supports Every-Other-Day Medium Replacement in the Generation and Long-Term Cultivation of Human Pluripotent Stem Cells. *PLoS One, 11*(9), e0161229. doi:10.1371/journal.pone.0161229

Amit, M., Laevsky, I., Miropolsky, Y., Shariki, K., Peri, M., & Itskovitz-Eldor, J. (2011). Dynamic suspension culture for scalable expansion of undifferentiated human pluripotent stem cells. *Nature Protocols, 6*, 572-579. doi:10.1038.nprot/2011.325

Balboa, D., & Otonkoski, T. (2015). Human pluripotent stem cell based islet models for diabetes research. *Best Pract Res Clin Endocrinol Metab, 29*(6), 899-909. doi:10.1016/j.beem.2015.10.012

Basford, C. L., Prentice, K. J., Hardy, A. B., Sarangi, F., Micallef, S. J., Li, X., . . . Wheeler, M. B. (2012). The functional and molecular characterisation of human embryonic stem cell-derived insulin-positive cells compared with adult pancreatic beta cells. *Diabetologia, 55*(2), 358-371. doi:10.1007/s00125-011-2335-x

Blauwkamp, T. A., Nigam, S., Ardehali, R., Weissman, I. L., & Nusse, R. (2012). Endogenous Wnt signalling in human embryonic stem cells generates an equilibrium of distinct lineage-specified progenitors. *Nat Commun, 3*, 1070. doi:10.1038/ncomms2064

Bonfanti, P., Nobecourt, E., Oshima, M., Albagli-Curiel, O., Laurysens, V., Stange, G., . . . Scharfmann, R. (2015). Ex Vivo Expansion and Differentiation of Human and Mouse Fetal Pancreatic Progenitors Are Modulated by Epidermal Growth Factor. *Stem Cells Dev, 24*(15), 1766-1778. doi:10.1089/scd.2014.0550

Burridge, P. W., Holmstrom, A., & Wu, J. C. (2015). Chemically Defined Culture and Cardiomyocyte Differentiation of Human Pluripotent Stem Cells. *Curr Protoc Hum Genet, 87*, 21 23 21-21 23 15. doi:10.1002/0471142905.hg2103s87

Cebola, I., Rodriguez-Segui, S. A., Cho, C. H., Bessa, J., Rovira, M., Luengo, M., . . . Ferrer, J. (2015). TEAD and YAP regulate the enhancer network of human embryonic pancreatic progenitors. *Nat Cell Biol, 17*(5), 615-626. doi:10.1038/ncb3160

Chen, G., Gulbranson, D. R., Hou, Z., Bolin, J. M., Ruotti, V., Probasco, M. D., . . . Thomson, J. A. (2011). Chemically defined conditions for human iPSC derivation and culture. *Nat Methods, 8*(5), 424-429. doi:10.1038/nmeth.1593

Chen, G., Gulbranson, D. R., Yu, P., Hou, Z., & Thomson, J. A. (2012). Thermal stability of fibroblast growth factor protein is a determinant factor in regulating self-renewal, differentiation, and reprogramming in human pluripotent stem cells. *Stem Cells, 30*(4), 623-630. doi:10.1002/stem.1021

Chen, X., Chen, A., Liang Woo, T., Choo, A. B. H., Reuveny, S., & Oh, S. K. W. (2010). Investigations into the Metabolism of Two-Dimensional Colony and Suspended Microcarrier Cultures of Human Embryonic Stem Cells in Serum-Free Media. *STEM CELLS AND DEVELOPMENT, 19*(11), 1781-1792.

D'Amour, K. A., Bang, A. G., Eliazer, S., Kelly, O. G., Agulnick, A. D., Smart, N. G., . . . Baetge, E. E. (2006). Production of pancreatic hormone-expressing endocrine cells from human embryonic stem cells. *Nat Biotechnol, 24*(11), 1392-1401. doi:10.1038/nbt1259

Diekmann, U., Lenzen, S., & Naujok, O. (2015). A reliable and efficient protocol for human pluripotent stem cell differentiation into the definitive endoderm based on dispersed single cells. *Stem Cells Dev, 24*(2), 190-204. doi:10.1089/scd.2014.0143

Diekmann, U., Wolling, H., Dettmer, R., Niwolik, I., Naujok, O., & Buettner, F. F. R. (2019). Chemically defined and xenogeneic-free differentiation of human pluripotent stem cells into definitive endoderm in 3D culture. *Sci Rep, 9*(1), 996. doi:10.1038/s41598-018-37650-z

Edlund, H. (2002). Pancreatic organogenesis--developmental mechanisms and implications for therapy. *Nat Rev Genet, 3*(7), 524-532. doi:10.1038/nrg841

Elanzew, A., Sommer, A., Pusch-Klein, A., Brustle, O., & Haupt, S. (2015). A reproducible and versatile system for the dynamic expansion of human pluripotent stem cells in suspension. *Biotechnol J, 10*(10), 1589-1599. doi:10.1002/biot.201400757

Gagnon, M., Hiller, G., Luan, Y. T., Kittredge, A., DeFelice, J., & Drapeau, D. (2011). High-end pH-controlled delivery of glucose effectively suppresses lactate accumulation in CHO fed-batch cultures. *Biotechnol Bioeng, 108*(6), 1328-1337. doi:10.1002/bit.23072

Guo, S., Mao, X., He, F., Liu, H., & Ming, L. (2014). Activin A supplement in the hESCs culture enhances the endoderm differentiation efficiency. *Cell Biol Int, 38*(7), 849-856. doi:10.1002/cbin.10274

Hai, N., Shin, D. W., Bi, H., Ye, K., & Jin, S. (2018). Mechanistic Analysis of Physicochemical Cues in Promoting Human Pluripotent Stem Cell Self-Renewal and Metabolism. *Int J Mol Sci, 19*(11). doi:10.3390/ijms19113459

Hashemzadeh, S., Omidi, Y., & Rafii-Tabar, H. (2019). Amperometric lactate nanobiosensor based on reduced graphene oxide, carbon nanotube and gold nanoparticle nanocomposite. *Mikrochim Acta, 186*(10), 680. doi:10.1007/s00604-019-3791-0

Hebrok, M., Kim, S. K., & Melton, D. A. (1998). Notochord repression of endodermal Sonic hedgehog permits pancreas development. *Genes & Development, 12*, 1705-1713.

Hebrok, M., Kim, S. K., St-Jacques, B., McMahon, A. P., & Melton, D. A. (2000). Regulation of pancreas development by hedgehog signaling. *Development, 127*, 4905-4913.

Herrera, P. L., Nepote, V., & Delacour, A. (2002). Pancreatic Cell Lineage Analyses in Mice. *Endocrine, 19*(3), 267-277.

Hookway, T. A., Butts, J. C., Lee, E., Tang, H., & McDevitt, T. C. (2016). Aggregate formation and suspension culture of human pluripotent stem cells and differentiated progeny. *Methods, 101*, 11-20. doi:10.1016/j.ymeth.2015.11.027

Horiguchi, I., Urabe, Y., Kimura, K., & Sakai, Y. (2018). Effects of glucose, lactate and basic FGF as limiting factors on the expansion of human induced pluripotent stem cells. *Journal of Bioscience and Bioengineering, 125*(1). doi:10.1016/j.jbiosc.2017.08.004

Jacobs, K., Zambelli, F., Mertzanidou, A., Smolders, I., Geens, M., Nguyen, H. T., . . . Spits, C. (2016). Higher-Density Culture in Human Embryonic Stem Cells Results in DNA Damage and Genome Instability. *Stem Cell Reports, 6*(3), 330-341. doi:10.1016/j.stemcr.2016.01.015

Jacobson, E. F., & Tzanakakis, E. S. (2017). Human pluripotent stem cell differentiation to functional pancreatic cells for diabetes therapies: Innovations, challenges and future directions. *J Biol Eng, 11*, 21. doi:10.1186/s13036-017-0066-3

Jacobson, E. F., & Tzanakakis, E. S. (2018). Who Will Win: Induced Pluripotent Stem Cells Versus Embryonic Stem Cells for beta Cell Replacement and Diabetes Disease Modeling? *Curr Diab Rep, 18*(12), 133. doi:10.1007/s11892-018-1109-y

Jennings, R. E., Berry, A. A., Kirkwood-Wilson, R., Roberts, N. A., Hearn, T., Salisbury, R. J., . . . Hanley, N. A. (2013). Development of the human pancreas from foregut to endocrine commitment. *Diabetes, 62*(10), 3514-3522. doi:10.2337/db12-1479

Jennings, R. E., Berry, A. A., Strutt, J. P., Gerrard, D. T., & Hanley, N. A. (2015). Human pancreas development. *Development, 142*(18), 3126-3137. doi:10.1242/dev.120063

Jeon, J., Correa-Medina, M., Ricordi, C., Edlund, H., & Diez, J. A. (2009). Endocrine cell clustering during human pancreas development. *J Histochem Cytochem, 57*(9), 811-824. doi:10.1369/jhc.2009.953307

Jin, S. M., & Kim, K. W. (2017). Is islet transplantation a realistic approach to curing diabetes? *Korean J Intern Med, 32*(1), 62-66. doi:10.3904/kjim.2016.224

Kattman, S. J., Witty, A. D., Gagliardi, M., Dubois, N. C., Niapour, M., Hotta, A., . . . Keller, G. (2011). Stage-specific optimization of activin/nodal and BMP signaling promotes cardiac differentiation of mouse and human pluripotent stem cell lines. *Cell Stem Cell, 8*(2), 228-240. doi:10.1016/j.stem.2010.12.008

Kempf, H., Olmer, R., Kropp, C., Ruckert, M., Jara-Avaca, M., Robles-Diaz, D., . . . Zweigerdt, R. (2014). Controlling expansion and cardiomyogenic differentiation of human pluripotent

stem cells in scalable suspension culture. *Stem Cell Reports, 3*(6), 1132-1146. doi:10.1016/j.stemcr.2014.09.017

Kroon, E., Martinson, L. A., Kadoya, K., Bang, A. G., Kelly, O. G., Eliazer, S., . . . Baetge, E. E. (2008). Pancreatic endoderm derived from human embryonic stem cells generates glucose-responsive insulin-secreting cells in vivo. *Nat Biotechnol, 26*(4), 443-452. doi:10.1038/nbt1393

Kropp, C., Kempf, H., Halloin, C., Robles-Diaz, D., Franke, A., Scheper, T., . . . Olmer, R. (2016). Impact of Feeding Strategies on the Scalable Expansion of Human Pluripotent Stem Cells in Single-Use Stirred Tank Bioreactors. *Stem Cells Transl Med, 5*(10), 1289-1301. doi:10.5966/sctm.2015-0253

Kuma, A., Tamura, M., Ishimatsu, N., Harada, Y., Izumi, H., Miyamoto, T., . . . Otsuji, Y. (2017). Monocarboxylate Transporter-1 Mediates the Protective Effects of Neutral-pH Bicarbonate/Lactate-Buffered Peritoneal Dialysis Fluid on Cell Viability and Apoptosis. *Ther Apher Dial, 21*(1), 62-70. doi:10.1111/1744-9987.12476

Kurek, D., Neagu, A., Tastemel, M., Tuysuz, N., Lehmann, J., van de Werken, H. J. G., . . . Ten Berge, D. (2015). Endogenous WNT signals mediate BMP-induced and spontaneous differentiation of epiblast stem cells and human embryonic stem cells. *Stem Cell Reports, 4*(1), 114-128. doi:10.1016/j.stemcr.2014.11.007

Kwok, C. K., Ueda, Y., Kadari, A., Gunther, K., Heron, A., Schnitzler, A. C., . . . Edenhofer, F. (2017). Scalable stirred suspension culture for the generation of billions of human induced pluripotent stem cells using single-use bioreactors. *J Tissue Eng Regen Med*. doi:10.1002/term.2435

Lang, V., & Light, P. E. (2010). The molecular mechanisms and pharmacotherapy of ATP-sensitive potassium channel gene mutations underlying neonatal diabetes. *Pharmgenomics Pers Med, 3*, 145-161. doi:10.2147/PGPM.S6969

Leung, H. W., Chen, A., Choo, A. B., Reuveny, S., & Oh, S. K. (2011). Agitation can induce differentiation of human pluripotent stem cells in microcarrier cultures. *Tissue Eng Part C Methods, 17*(2), 165-172. doi:10.1089/ten.TEC.2010.0320

Lian, X., Hsiao, C., Wilson, G., Zhu, K., Hazeltine, L. B., Azarin, S. M., . . . Palecek, S. P. (2012). Robust cardiomyocyte differentiation from human pluripotent stem cells via temporal modulation of canonical Wnt signaling. *Proc Natl Acad Sci U S A, 109*(27), E1848-1857. doi:10.1073/pnas.1200250109

Lin, K. C., Muthukumar, S., & Prasad, S. (2020). Flex-GO (Flexible graphene oxide) sensor for electrochemical monitoring lactate in low-volume passive perspired human sweat. *Talanta, 214*, 120810. doi:10.1016/j.talanta.2020.120810

Liu, W., Ren, Z., Lu, K., Song, C., Cheung, E. C. W., Zhou, Z., & Chen, G. (2018). The Suppression of Medium Acidosis Improves the Maintenance and Differentiation of Human Pluripotent Stem Cells at High Density in Defined Cell Culture Medium. *Int J Biol Sci, 14*(5), 485-496. doi:10.7150/ijbs.24681

Liu, Z., Pouli, D., Alonzo, C. A., A., V., Karaliota, S., Quinn, K. P., . . . Georgakoudi, I. (2018). Mapping metabolic changes by noninvasive, multiparametric, high-resolution imaging using endogenous contrast. *Science Advances, 4*(4), 1-14. doi:10.1126/sciadv.aap9302

Livak, K. J., & Schmittgen, T. D. (2001). Analysis of relative gene expression data using real-time quantitative PCR and the 2(-Delta Delta C(T)) Method. *Methods, 25*(4), 402-408. doi:10.1006/meth.2001.1262

Lock, L. T., & Tzanakakis, E. S. (2007). Stem/Progenitor cell sources of insulin-producing cells for the treatment of diabetes. *Tissue Eng, 13*(7), 1399-1412. doi:10.1089/ten.2007.0047

Marinho, P. A., Chailangkarn, T., & Muotri, A. R. (2015). Systematic optimization of human pluripotent stem cells media using Design of Experiments. *Sci Rep, 5*, 9834. doi:10.1038/srep09834

Martin, M., Gallego-Llamas, J., Ribes, V., Kedinger, M., Niederreither, K., Chambon, P., . . . Gradwohl, G. (2005). Dorsal pancreas agenesis in retinoic acid-deficient Raldh2 mutant mice. *Dev Biol, 284*(2), 399-411. doi:10.1016/j.ydbio.2005.05.035

McCluskey, J. T., Hamid, M., Guo-Parke, H., McClenaghan, N. H., Gomis, R., & Flatt, P. R. (2011). Development and functional characterization of insulin-releasing human pancreatic beta cell lines produced by electrofusion. *J Biol Chem, 286*(25), 21982-21992. doi:10.1074/jbc.M111.226795

Mihara, Y., Matsuura, K., Sakamoto, Y., Okano, T., Kokudo, N., & Shimizu, T. (2017). Production of pancreatic progenitor cells from human induced pluripotent stem cells using a three-dimensional suspension bioreactor system. *J Tissue Eng Regen Med, 11*(11), 3193-3201. doi:10.1002/term.2228

Miralles, F., Lamotte, L., Couton, D., & Joshi, R. L. (2006). Interplay between FGF10 and Notch signalling is required for the self-renewal of pancreatic progenitors. *Int J Dev Biol, 50*(1), 17-26. doi:10.1387/ijdb.052080fm

Moya, N., Cutts, J., Gaasterland, T., Willert, K., & Brafman, D. A. (2014). Endogenous WNT signaling regulates hPSC-derived neural progenitor cell heterogeneity and specifies their regional identity. *Stem Cell Reports, 3*(6), 1015-1028. doi:10.1016/j.stemcr.2014.10.004

Nair, G., & Hebrok, M. (2015). Islet formation in mice and men: lessons for the generation of functional insulin-producing beta-cells from human pluripotent stem cells. *Curr Opin Genet Dev, 32*, 171-180. doi:10.1016/j.gde.2015.03.004

Nair, G. G., Liu, J. S., Russ, H. A., Tran, S., Saxton, M. S., Chen, R., . . . Hebrok, M. (2019). Recapitulating endocrine cell clustering in culture promotes maturation of human stem-cell-derived beta cells. *Nat Cell Biol, 21*(2), 263-274. doi:10.1038/s41556-018-0271-4

Nath, S. C., Nagamori, E., Horie, M., & Kino-Oka, M. (2017). Culture medium refinement by dialysis for the expansion of human induced pluripotent stem cells in suspension culture. *Bioprocess Biosyst Eng, 40*(1), 123-131. doi:10.1007/s00449-016-1680-z

Norrman, K., Strombeck, A., Semb, H., & Stahlberg, A. (2013). Distinct gene expression signatures in human embryonic stem cells differentiated towards definitive endoderm at single-cell level. *Methods, 59*(1), 59-70. doi:10.1016/j.ymeth.2012.03.030

Olmer, R., Lange, A., Selzer, S., Kasper, C., Haverich, A., Martin, U., & Zweigerdt, R. (2012). Suspension culture of human pluripotent stem cells in controlled, stirred bioreactors. *Tissue Eng Part C Methods, 18*(10), 772-784. doi:10.1089/ten.TEC.2011.0717

Pagliuca, F. W., Millman, J. R., Gurtler, M., Segel, M., Van Dervort, A., Ryu, J. H., . . . Melton, D. A. (2014). Generation of functional human pancreatic beta cells in vitro. *Cell, 159*(2), 428-439. doi:10.1016/j.cell.2014.09.040

Payne, M. E., Zamarayeva, A., Pister, V. I., Yamamoto, N. A. D., & Arias, A. C. (2019). Printed, Flexible Lactate Sensors: Design Considerations Before Performing On-Body Measurements. *Sci Rep, 9*(1), 13720. doi:10.1038/s41598-019-49689-7

Pesl, M., Acimovic, I., Pribyl, J., Hezova, R., Vilotic, A., Fauconnier, J., . . . Meli, A. C. (2014). Forced aggregation and defined factors allow highly uniform-sized embryoid bodies and functional cardiomyocytes from human embryonic and induced pluripotent stem cells. *Heart Vessels, 29*(6), 834-846. doi:10.1007/s00380-013-0436-9

Promphet, N., Rattanawaleedirojn, P., Siralertmukul, K., Soatthiyanon, N., Potiyaraj, P., Thanawattano, C., . . . Rodthongkum, N. (2019). Non-invasive textile based colorimetric sensor for the simultaneous detection of sweat pH and lactate. *Talanta, 192*, 424-430. doi:10.1016/j.talanta.2018.09.086

Ramos-Mejia, V., Melen, G. J., Sanchez, L., Gutierrez-Aranda, I., Ligero, G., Cortes, J. L., . . . Menendez, P. (2010). Nodal/Activin signaling predicts human pluripotent stem cell lines prone to differentiate toward the hematopoietic lineage. *Mol Ther, 18*(12), 2173-2181. doi:10.1038/mt.2010.179

Rezania, A., Bruin, J. E., Arora, P., Rubin, A., Batushansky, I., Asadi, A., . . . Kieffer, T. J. (2014). Reversal of diabetes with insulin-producing cells derived in vitro from human pluripotent stem cells. *Nat Biotechnol, 32*(11), 1121-1133. doi:10.1038/nbt.3033

Riedel, M. J., Asadi, A., Wang, R., Ao, Z., Warnock, G. L., & Kieffer, T. J. (2012). Immunohistochemical characterisation of cells co-producing insulin and glucagon in the developing human pancreas. *Diabetologia, 55*(2), 372-381. doi:10.1007/s00125-011-2344-9

Rodriguez-Seguel, E., Mah, N., Naumann, H., Pongrac, I. M., Cerda-Esteban, N., Fontaine, J. F., . . . Spagnoli, F. M. (2013). Mutually exclusive signaling signatures define the hepatic and pancreatic progenitor cell lineage divergence. *Genes Dev, 27*(17), 1932-1946. doi:10.1101/gad.220244.113

Rorsman, P., Arkhammar, P., Bokvist, K., Hellerstrom, C., Nilsson, T., Welsh, M., . . . BERGGREN, P. (1989). Failure of glucose to elicit a normal secretory response in fetal pancreatic beta cells results from glucose insensitivity of the ATP regulated K+ channels. *PNAS, 86*, 4505-4509.

Russ, H. A., Parent, A. V., Ringler, J. J., Hennings, T. G., Nair, G. G., Shveygert, M., . . . Hebrok, M. (2015). Controlled induction of human pancreatic progenitors produces functional beta-like cells in vitro. *EMBO J, 34*(13), 1759-1772. doi:10.15252/embj.201591058

Sahabian, A., Sgodda, M., Naujok, O., Dettmer, R., Dahlmann, J., Manstein, F., . . . Olmer, R. (2019). Chemically-Defined, Xeno-Free, Scalable Production of hPSC-Derived Definitive Endoderm Aggregates with Multi-Lineage Differentiation Potential. *Cells, 8*(12). doi:10.3390/cells8121571

Salisbury, R. J., Blaylock, J., Berry, A. A., Jennings, R. E., De Krijger, R., Piper Hanley, K., & Hanley, N. A. (2014). The window period of NEUROGENIN3 during human gestation. *Islets, 6*(3), e954436. doi:10.4161/19382014.2014.954436

Schmidt, S. R. (2016). The Benefits and Limits of Disposable Technologies In Manufacturing Protein Therapeutic. *American Pharmaceutical Review*, 1-3.

Schulz, T. C., Young, H. Y., Agulnick, A. D., Babin, M. J., Baetge, E. E., Bang, A. G., . . . Robins, A. J. (2012). A scalable system for production of functional pancreatic progenitors from human embryonic stem cells. *PLoS One, 7*(5), e37004. doi:10.1371/journal.pone.0037004

Serra, M., Brito, C., Sousa, M. F., Jensen, J., Tostoes, R., Clemente, J., . . . Alves, P. M. (2010). Improving expansion of pluripotent human embryonic stem cells in perfused bioreactors through oxygen control. *J Biotechnol, 148*(4), 208-215. doi:10.1016/j.jbiotec.2010.06.015

Shyh-Chang, N., Zheng, Y., Locasale, J. W., & Cantley, L. C. (2011). Human pluripotent stem cells decouple respiration from energy production. *EMBO J, 30*(24), 4851-4852. doi:10.1038/emboj.2011.436

Siller, R., Naumovska, E., Mathapati, S., Lycke, M., Greenhough, S., & Sullivan, G. J. (2016). Development of a rapid screen for the endodermal differentiation potential of human pluripotent stem cell lines. *Sci Rep, 6*, 37178. doi:10.1038/srep37178

Silva, M. M., Rodrigues, A. F., Correia, C., Sousa, M. F., Brito, C., Coroadinha, A. S., . . . Alves, P. M. (2015). Robust Expansion of Human Pluripotent Stem Cells: Integration of Bioprocess Design With Transcriptomic and Metabolomic Characterization. *Stem Cells Transl Med, 4*(7), 731-742. doi:10.5966/sctm.2014-0270

Spelke, D. P., Ortmann, D., Khademhosseini, A., Ferreira, L., & Karp, J. M. (2011). Methods for embryoid body formation: the microwell approach. *Methods Mol Biol, 690*, 151-162. doi:10.1007/978-1-60761-962-8_10

Varum, S., Rodrigues, A. S., Moura, M. B., Momcilovic, O., Easley, C. A. t., Ramalho-Santos, J., . . . Schatten, G. (2011). Energy metabolism in human pluripotent stem cells and their differentiated counterparts. *PLoS One, 6*(6), e20914. doi:10.1371/journal.pone.0020914

Wang, H., Luo, X., Yao, L., Lehman, D. M., & Wang, P. (2015). Improvement of Cell Survival During Human Pluripotent Stem Cell Definitive Endoderm Differentiation. *Stem Cells Dev, 24*(21), 2536-2546. doi:10.1089/scd.2015.0018

Wang, L., Schulz, T. C., Sherrer, E. S., Dauphin, D. S., Shin, S., Nelson, A. M., . . . Robins, A. J. (2007). Self-renewal of human embryonic stem cells requires insulin-like growth factor-1

receptor and ERBB2 receptor signaling. *Blood, 110*(12), 4111-4119. doi:10.1182/blood-2007-03-082586

Weiss, R. J., Spahn, P. N., Toledo, A. G., Chiang, A. W. T., Kellman, B. P., Li, J., . . . Esko, J. D. (2020). ZNF263 is a transcriptional regulator of heparin and heparan sulfate biosynthesis. *Proc Natl Acad Sci U S A, 117*(17), 9311-9317. doi:10.1073/pnas.1920880117

Wells, J., & Melton, D. A. (2000). Early mouse endoderm is patterned by soluble factors from adjacent germ layers. *Development, 127*, 1563-1572.

Wilmes, A., Rauch, C., Carta, G., Kern, G., Meier, F., Posch, W., . . . Jennings, P. (2017). Towards optimisation of induced pluripotent cell culture: Extracellular acidification results in growth arrest of iPSC prior to nutrient exhaustion. *Toxicol In Vitro, 45*(Pt 3), 445-454. doi:10.1016/j.tiv.2017.07.023

Wilson, M. E., Scheel, D., & German, M. S. (2003). Gene expression cascades in pancreatic development. *Mechanisms of Development, 120*, 65-80.

Xu, X., Kahan, B., Forgianni, A., Jing, P., Jacobson, L., Browning, V., . . . Odorico, J. (2006). Endoderm and pancreatic islet lineage differentiation from human embryonic stem cells. *Cloning and Stem Cells, 8*(2).

Yabe, S. G., Nishida, J., Fukuda, S., Takeda, F., Nashiro, K., Ibuki, M., & Okochi, H. (2019). Definitive endoderm differentiation is promoted in suspension cultured human iPS-derived spheroids more than in adherent cells. *Int J Dev Biol, 63*(6-7), 271-280. doi:10.1387/ijdb.180251sy

Yanai, A., Laver, C., Joe, A. W., & Gregory-Evans, K. (2016). Efficient Production of Photoreceptor Precursor Cells from Human Embryonic Stem Cells. In K. Turksen (Ed.), *Human Embryonic Stem Cell Protocols* (pp. 357-369). New York, NY: Springer New York.

Ye, F., Duvillie, B., & Scharfmann, R. (2005). Fibroblast growth factors 7 and 10 are expressed in the human embryonic pancreatic mesenchyme and promote the proliferation of embryonic pancreatic epithelial cells. *Diabetologia, 48*(2), 277-281. doi:10.1007/s00125-004-1638-6

Zhu, Z., Li, Q. V., Lee, K., Rosen, B. P., Gonzalez, F., Soh, C. L., & Huangfu, D. (2016). Genome Editing of Lineage Determinants in Human Pluripotent Stem Cells Reveals Mechanisms of Pancreatic Development and Diabetes. *Cell Stem Cell, 18*(6), 755-768. doi:10.1016/j.stem.2016.03.015